
AN INTRODUCTION TO MATERIALS ENGINEERING AND SCIENCE

FOR CHEMICAL AND MATERIALS ENGINEERS

Brian S. Mitchell
Department of Chemical Engineering,
Tulane University



A JOHN WILEY & SONS, INC., PUBLICATION

Electrical, Magnetic, and Optical Properties of Materials

This chapter is organized much like Chapter 4. We will describe three related properties of materials, and we will subdivide each section into the five materials classes. Just as in Chapter 4, there are some fundamental equations that relate important fluxes to driving forces and, in doing so, create proportionality constants that are material properties. And, just as in Chapter 4, we will be more concerned with the constants—material properties—than with the driving forces. In fact, we will be even less concerned with the driving forces and fluxes of electricity and magnetism in this chapter than we were with momentum, heat, and mass transport topics, since the latter have more to do with materials processing, which we will touch upon in Chapter 7, whereas the former are more the realm of solid-state physics. This is not to say that neither the origins of the driving forces nor their resultant fluxes are unimportant to the engineer. On the contrary, these are the design parameters that must often be met. The point is that the derivations of many of these fundamental equations will be dispensed with in favor of concentration upon their application. The third topic of this chapter is related to the first two, although no fundamental equation of the driving-force form exists. It has to do with how electromagnetic radiation interacts with materials, and it is a logical extension of the description of electrical and magnetic phenomena.

The first topic will deal with *electrical conductivity*. The driving force for the flow of electrons that leads to electrical conduction is the *electric field*, \mathcal{E} , and the resulting flow of electrons is characterized by the *current density*, \mathbf{J} . The flow and driving force are related through *Ohm's Law*:

$$\mathbf{J} = \sigma \mathcal{E} \quad (6.1)$$

where \mathbf{J} is the current density in units of amps/m², \mathcal{E} is the electric field strength in units of volts/m, and σ is the *electrical conductivity* in units of ohms⁻¹/m or ($\Omega \cdot \text{m}$)⁻¹. It is indeed unfortunate that the symbol for conductivity is also the symbol we utilized for the strength of a material, but it is rare that the two are used in the same context, so that confusion should be easily avoided.

The second section will address the topic of *magnetism*. The magnetic driving force is the *magnetic field*, \mathbf{H} , and is related to a quantity known as the magnetic flux density, or *magnetic induction*, \mathbf{B} , through the magnetic analogue to Ohm's Law:

$$\mathbf{B} = \mu \mathbf{H} \quad (6.2)$$

where \mathbf{B} has units of teslas (webers/m²), and \mathbf{H} has units of amps/m. The proportionality constant, μ , is called the *magnetic permeability*. We will have much more to say about the units of permeability in Section 6.2, since there is some variability in its definition. It is once again unfortunate that the symbol for magnetic permeability is identical to that of another important engineering parameter, Newtonian viscosity, but there is little opportunity for confusion in real applications.

The third topic has to do with how materials interact with radiation that has both an electrical and a magnetic component—that is, electromagnetic radiation. This topic is often generically referred to as “optical properties” of materials, even though the full range of electromagnetic radiation, of which the optical portion is only a small segment, can be considered. There is no unifying, driving-force-containing equation to describe the optical properties of materials. However, there is one useful relationship that we will use to build most of the descriptions of Section 6.3 upon which relates the intensity of incident electromagnetic radiation, I_0 , to the transmitted, absorbed, and reflected intensities, I_T , I_A , and I_R , respectively:

$$I_0 = I_T + I_A + I_R \quad (6.3)$$

By the end of this chapter, you should be able to:

- Relate conductivity, resistivity, resistance, and conductance.
- Calculate conductivity from charge carrier concentration, charge, and mobility.
- Differentiate between a conductor, insulator, semiconductor, and superconductor.
- Differentiate between an intrinsic and an extrinsic semiconductor.
- Differentiate between a p - and n -type semiconductor.
- Identify different types of electrical polarizability, and determine if they are relevant to a given chemical structure.
- Describe how a p - n semiconductor junction works.
- Differentiate between diamagnetism, paramagnetism, ferromagnetism, ferrimagnetism, and antiferromagnetism.
- Describe the temperature dependence of magnetic susceptibility.
- Define the Curie temperature for a substance.
- Define the Néel temperature for a substance.
- Determine coercivity and remnant induction from a hysteresis loop.
- Relate transmissivity, absorptivity, and reflectivity.
- Define refractive index.
- Calculate reflectivity from refractive index differences at an interface.
- Describe the interactions of light with materials that result in color.

6.1 ELECTRICAL PROPERTIES OF MATERIALS

Without going into a complete derivation, let us examine Eq. (6.1) more closely to see where the driving force, electrical current, and electrical conductivity come from.

The electric field, \mathcal{E} , is a vector quantity, as indicated by the boldfaced type. For the time-being, we will limit the description to an electric field in one direction only and

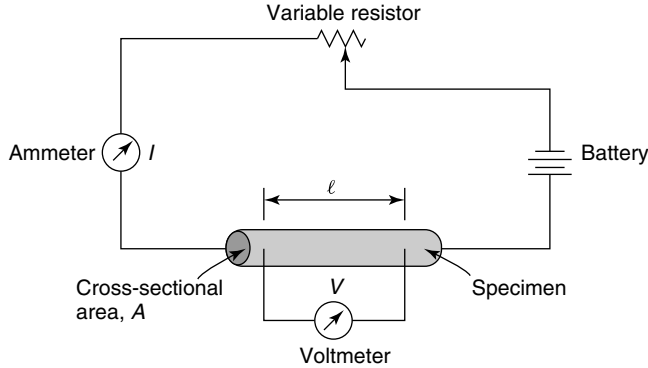


Figure 6.1 Schematic diagram of conductivity measurement in a material. Reprinted, by permission, from W. Callister, *Materials Science and Engineering: An Introduction*, 5th ed., p. 607. Copyright © 2000 by John Wiley & Sons, Inc.

will consider only the magnitude of the electric field, \mathcal{E} . An electric field is generated by applying a voltage, V , across a distance, l , as illustrated in Figure 6.1. The electric field strength is then given by

$$\mathcal{E} = V/l \quad (6.4)$$

When a conductive material is placed within the electric field, current begins to flow, as characterized by the current density, \mathbf{J} , of Eq. (6.1). The current density is also a vector quantity, but since our field is in one dimension only, current will similarly flow only in one direction, so that we will use only the scalar quantity from here on, J . The current density is simply the *current*, I , per unit area in the specimen, A :

$$J = \frac{I}{A} \quad (6.5)$$

where I is in units of ampere (amps, A, for short) and A is in units of m^2 . The current, in turn, is defined as the rate of charge passage per unit time:

$$I = \frac{dq}{dt} \quad (6.6)$$

where q is the charge in units of coulombs, so that an ampere is equal to a coulomb/s. Substitution of Eqs. (6.4) and (6.5) into Eq. (6.1) and isolation of V gives

$$V = I \left(\frac{l}{\sigma A} \right) \quad (6.7)$$

We define the quantity in parentheses as the *resistance*, R , to obtain the more familiar form of Ohm's Law:

$$V = I \times R \quad (6.8)$$

Cooperative Learning Exercise 6.1

Consider a wire, 3 mm in diameter and 2 m long. Use the data in Appendix 8 to answer the following questions.

Person 1: What is the resistance in the wire if it is made of copper?

Person 2: What is the resistance in the wire if it is made of stainless steel?

Exchange the results of your calculations, check them, and use them to make the following calculations, assuming that a potential difference of 0.05 V is placed across the ends of the wire.

Person 1: If the wire is made of stainless steel, calculate the current flow, current density, and magnitude of the electric field.

Person 2: If the wire is made of copper, calculate the current flow, current density, and magnitude of the electric field.

Answers: $R_{Cu} = 4.84 \times 10^{-3} \Omega$; $R_{SS} = 0.202 \Omega$; $I_{SS} = 0.25 \text{ A}$, $I_{Cu} = 10.3 \text{ A}$; $J_{Cu} = 1.5 \times 10^6 \text{ A/m}^2$, $J_{SS} = 0.025 \text{ A/m}^2$; $E_{Cu} = 0.025 \text{ V/m}$, $E_{SS} = 0.025 \text{ V/m}$.

The relationship between conductivity and resistance is an important one, and it can be further generalized through the introduction of two additional quantities called the *conductance*, G , and the *resistivity*, ρ . The resistivity is simply the resistance per unit length times the cross-sectional area, $\rho = RA/l$, and as such is a geometry-independent material property, as is the conductivity, σ . Similarly, the conductance is the conductivity per unit area times length, $G = \sigma l/A$. It is important to remember that the geometry of the sample must be known to calculate its resistance and/or conductance, whereas the resistivity and conductivity are inherent material properties that can vary with temperature and composition, but are generally independent of sample geometry. Moreover, it is useful to keep in mind that conductivity and resistivity are inverses of one another, and if we know one, we can find the other.

Conductivity requires a *charge carrier*. There are two types of charge carriers we will consider: electrons and ions. The structural descriptions of Chapter 1 will be helpful in determining the primary type of charge carrier within a material, if any. In subsequent sections, we explore the molecular origins of each type of conductivity, investigate the important parameters that cause conductivity to vary in materials, and describe additional electrical conduction phenomena that have revolutionized our lives.

6.1.1 Electrical Properties of Metals and Alloys

Electrical conduction in metals and alloys occurs by the motion of electrons. It can be shown that the conductivity is proportional to the number of electrons per unit volume, n_e , the charge per electron, q_e , and the *electron mobility*, μ_e :

$$\sigma = n_e q_e \mu_e \quad (6.9)$$

where the units of n_e are m^{-3} , q_e is the magnitude of charge on an electron (1.602×10^{-19} coulombs), and μ_e is in $\text{m}^2/\text{V} \cdot \text{s}$. Any of these three quantities can, and do, affect the overall conductivity of a material, leading to an astounding 27 orders of magnitude in the variation of electrical conductivity values. This immense variation

in a physical property causes us to further classify materials according to their ability to conduct electricity. Those materials for which the value of σ is low, ranging from 10^{-20} to $10^{-10}(\Omega \cdot \text{m})^{-1}$, are termed *insulators*, while those with intermediate values on the order of 10^{-6} to $10^4(\Omega \cdot \text{m})^{-1}$ are called *semiconductors*. Materials with high electrical conductivities above $10^7(\Omega \cdot \text{m})^{-1}$, such as most metals and alloys, are called *conductors*. Notice that the range of conductivities for these classes are still very large and that there are significant gaps between them for which absolute classification is difficult. In fact, a given material can cross over from one classification to another, depending on such factors as temperature. As a result, it is important to understand the origins of electrical conduction in these materials.

6.1.1.1 The Molecular Origins of Electrical Conduction. Recall from Section 1.0.4.3 that the bonds in metals tend to form bands of electrons. The electrons involved in bonding are found in the valence band, inner electrons not involved in bonding are found in the core band, and the remaining unfilled orbitals of the outer bands form the conduction band. It is the conduction band that gives metals and alloys the ability to freely conduct electrons. As shown in Figure 6.2, the “distance” between the conduction and valence bands in a solid, called the *band gap*, E_g , can be used to characterize the electrical behavior of a material. Insulators have large band gaps of several electron volts (eV), whereas conductors have small band gaps, or even overlapping valence and conduction bands, as illustrated in Figure 6.2b. Metallic solids are good electrical conductors because their valence band is not completely filled or because it may overlap with a second empty valence band, thereby causing the total energy band to be only partially filled.

According to the band theory, the motion of electrons under an external electric field is possible only for electrons in partially filled energy bands. The *probability function*,

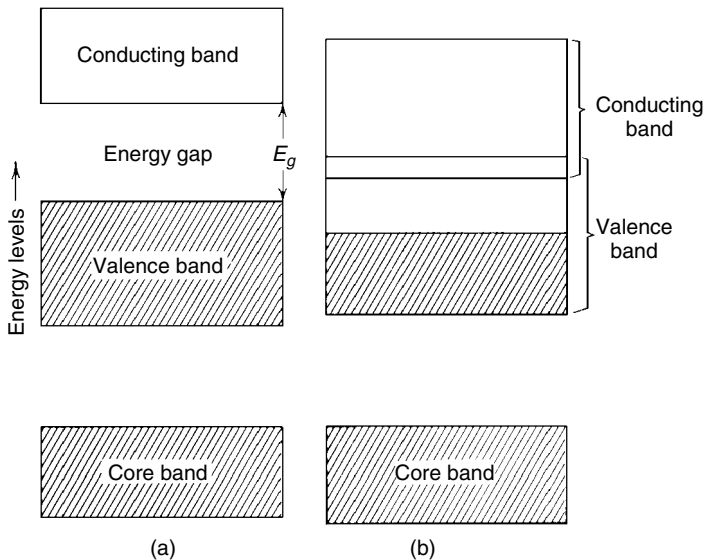


Figure 6.2 Schematic illustration of band gaps in (a) an insulator and (b) conductor. From Z. Jastrzebski, *The Nature and Properties of Engineering Materials*, 2nd ed. Copyright © 1976 by John Wiley & Sons, Inc. This material is used by permission of John Wiley & Sons, Inc.

$f(E)$, that describes the probability that an energy level E is occupied by an electron is given by Fermi as

$$f(E) = \frac{1}{\exp[(E - E_f)/k_B T] + 1} \quad (6.10)$$

where E_f is called the Fermi energy, k_B is Boltzmann's constant, and T is the absolute temperature. The Fermi energy in a metal represents the kinetic energy of the electrons having the maximum energy level that some electrons can attain. At absolute zero, the Fermi–Dirac distribution law requires that the Fermi function, $f(E)$, must have a value of 1 or 0 (see Figure 6.3a). Thus, at $T = 0$ K we have $f(E) = 1$ and $E < E_f$. At temperatures greater than 0 K, $f(E)$ changes from 1 to 0 over an energy range of about one unit of $k_B T$. At $E = E_f$ we obtain $f(E) = \frac{1}{2}$ (see Figure 6.3b). If $E - E_f \gg k_B T$, the exponential term in the denominator of Eq. (6.10) becomes very large relative to unity, and $f(E)$ becomes

$$f(E) = \exp\left[\frac{-(E - E_f)}{k_B T}\right] \quad (6.11)$$

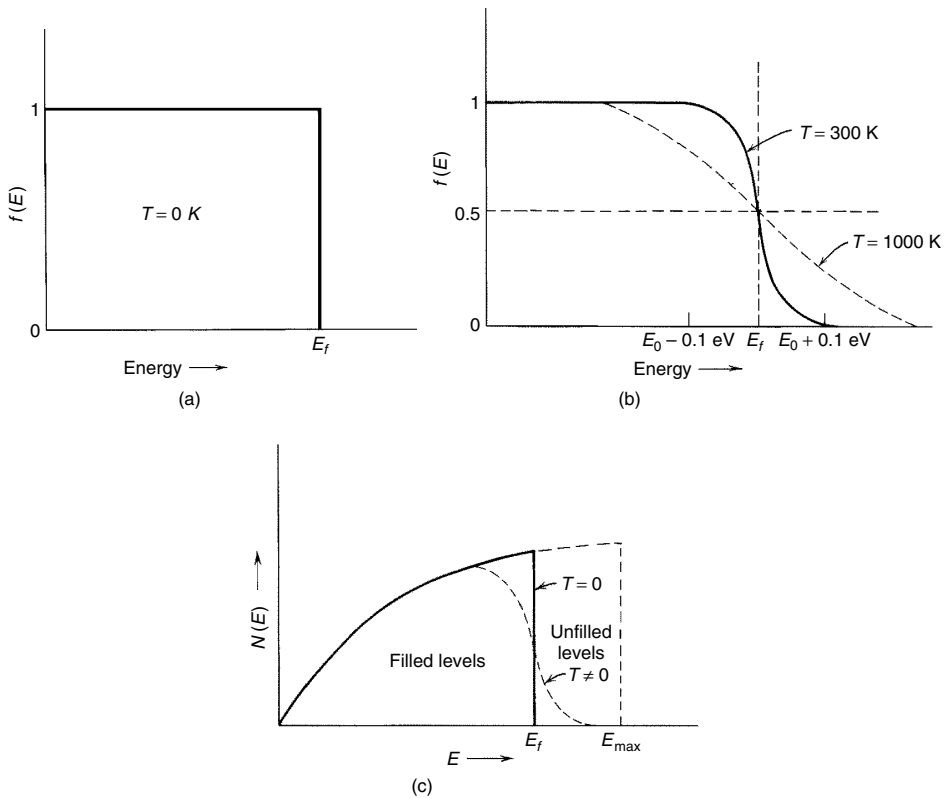


Figure 6.3 The Fermi distribution function (a) at absolute zero and (b) at a finite temperature. (c) The population density of electrons in a metal as a function of energy. From Z. Jastrzebski, *The Nature and Properties of Engineering Materials*, 2nd ed. Copyright © 1976 by John Wiley & Sons, Inc. This material is used by permission of John Wiley & Sons, Inc.

For electron energies, E , below the Fermi level, $E_f - E \gg k_B T$, and Eq. (6.11) can be approximated as

$$f(E) \approx 1 - \exp\left[-\frac{E - E_f}{k_B T}\right] \quad (6.12)$$

indicating that the probability of occupation of the energy band is nearly unity.

The state densities are not uniform across the energy band, and their *population density*, $N(E)$, is the greatest in the center of the band. The number of electrons in the band, n_e , can then be evaluated and used in Eq. (6.9) by integrating the product of the density of state $N(E)$ and the probability of their occupation, $f(E)$, over the band energy range (see Figure 6.3c). Thus, for metals,

$$n_e = \int_0^{E_f} N(E) \cdot f(E) dE \quad (6.13)$$

The energy distribution in the conduction zone extends over several electron volts and is about 5 eV for some metals at absolute zero. Thus, only a small fraction of the electrons in the energy band can be excited above the Fermi level, and only those within an energy range of the order $k_B T$ can be excited thermally.

In addition to the number of electrons, the other factor in Eq. (6.9) that affects conductivity is the electron mobility, μ_e . The mobility is the average charge carrier velocity, or *drift velocity*, \bar{v} , divided by the electric field strength, \mathcal{E} :

$$\mu_e = \bar{v} / \mathcal{E} \quad (6.14)$$

In a typical metal, $\mu_e = 5 \times 10^{-3} \text{ m}^2/\text{V} \cdot \text{s}$, which gives a drift velocity of $5 \times 10^{-3} \text{ m/s}$ for an electric field of 1 V/m. The average electron velocity, in turn, is related to an important structural parameter, the mean free path, l , which we utilized in Section 4.2.1.4 to describe thermal conductivity:

$$l = \tau \bar{v} \quad (6.15)$$

where τ is a quantity known as the *relaxation time* and has units of sec^{-1} . The relaxation time is closely related to the mean time of flight between electron collisions and also to the mean free path of the conduction electrons, as indicated above.

As the mobilities are likely to depend on temperature only as a simple power law over an appropriate region, the temperature dependence on conductivity will be dominated by the exponential dependence of the carrier concentration. We will have more to say about carrier mobility in the section on semiconductors.

In summary, metals are good electrical conductors because thermal energy is sufficient to promote electrons above the Fermi level to otherwise unoccupied energy levels. At these levels ($E > E_f$), the accessibility of unoccupied levels in adjacent atoms yields high mobility of conduction electrons known as *free electrons* through the solid.

6.1.1.2 Resistivity in Metals and Alloys. Resistivity is the reciprocal of conductivity. We will find it useful to momentarily concentrate on resistivity instead of conductivity to explain some important electrical phenomena. If the metal crystal lattice were perfect and there were no lattice vibrations, the electrons would pass through

the lattice unscattered, encountering no resistance. But, as we saw in the description of thermal conductivity (cf. Section 4.2.2.1), lattice vibrations and phonon scattering play a role in disrupting the mean free path of electrons. Working backwards through the previous equations, then, shows that a reduction in mean free path, l [Eq. (6.15)], due to phonon scattering and lattice vibrations decreases the electron mobility [Eq. (6.14)], which in turn can reduced electrical conductivity [Eq. (6.9)] or increase resistivity. This effect leads to the temperature-dependent portion of resistivity, ρ_t . Since the thermal lattice vibrations increase directly with increasing temperature, the electrical resistivity of metals will increase with temperature in a linear manner. At high temperatures approaching the melting point, the resistivity usually rises somewhat more rapidly than linearly with temperature. Only at very low temperatures can lattice defects and impurity atoms affect conductivity and resistivity, rather than thermal lattice vibrations. This type of resistivity is known as the *residual resistivity*, ρ_r , and is relatively temperature-independent. The two types of resistivity are additive, such that the total resistivity is given by

$$\rho = \rho_t + \rho_r \quad (6.16)$$

This relationship is shown in Figure 6.4 for a series of copper alloys. The variation of resistivity with temperature is approximately linear over a wide temperature range, and near absolute zero the alloys have a relatively temperature-independent residual resistivity. Notice that as the level of nickel impurities increases, so do both the residual

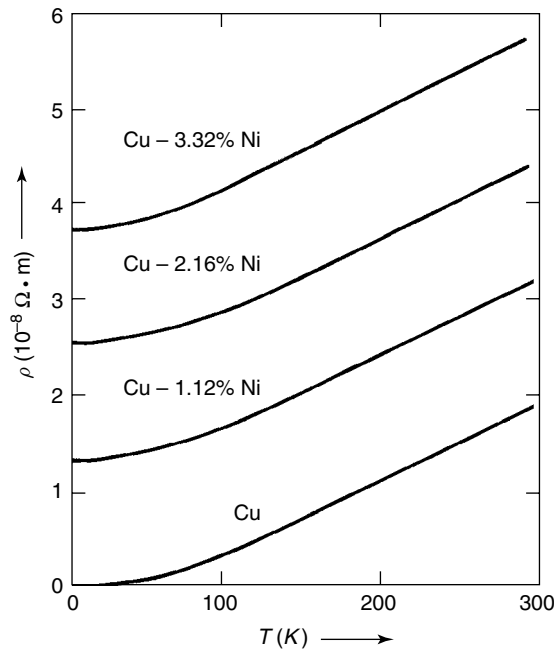


Figure 6.4 Variation of resistivity with temperature for several copper alloys. From K. M. Ralls, T. H. Courtney, and J. Wulff, *Introduction to Materials Science and Engineering*. Copyright © 1976 by John Wiley & Sons, Inc. This material is used by permission John Wiley & Sons, Inc.

and thermal vibration resistivities. This is directly related to a reduction in the electron mean free path.

Oftentimes the variation of resistivity with temperature in the linear region is approximated with an empirical expression of the form

$$\rho_t = \rho_0 + aT \quad (6.17)$$

where ρ_0 and a are experimentally determined constants for a particular metal. Do not confuse the empirical parameter ρ_0 with the residual resistivity, ρ_r - the former is an equation-fitting parameter only for the linear region of the resistivity-temperature plot, whereas the latter is a fundamental property of a material. The resistivities of some metals and alloys are presented in Appendix 8.

The variation of resistivity with composition is also expressed in an empirical fashion. For two-phase alloys consisting of phases α and β , the rule of mixtures can be used to approximate the alloy resistivity from the individual metal resistivities:

$$\rho = V_\alpha \rho_\alpha + (1 - V_\alpha) \rho_\beta \quad (6.18)$$

where V_α is the volume fraction of phase α .

Other factors such as cold deformation and processing conditions can affect resistivity. The cold deformation effect is not as pronounced as the addition of impurity or alloying elements, but the effect of processing on resistivity can be large, as illustrated in Figure 6.5 for a Cu_3Au compound. The effect on resistivity is again related to structure. The rapidly quenched compound maintains its disordered structure, which

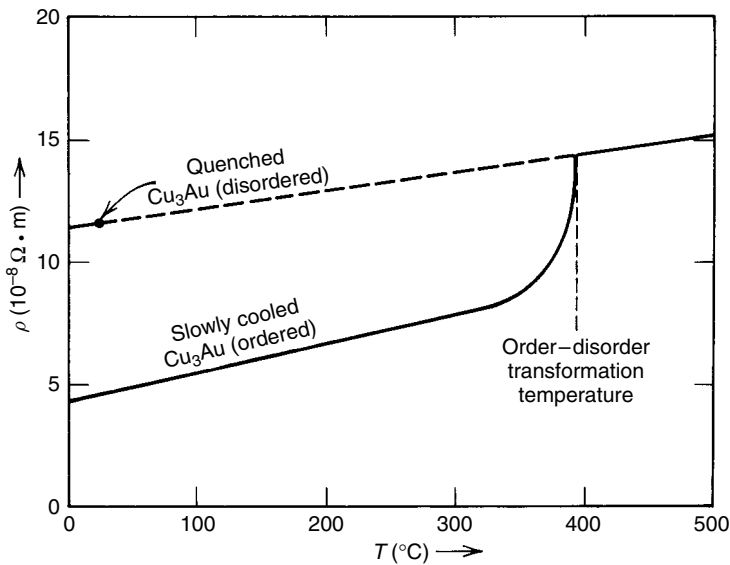


Figure 6.5 Temperature variation of the resistivity for Cu_3Au under two different processing conditions. From K. M. Ralls, T. H. Courtney, and J. Wulff, *Introduction to Materials Science and Engineering*. Copyright © 1976 by John Wiley & Sons, Inc. This material is used by permission John Wiley & Sons, Inc.

causes an increase in the resistivity relative to the slowly cooled, ordered structure. In the ordered structure, gold atoms occupy the corner positions and copper atoms occupy the face-centered positions of the FCC unit cell, which results in less electron scattering than the disordered structure in which copper and gold atoms occupy FCC atomic sites at random within each unit cell. Only at the order–disorder transition temperature do the two resistivity curves become coincident, corresponding to a transformation from the ordered to the disordered FCC structure as a result of increased thermal motion.

For metals in general, any mechanical or chemical action that alters the crystalline perfection will raise the residual resistivity and, therefore, the total resistivity, according to Eq. (6.16). Thus, vacancies in metals, in contrast to those in ionic solids, increase the resistivity. The reason for this lies in the inherent differences between conduction mechanisms in these two classes of materials. The differences between ionic and electronic conduction will be elaborated upon in Section 6.1.2.

6.1.1.3 Superconduction. You may have noticed in Figure 6.3 that the resistivity of pure copper approaches zero at absolute zero temperature; that is, the residual resistivity is zero. An expanded scale shows that this is not really the case. Figure 6.6 shows that the residual resistivity in pure copper is about $10^{-10} \, \Omega \cdot \text{m}$. This is the “normal” behavior of many metals. Some metals, however, such as Pb, lose all resistivity abruptly and completely at some low temperature. This phenomenon is called *superconductivity*, and the materials that exhibit it are called *superconductors*. The temperature at which the resistivity vanishes is called the *critical transition temperature*, T_c . For example, lead has a $T_c = 7.19 \, \text{K}$, and it has a resistivity that is less than $10^{-25} \, \Omega \cdot \text{m}$ at 4.2 K. Many elemental metals (see Figure 6.7), solid–solution alloys, and intermetallic compounds exhibit superconductivity. Often, such materials have relatively high electrical resistivities above T_c , compared to other nonsuperconducting metals such as Ag and Cu. Observed T_c values range from a few millidegrees Kelvin to over 21 K for intermetallic compounds such as Nb_3Ge .

In 1957 the research team of Bardeen, Cooper, and Schrieffer produced a theory, now known as the *BCS theory*, that managed to explain all the major properties of

HISTORICAL HIGHLIGHT

The discovery of superconductivity was not very dramatic. When Dutch physicist Heike Kamerlingh Onnes succeeded in liquefying helium in 1908 he looked around for something worth measuring at that temperature range. His choice fell upon the resistivity of metals. He tried platinum first and found that its resistivity continued to decline at lower temperatures, tending to some small but finite value as the temperature approached absolute zero. He could have tried a large number of other metals with similar prosaic results. But he was in luck. His second metal, mercury, showed quite unorthodox behavior, and in 1911 he showed that its resistivity suddenly

decreased to such a small value that he was unable to measure it—and no one has succeeded in measuring it ever since.

In the subsequent years, many more superconductors were found at these very low temperatures. By the 1960s, certain alloys of niobium were made that became superconductors at 10–23 K. It was generally believed on theoretical grounds that there would be no superconductors above 30 K. See Section 6.1.2.4 to see if this belief is still held today.

Source: Adapted from Solymar and Walsh [1] and Sheahan [2].

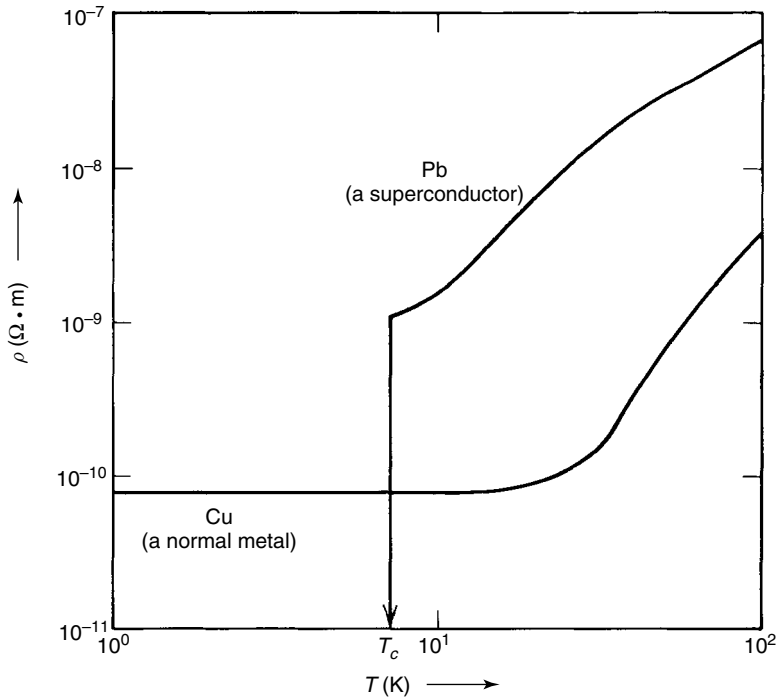


Figure 6.6 Variation of resistance at low temperatures for a nonsuperconductor and a superconductor. From K. M. Ralls, T. H. Courtney, and J. Wulff, *Introduction to Materials Science and Engineering*. Copyright © 1976 by John Wiley & Sons, Inc. This material is used by permission John Wiley & Sons, Inc.

[illegible]

Figure 6.7 The superconducting elements. Reprinted, by permission, from I. Amato, *Stuff*, p. 68. Copyright © 1997 by Ivan Amato.

superconductivity. The essence of the theory is that superconductivity is caused by electron–lattice interaction and that the superconducting electrons consist of paired ordinary electrons called a *Cooper pair*. We give here a qualitative description of how Cooper pairs form and how they lead to superconductivity.

Figure 6.8a shows the energy–momentum curve of an ordinary conductor with seven electrons in their discrete energy levels. In the absence of an electric field, the current from electrons moving to the right is exactly balanced by the electrons moving to the left, and the net current is zero. When an electric field is applied, all the electrons acquire some extra momentum, and this is equivalent to shifting the whole distribution in the direction of the electric field, as shown in Figure 6.8b. When the electric field is once again removed, the faster electrons will be scattered into lower energy states due to collisions with the vibrating lattice or impurity atoms, and the original distribution in Figure 6.8a is reestablished. For the model of Figure 6.8b, it means that the electron is scattered from energy level *a* to energy level *b* in order to reestablish the original distribution.

In the case of a superconductor, it becomes energetically more favorable for the electrons to pair up. Those of opposite momenta pair up to form a new particle called a superconducting electron or Cooper pair. This link between two electrons is shown in Figure 6.9a by an imaginary spring. The velocity of the entire center of mass is zero. According to the *de Broglie relationship* ($\lambda = h/p$, where λ is the wavelength, h is Planck's constant, and p is the momentum), this means that the wavelength associated with the new particle, λ , is infinitely long. This is valid for all the Cooper pairs. So, there is a large number of identical particles all with infinite wavelength—that is, a quantum phenomenon on a macroscopic scale. An applied electric field will displace all the particles again as shown in Figure 6.9b, but this time, when the electric field disappears, there is no return to the previous state. Scattering from energy level *a* to energy level *b* is no longer possible because then the electrons at both *b* and *c* would become pairless, which is energetically unfavorable. So, the asymmetrical distribution remains and there will be more electrons going to the right than to the left, and the current persists, in theory, forever. As the temperature rises, thermal energy eventually overcomes the pairing interaction, and the superconductivity effect vanishes.

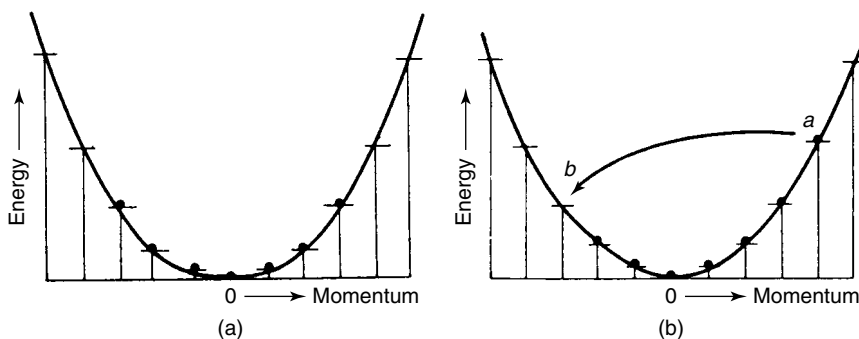


Figure 6.8 One dimensional schematic representation of the energy momentum curve for seven electrons in a conductor with (a) no applied electric field and (b) an applied electric field. Reprinted, by permission, from L. Solymar, and D. Walsh, *Lectures on the Electrical Properties of Materials*, 5th ed., p. 427. Copyright © 1993 by Oxford University Press.

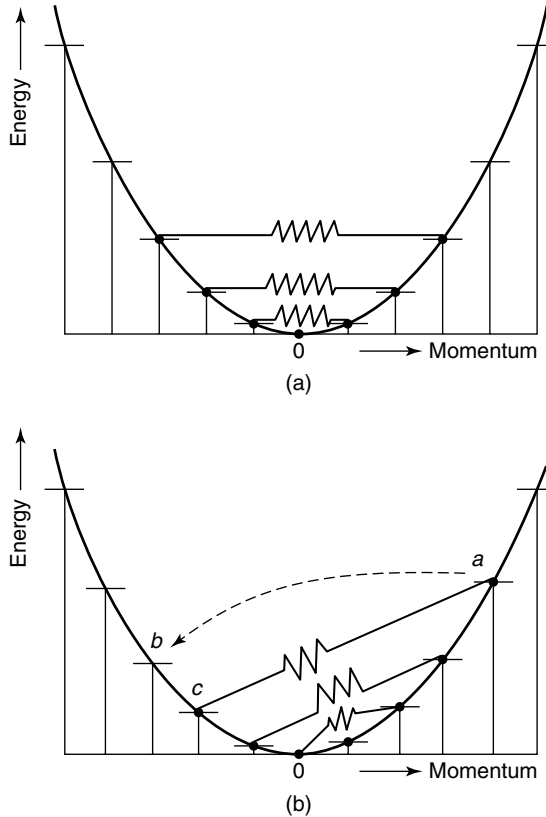


Figure 6.9 The energy–momentum curve for seven electrons in a superconductor with (a) no applied electric field and (b) an applied electric field. Reprinted, by permission, from L. Solymar and D. Walsh, *Lectures on the Electrical Properties of Materials*, 5th ed., p. 428. Copyright © 1993 by Oxford University Press.

One technologically significant application for superconductivity is in the use of electromagnets. It would be beneficial to have high magnetic fields without any power dissipation. Early experimenters, however, found that above certain magnetic fields, the superconductor became normal, regardless of the temperature. Thus, in order to have zero resistance, a superconductor must be held not only below the critical transition temperature, T_c , but also below a *critical magnetic field*, H_c . The interrelation between H_c and T_c is well described by the formula

$$H_c = H_0 \left[1 - \left(\frac{T}{T_c} \right)^2 \right] \quad (6.19)$$

where H_0 is the critical magnetic field at absolute zero. This relationship is graphically illustrated in Figure 6.10, where the material is a “normal” conductor above the curve and a superconductor below the curve. The values of H_0 and T_c for a number of elemental superconductors are given in Table 6.1. We will have more to say about superconductors in Section 6.1.2.4.

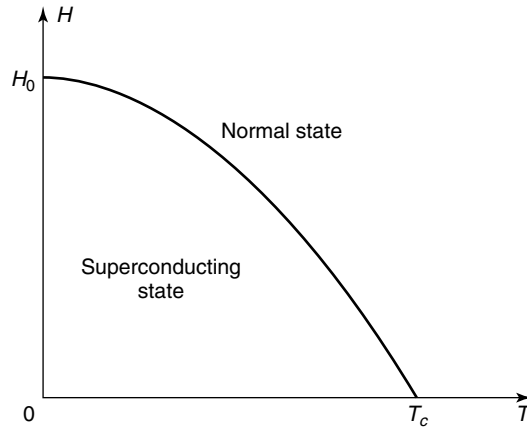


Figure 6.10 Temperature dependence of critical magnetic field for a superconductor. Reprinted, by permission, from L. Solymar and D. Walsh, *Lectures on the Electrical Properties of Materials*, 5th ed., p. 429. Copyright © 1993 by Oxford University Press.

Table 6.1 Critical Temperature and Critical Magnetic Field of a Number of Superconducting Elements

Element	T_c (K)	$H_0 \times 10^{-4}$ (A/m)	Element	T_c (K)	$H_0 \times 10^{-4}$ (A/m)
Al	1.19	0.8	Pb	7.18	6.5
Ga	1.09	0.4	Sn	3.72	2.5
Hg α	4.15	3.3	Ta	4.48	6.7
Hg β	3.95	2.7	Th	1.37	1.3
In	3.41	2.3	V	5.30	10.5
Nb	9.46	15.6	Zn	0.92	0.4

Source: L. Solymar, and D. Walsh, *Lectures on the Electrical Properties of Materials*, 5th ed. Copyright © 1993 by Oxford University Press.

6.1.1.4 Intrinsic Semiconduction. We return now to our description of band gaps from Section 6.1.1.1 in order to elaborate upon those materials with conductivities in the range 10^{-6} to $10^4(\Omega \cdot \text{m})^{-1}$. At first, it may not seem important to study materials that neither readily conduct electricity nor protect against it, as do insulators. However, the development of semiconducting materials has, and continues to, revolutionize our lives.

Recall from Figure 6.2 that the gap between the valence and conduction bands called the band gap, E_g , can be used to classify materials as conductors, insulators, or semiconductors; also recall that for semiconductors the value of E_g is typically on the order of 1–2 eV. The magnitude of the band gap is characteristic of the lattice alone and varies widely for different crystals. In semiconductors, the valence and conduction bands do not overlap as in metals, but there are enough electrons in the valence band that can be “promoted” to the conduction band at a certain temperature to allow for limited electrical conduction. For example, in silicon, the energies of the valence electrons that bind the crystal together lie in the valence band. All four

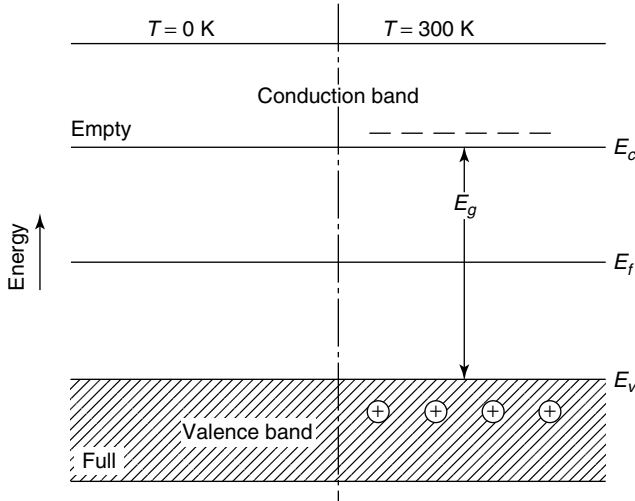


Figure 6.11 Energy bands of an intrinsic semiconductor: E_f is the Fermi energy level; E_c is the lower edge of the conduction band; E_v is the upper edge of the valence band; and E_g is the band gap. From Z. Jastrzebski, *The Nature and Properties of Engineering Materials*, 2nd ed. Copyright © 1976 by John Wiley & Sons, Inc. This material is used by permission of John Wiley & Sons, Inc.

valence electrons for each atom are tied in place, forming covalent bonds. There are no electrons in the conduction band at absolute zero, and the material is effectively an insulator (see Figure 6.11). At an elevated temperature, enough electrons have been thermally promoted to the conduction band to permit limited conduction. Promotion of electrons leaves behind positively charged “holes” in the valence band which maintain charge neutrality. The term *hole* denotes a mobile vacancy in the electronic valence structure of a semiconductor that is produced by removing one electron from a valence band. Holes, in almost all respects, can be regarded as moving positive charges through the crystal with a charge magnitude and mass the same as that of an electron.

Conduction that arises from thermally or optically excited electrons is called *intrinsic semiconduction*. The conduction of intrinsic semiconductors usually takes place at elevated temperatures, since sufficient thermal agitation is necessary to transfer a reasonable number of electrons from the valence band to the conduction band. The elements that are capable of intrinsic semiconduction are relatively limited and are shown in Figure 6.12. The most important of these are silicon and germanium.

In intrinsic semiconductors, the number of holes equals the number of mobile electrons. The resulting electrical conductivity is the sum of the conductivities of the valence band and conduction band charge carriers, which are holes and electrons, respectively. In this case, the conductivity can be expressed by modifying Eq. (6.9) to account for both charge carriers:

$$\sigma = n_e q_e \mu_e + n_h q_h \mu_h \quad (6.20)$$

where n_h , q_h , and μ_h are now the number, charge, and mobility of the holes, respectively, and contribute to the overall conductivity in addition to the corresponding

and

$$N_v = 2 \left(\frac{2\pi m_h^* k_B T}{h^2} \right)^{3/2} \quad (6.23)$$

where m_e^* and m_h^* are the effective mass of electrons and holes, respectively, k_B is Boltzmann's constant, T is absolute temperature, and h is Planck's constant. If we multiply these densities of state by the distribution of Eq. (6.11), in which we replace the energy, E , with the respective energy of the conduction and valence bands (E_v is lower in energy than the Fermi energy, E_f , and E_c is higher), we can obtain the number of mobile charge carriers in each band:

$$n_e = N_c \exp \left[\frac{-(E_c - E_f)}{k_B T} \right] \quad (6.24)$$

and

$$n_h = N_v \exp \left[\frac{-(E_f - E_v)}{k_B T} \right] \quad (6.25)$$

The product of the mobile positive and negative charge carriers is then obtained by multiplication of Eqs. (6.24) and (6.25), and recalling that $n_e = n_h$ we obtain

$$n_h \cdot n_e = n_e^2 = N_c N_v \exp \left[\frac{-(E_c - E_v)}{k_B T} \right] \quad (6.26)$$

and since $E_c - E_v = E_g$, the band gap energy is

$$n_e = (N_v N_c)^{1/2} \exp \left[\frac{-E_g}{2k_B T} \right] \quad (6.27)$$

Equation (6.27) illustrates that the product of charge carriers, $n_e n_h$, is independent of the position of the Fermi level and depends on the energy gap. It is a further result of this relationship that

$$E_f = \frac{E_c + E_v}{2} \quad (6.28)$$

Thus, the Fermi level is halfway between the conduction and valence bands.

The term $(N_v N_c)^{1/2}$ in Eq. (6.27) depends on the band structure of the semiconductor and is usually a constant for a specific material, outside of its temperature dependence. Thus, we can remove the temperature dependence of N_v and N_c from Eqs. (6.22) and (6.23) and simplify Eq. (6.27) to

$$n_e = C T^{3/2} \exp \left[\frac{-E_g}{2k_B T} \right] \quad (6.29)$$

where C is a constant. Substitution of Eq. (6.29) into Eq. (6.21) gives

$$\sigma = C T^{3/2} q_e (\mu_e + \mu_h) \exp \left[\frac{-E_g}{2k_B T} \right] \quad (6.30)$$

Neglecting the variation of the $T^{3/2}$ term, which is negligible compared to the variation with temperature in the exponential term, and recalling that the mobilities are less sensitive to temperature than are the charge carrier densities, Eq. (6.30) can be rewritten as

$$\sigma = \sigma_0 \exp\left(\frac{-E_g}{2k_B T}\right) \quad (6.31)$$

where σ_0 is the overall constant.

Equation (6.31) indicates that the conductivity of intrinsic semiconductors drops nearly exponentially with increasing temperature. At still higher temperatures, the concentration of thermally excited electrons in the conduction band may become so high that the semiconductor behaves more like a metal.

6.1.1.5 Extrinsic Semiconduction. The charge carrier density can also be increased through impurities of either higher or lower valence. For example, if pentavalent substitutional atoms such as P, As, or Sb are placed into a covalently bonded tetravalent material such as Si or Ge, in a process known as *doping*, only four of their five valence electrons are required to participate in covalent bonding. Since the fifth electron remains weakly bound to the impurity or *donor* atom, it is not entirely free in the crystal. Nevertheless, the binding energy, which is of the order 0.01 eV, is much less than that of a covalently bonded electron. This “extra” electron can be easily detached from the impurity or donor atom. The energy state of this electron is indicated by E_d , since it is the donor level, and the energy required to excite it to the conduction band can be represented by the band model shown in Figure 6.13. Notice that the energy gap between the donor and conducting bands is much smaller than that between the valence and conduction bands, or the normal band gap, E_g . Thermal agitation, even at room temperature, is sufficient to transfer this electron to the conduction band, leaving behind a positively charged hole in the donor

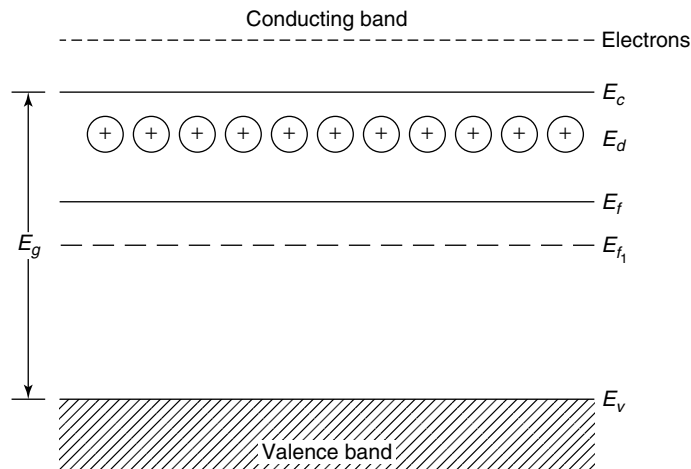


Figure 6.13 Schematic illustration of energy bands in an *n*-type, extrinsic semiconductor. From Z. Jastrzebski, *The Nature and Properties of Engineering Materials*, 2nd ed. Copyright © 1976 by John Wiley & Sons, Inc. This material is used by permission of John Wiley & Sons, Inc.

band. The conductivity in this case is due to motion of electrons in the conduction band, and this type of material is called an *n-type semiconductor*. This is one type of *extrinsic semiconductor*, or *impurity semiconductor*, in which an insulating or intrinsic semiconducting material is made to increase its semiconduction capabilities through the addition of impurity atoms. Notice also, in Figure 6.13, that the Fermi level of the *n*-type extrinsic semiconductor, E_f , is higher than that of the undoped, intrinsic semiconductor, E_{f1} .

From a conductivity standpoint, the other possibility in the addition of impurity atoms is to substitute with an impurity of lower valence, such as a trivalent element in a tetravalent lattice. Examples would be the addition of boron, aluminum, gallium, indium, and thallium to silicon or germanium. In this case, a *p-type*, extrinsic semiconductor is created. Since the substitutional atoms are deficient in bonding electrons, one of their bonding orbitals will contain a hole that is capable of “accepting” an electron from elsewhere in the crystal. As shown in Figure 6.14, the binding energy is small, and the promotion of an electron from the valence band to the acceptor band, E_a , leaves a hole in the valence band that can act as a charge carrier. In summary, then, for an *n*-type semiconductor, electrons in the conduction band are charge carriers and holes participate in bonding, whereas for a *p*-type semiconductor, the electrons participate in bonding, and the holes are the charge carriers.

In both types of extrinsic semiconductors, the doping elements are chosen so that both acceptor and donor levels are located closer to the corresponding energy bands and only a small energy gap is involved when exciting electrons. Intrinsic semiconductors are prepared routinely with initial total impurity contents less than one part per million (ppm), along with unwanted donor or acceptor atoms at less than one part in 10^7 . To such highly purified materials, controlled amounts of substitutional donor or acceptor impurities are intentionally added on the order of 1–1000 ppm to produce extrinsic semiconductors having specific room temperature conductivities.

Unlike intrinsic semiconductors, in which the conductivity is dominated by the exponential temperature and band-gap expression of Eq. (6.31), the conductivity of extrinsic semiconductors is governed by competing forces: charge carrier density and charge carrier mobility. At low temperatures, the number of charge carriers initially

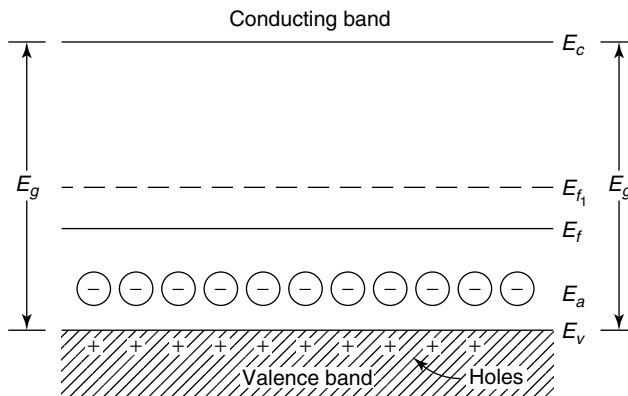


Figure 6.14 Schematic illustration of energy bands in a *p*-type, extrinsic semiconductor. From Z. Jastrzebski; *The Nature and Properties of Engineering Materials*, 2nd ed. Copyright © 1976 by John Wiley & Sons, Inc. This material is used by permission of John Wiley & Sons, Inc.

Cooperative Learning Exercise 6.2

The following electrical conductivity characteristics for both the intrinsic and extrinsic forms of a semiconductor have been determined at room temperature. Recall that $q_e = q_h = 1.602 \times 10^{-19}$ coulombs.

	$\sigma (\Omega \cdot \text{m})^{-1}$	$n_e (\text{m}^{-3})$	$n_h (\text{m}^{-3})$
Intrinsic	2.5×10^{-6}	3.0×10^{13}	3.0×10^{13}
Extrinsic	3.6×10^{-5}	4.5×10^{14}	2.0×10^{12}

Person 1: Use the data to write a relationship for the intrinsic conductivity of this substance as a function of the electron and hole mobilities.

Person 2: Use the data to write a relationship for the extrinsic conductivity of this substance as a function of the electron and hole mobilities.

Assuming that the mobilities are the same in both the intrinsic and extrinsic states, combine your information to solve for the electron and hole mobilities of this substance. Can you tell whether the substance is an n -type or p -type extrinsic semiconductor by looking at the data?

Answers: Equation (6.20) can be used for both; $0.52 = \mu_e + \mu_h$; $112.4 = 225\mu_e + \mu_h$. Solve simultaneously to get $\mu_e = 0.50 \text{ m}^2/\text{V}\cdot\text{s}$; $\mu_h = 0.02 \text{ m}^2/\text{V}\cdot\text{s}$. This is an n -type semiconductor, since $n_e \gg n_h$.

increases with temperature, as shown in Figure 6.15 for an n -type semiconductor, because thermal activation promotes donor electrons to the conduction band. At intermediate temperatures, most of the donor electrons have been promoted and the number of charge carriers is nearly independent of temperature in what is known as the *exhaustion range*. At higher temperatures, the number of valence (bonding) electrons excited to the conduction band greatly exceeds the total number of electrons from substitutional donor atoms, and the extrinsic semiconductor behaves like an intrinsic semiconductor (dashed line in Figure 6.15).

On the basis of charge carrier density (conduction electrons) alone, then, the conductivity of an extrinsic semiconductor should vary with temperature as shown in Figure 6.16. However, charge carrier mobility has a temperature-dependent effect. As mentioned in the previous section, the temperature dependence of carrier mobility has little effect on intrinsic conductivity. However, when extrinsic conductivity predominates and donor levels are close the conduction band, the carrier mobility can determine the temperature dependence of conductivity. This occurs in the exhaustion range where mobility typically decreases with increasing temperature because of increased phonon scattering. Thus, in this region, characterized by an approximately constant number of charge carriers and a decreasing carrier mobility with temperature, the temperature dependence of conductivity of an extrinsic semiconductor is similar to that of a pure metal (cf. resistivity plot for pure copper in Figure 6.4). In summary, at low temperature the conductivity varies with temperature as the charge carrier concentration, at higher temperatures the charge carrier mobility dominates and the conductivity decreases with

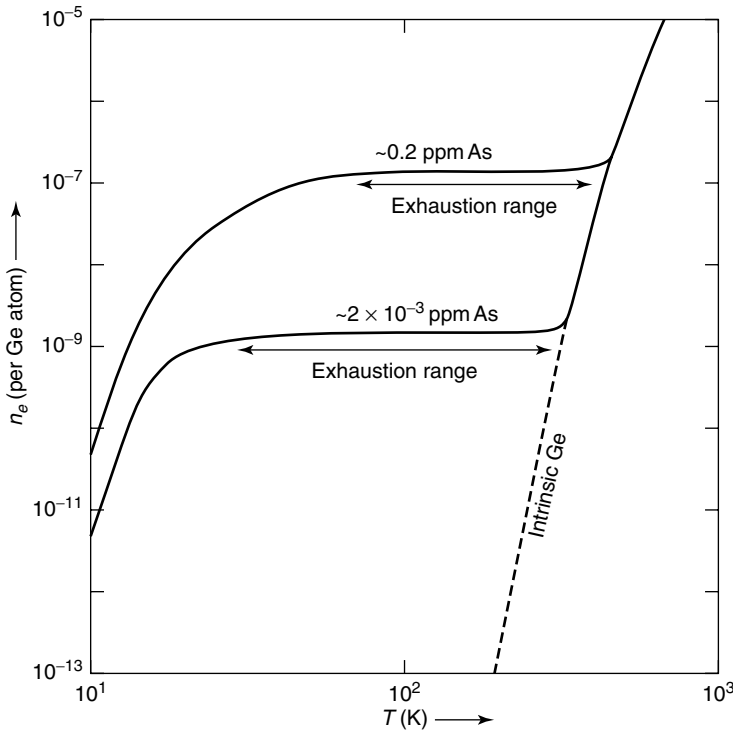


Figure 6.15 Temperature dependence of charge carrier concentration of n -type extrinsic germanium with two different As impurity levels. From K. M. Ralls, T. H. Courtney, and J. Wulff, *Introduction to Materials Science and Engineering*. Copyright © 1976 by John Wiley & Sons, Inc. This material is used by permission John Wiley & Sons, Inc.

temperature, and at still higher temperatures the extrinsic semiconductor behaves as an intrinsic semiconductor. This behavior is summarized in Figure 6.16.

6.1.1.6 Semiconductor Junctions and Devices*. Semiconductor crystals can be made in such a way that an n -type region can be made adjacent to a p -type region. This is normally accomplished by selective doping during the growth of a single crystal. The boundary between such regions within a single crystal is called the *pn junction*, and it has important applications to the development of transistors, rectifiers, and solar energy cells. Let us examine some of these devices.

The *rectifier*, or *diode*, is an electronic device that allows current to flow in only one direction. There is low resistance to current flow in one direction, called the *forward bias*, and a high resistance to current flow in the opposite direction, known as the *reverse bias*. The operation of a pn rectifying junction is shown in Figure 6.17. If initially there is no electric field across the junction, no net current flows across the junction under thermal equilibrium conditions (Figure 6.17a). Holes are the dominant carriers on the p -side, and electrons predominate on the n -side. This is a dynamic equilibrium: Holes and conduction electrons are being formed due to thermal agitation. When a hole and an electron meet at the interface, they recombine with the simultaneous emission of radiation photons. This causes a small flow of holes from the p -region

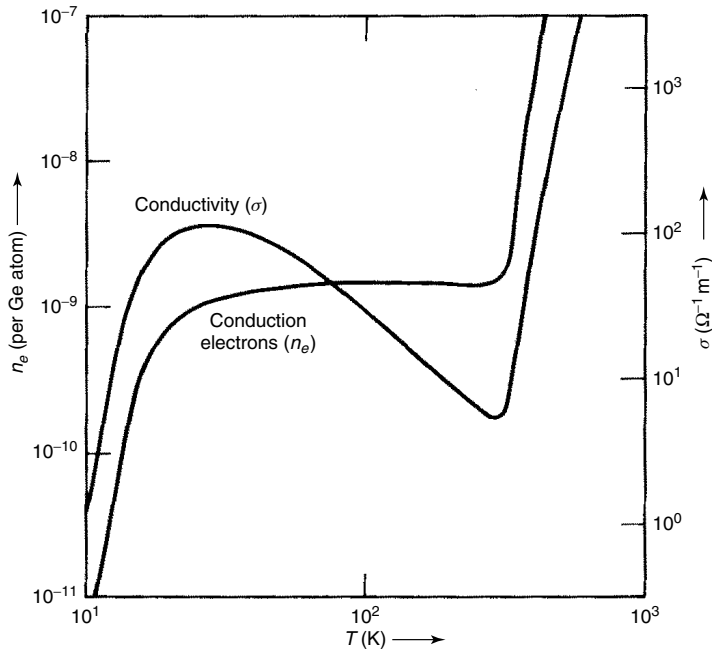


Figure 6.16 Temperature dependence of charge carrier density and conductivity of extrinsic semiconductor Ge doped with 2 ppb As. From K. M. Ralls, T. H. Courtney, and J. Wulff, *Introduction to Materials Science and Engineering*. Copyright © 1976 by John Wiley & Sons, Inc. This material is used by permission John Wiley & Sons, Inc.

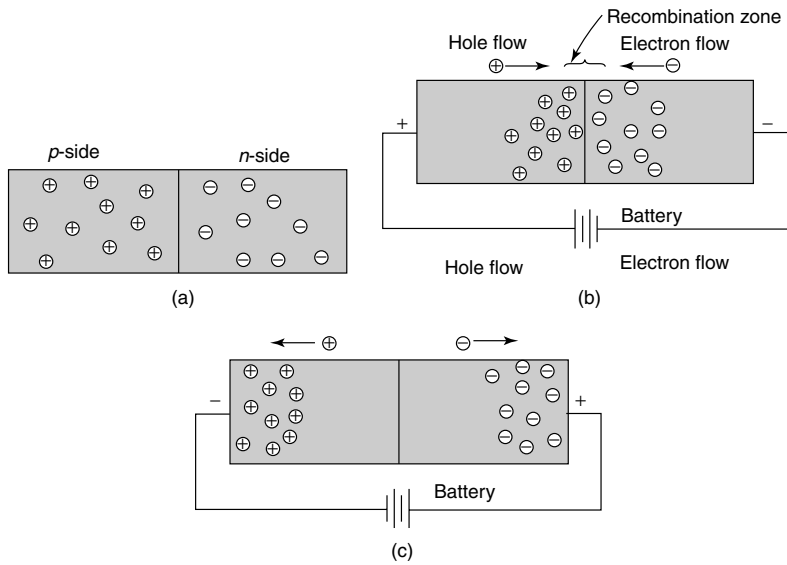


Figure 6.17 Schematic illustration of electron and hole distribution for a *pn*-rectifying junction for (a) no applied electrical potential, (b) forward bias, and (c) reverse bias. Reprinted, by permission, from W. Callister, *Materials Science and Engineering: An Introduction*, 5th ed., p. 631. Copyright © 2000 by John Wiley & Sons, Inc.

to the n -region and a flow of electrons from the n -region to the p -region. New holes and electrons continue to form to balance this flow, and an equilibrium is established with no external current flowing through the system.

If the n -region is connected to the negative terminal and the p -region to the positive terminal of a battery (Figure 6.17b), holes will move from left to right while electrons will move from right to left. These meet each other and recombine as before in the *recombination zone*. This produces an abundant number of current carriers flowing across the junction; hence the resistance in the forward direction is low. Only a small voltage is necessary to maintain a large current flow.

For reverse bias (Figure 6.17c), holes are attracted to the negative terminal, and electrons are attracted to the positive terminal. Thus, electrons and holes move away from each other and the junction region will be relatively free from charge carriers, in which case it is called the *barrier region*. Recombination will not occur to any appreciable extent, so that the junction is now highly insulative. There may be, however, a small flow of current as the result of the thermal generation of holes and electrons in the semiconductor, termed *leakage current*. The current–voltage behavior of the pn junction under both forward and reverse biases is shown in Figure 6.18. If the voltage is allowed to vary sinusoidally (Figure 6.19a), as in an alternating current, the current also varies, but the maximum current for the reverse bias, I_R , is extremely small compared to that for the forward bias, I_F .

The pn junction can be fabricated so that the leakage current in the reverse bias is extremely small, and potentials of up to several hundred volts can be applied before *breakdown* will occur. Breakdown occurs at high reverse voltages (over several hundred volts), when large numbers of charge carriers are generated, giving rise to an abrupt increase in current. Atoms may actually be ionized during breakdown due to the acceleration of electrons and holes in a phenomenon known as the *avalanche effect*. Some devices, called *Zener diodes*, are designed to utilize breakdown behavior

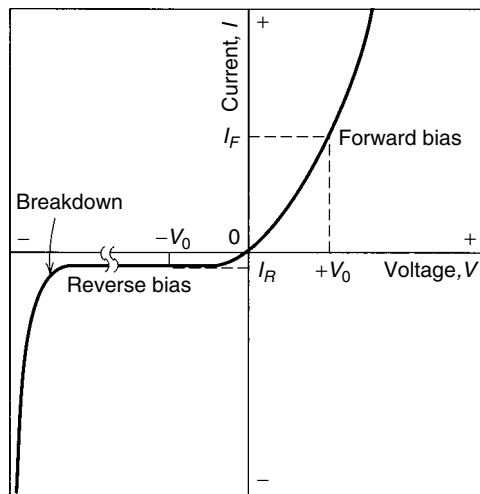


Figure 6.18 The current–voltage characteristics of a pn -junction. for forward and reverse biases. Reprinted, by permission, from W. Callister, *Materials Science and Engineering: An Introduction*, 5th ed., p. 632. Copyright © 2000 by John Wiley & Sons, Inc.

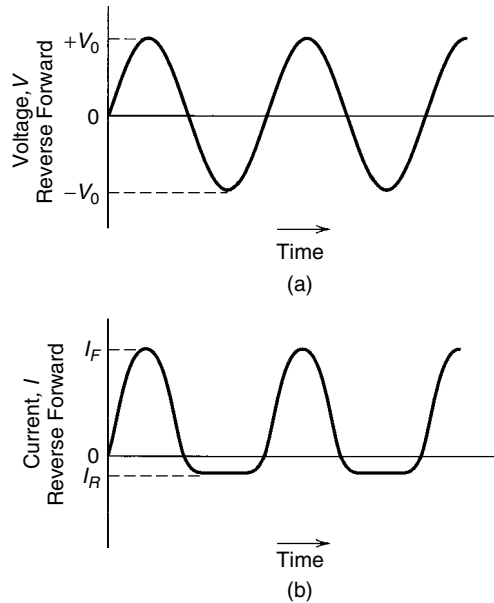


Figure 6.19 (a) Voltage–time and (b) current–time for a pn -rectifying junction. Reprinted, by permission, from W. Callister, *Materials Science and Engineering: An Introduction*, 5th ed., p. 632. Copyright © 2000 by John Wiley & Sons, Inc.

as voltage regulators. The voltage breakdown can be varied by controlling the dopant level; generally, the higher the impurity concentration, the lower the breakdown voltage. In silicon semiconductors, for example, the breakdown voltage can be varied from about 10 V to about 1000 V by regulating the impurity concentration.

Another type of semiconductor junction device is a transistor, which is capable of two primary types of functions. The first is to amplify an electrical signal. The second is to serve as a switching device for the processing and storage of information. We will briefly describe the *junction transistor* here, and we will defer the description of another type of transistor called a *MOSFET* to Section 6.1.2.6.

The junction transistor is composed of two pn junctions arranged back to back in either the p - n - p or n - p - n configurations. The latter configuration is shown in Figure 6.20. It is composed of a thin n -type *base* region, sandwiched between a p -type *emitter* and a p -type *collector*. The first pn junction is forward-biased, and the second np junction is reverse-biased. Since the emitter is p -type and Junction 1 is forward biased, a large number of holes enter the n -type base region. These holes combine with electrons in the base. However, in a properly prepared junction transistor, the base is thin enough to allow most of the holes to pass through the base without recombination and into the p -type collector. A small increase in input voltage within the emitter-base circuit produces a large increase in current across Junction 2 due to the passage of holes. The large increase in collector current also results in a large increase in voltage across the load resistor. Thus, a voltage signal that passes through a junction transistor experiences *amplification*, as illustrated by the input and output voltage plots in Figure 6.20. A similar effect is observed in an n - p - n junction transistor, except that electrons instead of holes are injected across the base to the collector.

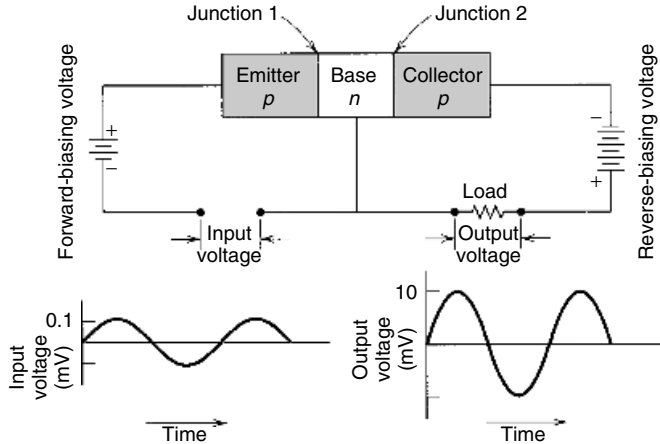


Figure 6.20 Schematic diagram of a *pnp*-junction transistor and associated input and output voltage characteristics. Reprinted, by permission, from W. Callister, *Materials Science and Engineering: An Introduction*, 5th ed., p. 633. Copyright © 2000 by John Wiley & Sons, Inc.

In addition to their ability to amplify electrical signals, transistors and diodes may act as switching and information storage devices. Computer information is stored in terms of binary code—for example, zeros and ones. Transistors and diodes can operate as switches that have two states: on and off, or conducting and nonconducting. Thus, a conducting circuit can represent a zero while a nonconducting circuit can represent a one. In this way, information and logical operations can be stored and retrieved from a series of semiconducting circuits known as *integrated circuits*. Inexpensive integrated circuits are mass produced by forming layers of high-purity silicon in a precisely detailed pattern and introducing specific dopants into specific areas by diffusion or ion implantation. The details of some of these processes will be described in Chapter 7.

6.1.2 Electrical Properties of Ceramics and Glasses

Many of the fundamental relationships and concepts governing the electrical properties of materials have been introduced in the previous section. In this section, we elaborate upon those topics that are more prevalent or technologically relevant in ceramics and glasses than in metals, such as electrical insulation and superconductivity, and introduce some topics that were omitted in Section 6.1.1, such as dielectric properties.

6.1.2.1 Electrical Resistance. At room temperature, many ceramics (and polymers, for that matter) have electrical resistivities that are approximately 20 orders of magnitude higher than those of metals (see Figure 6.21). As a result, they are often used as electrical insulators. With rising temperature, however, insulating materials experience an increase in electrical conductivity, which may ultimately be greater than that for semiconductors. In fact, some oxide ceramics such as ReO_3 can achieve metallic levels of electrical conductivity at high temperatures. In all cases, the electrical conductivity can be interpreted in terms of carrier concentrations and carrier mobilities as previously described, though we shall see in Section 6.1.2.3 that the carriers may be different for ceramics and glasses than for metals.

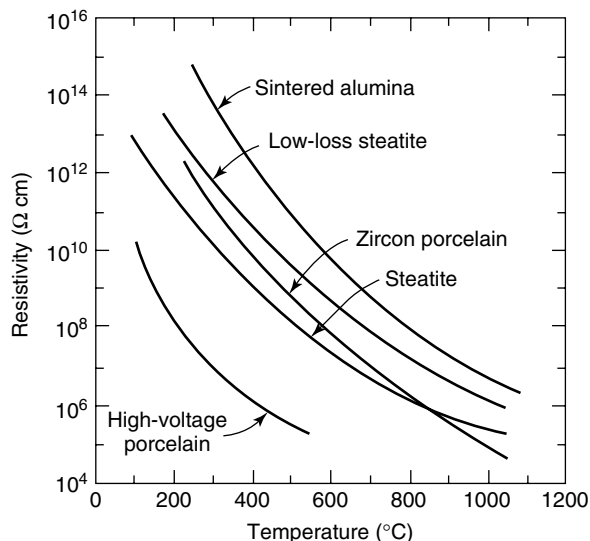


Figure 6.21 Temperature dependence of resistivity for some typical oxide ceramics. From W. D. Kingery, H. K. Bowen, and D. R. Uhlmann, *Introduction to Ceramics*. Copyright © 1976 by John Wiley & Sons, Inc. This material is used by permission of John Wiley & Sons, Inc.

Despite the potential for high electrical conductivities, we will concentrate on the more common high-resistivity aspects of ceramics in this section and will describe some of the factors that affect the use of ceramics and glasses as electrical insulators. For ceramics and glasses having electrical resistivities above about $10^5 \Omega \cdot \text{cm}$, the concentration–mobility product of the charge carriers is small; as a result, minor variations in composition, impurities, heat treatment, stoichiometry, porosity, oxygen partial pressure, and other variables can have a significant effect on the resistivity. The effect of porosity is similar to that described for thermal conductivity in Section 4.2. As porosity increases, the electrical resistivity increases proportionally for small values of porosity. At higher porosities, the effect is more substantial. The effect of grain boundaries in polycrystalline materials is related to the mean free path of the ions, as described in Section 6.1.1.1. Except for very thin films or extremely fine-grained materials (less than $0.1 \mu\text{m}$), the effects of grain boundary scattering are small compared to lattice scattering. Consequently, the grain size in uniform-composition materials has little effect on resistivity. However, substantial effects can result from impurity concentrations at grain boundaries. Particularly for oxide materials, there is a tendency to form a glassy silicate phase at the boundary between particles. Ceramic compositions with the highest glassy phase have the lower resistivities at moderate temperatures. In glasses, the alkali content should be kept to a minimum when high resistivities are required. The reasons for this are related to the electrical conduction via ions, which will be described in Section 6.1.2.3. For now, we maintain our emphasis on the electrical insulating properties of ceramics and glasses in order to describe a unique application known as dielectrics.

6.1.2.2 Dielectrics, Ferroelectricity, and Piezoelectricity. A *dielectric* is a material separating two charged bodies, as illustrated in Figure 6.22b. For a substance

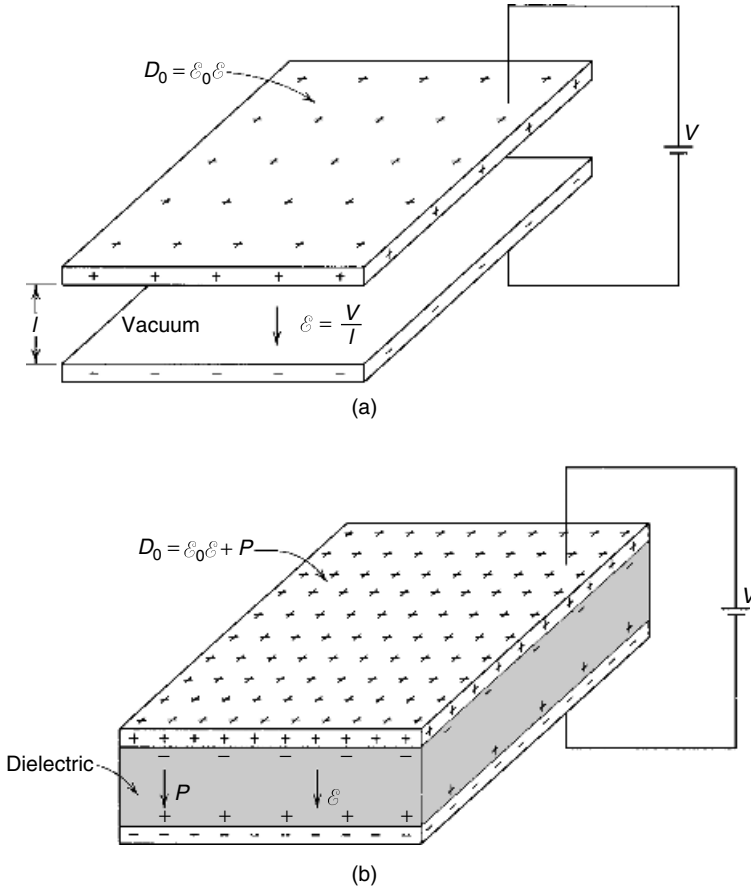


Figure 6.22 A parallel-plate capacitor (a) in vacuum and (b) with a dielectric material between the plates. Reprinted, by permission, from W. Callister, *Materials Science and Engineering: An Introduction*, 5th ed., p. 640. Copyright © 2000 by John Wiley & Sons, Inc.

to be a good dielectric, it must be an electrical insulator. As a result, any electrical insulator is also called a dielectric.

The interaction of a dielectric with an electric field is conveniently described in terms of a parallel plate capacitor. When a voltage is applied between two parallel plates in a vacuum (Figure 6.22a), one plate becomes positively charged and the other becomes negatively charged. If an electrical conductor were to be placed in contact with the plates, current would flow. In a vacuum, however, no current flows, and the electric field strength is a function of the applied voltage, V , and the separation distance between the plates, l , as given earlier by Eq. (6.4):

$$\mathcal{E} = V/l \quad (6.4)$$

The magnitude of the charge per unit area on either plate, called the *electric displacement* or *flux density*, \mathbf{D}_0 , is directly proportional to the field:

$$\mathbf{D}_0 = \epsilon_0 \mathcal{E} \quad (6.32)$$

where ε_0 is a constant called *electric permittivity* and has a value of 8.854×10^{-12} C/V · m (or farad/m, F/m, where a farad equals a coulomb/volt). The electric displacement therefore has units of C/m². Notice the similarity in form of Eq. (6.32) to Eq. (6.2) for the magnetic flux in a magnetic field. As before, both \mathbf{D}_0 and \mathcal{E} are vector quantities, but for our purposes a description of their magnitudes is sufficient, so the boldface will be dropped.

Since D_0 is the surface charge density on the plate in vacuum, it can be related to the capacitance of a parallel plate capacitor in vacuum, C_0 , which is defined as

$$C_0 = q/V \quad (6.33)$$

where q is the magnitude of charge on each plate and V is the applied voltage. With A the plate area and l the separation between plates, along with $q = D_0 A$, Eq. (6.33) becomes

$$C_0 = \varepsilon_0 \frac{A}{l} \quad (6.34)$$

when a vacuum exists between the plates.

If we now place a dielectric (insulator) material between the plates, as in Figure 6.22b, a displacement of charge within the material is created through a progressive orientation of permanent or induced dipoles. Recall that a dipole is simply any type of charge separation, as first described in Section 1.0.3.2 and illustrated in Figure 6.23, and that it may be permanent or temporarily induced. The magnitude of the electric dipole, p_e , is simply proportional to the charge, q , and the separation distance, a , as $p_e = qa$.

The interaction between permanent or induced electric dipoles with an applied electric field is called *polarization*, which is the induced dipole moment per unit volume. Polarization causes positive charge to accumulate on the bottom surface next to the

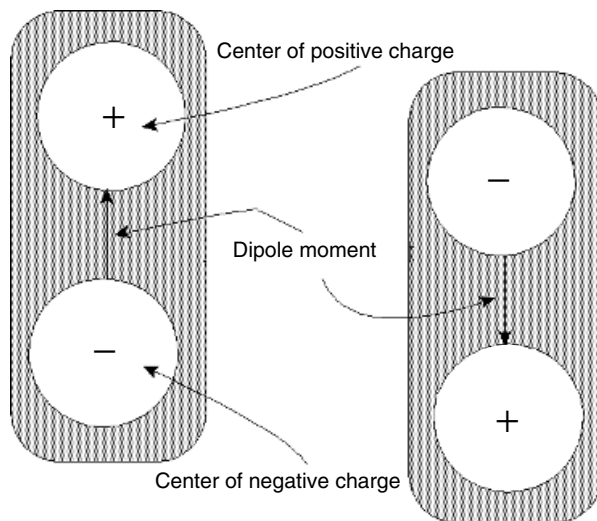


Figure 6.23 Schematic illustration of an electric dipole.

negatively charged plate and causes negative charge to accumulate toward the positively charged plate on the top. This tends to decrease the effective surface charge density on either plate. The expected decrease in effective charge corresponds to the polarization, P , of the material, which equals the induced dipole moment per unit volume of polarizable material. The electric field is now found from Eq. (6.32) by accounting for the reduction in displacement due to polarization:

$$\mathcal{E} = (D - P)/\epsilon_0 \quad (6.35)$$

The displacement can now be found by rearranging Eq. (6.2) to

$$D = \epsilon_0 \mathcal{E} + P \quad (6.36)$$

Equation (6.36) is often written

$$D = \epsilon \mathcal{E} \quad (6.37)$$

where ϵ is called the *permittivity*.

The ratio of permittivity with the dielectric to the permittivity in vacuum, ϵ/ϵ_0 , is called the *relative permittivity*, ϵ_r , or *dielectric constant*. The dielectric constant is a material property. Some values of dielectric constants for common ceramic and glass insulators are given in Table 6.3. Since a polarizable material causes an increase in charge per unit area on the plates of a capacitor, the capacitance also increases, and it can be shown that the dielectric constant is related to the capacitance and displacement in vacuum and with the dielectric material as follows:

$$\epsilon_r = \frac{\epsilon}{\epsilon_0} = \frac{D}{D_0} = \frac{C}{C_0} \quad (6.38)$$

Cooperative Learning Exercise 6.3

A voltage of 10 V is applied across a parallel-plate capacitor with a plate separation of 2×10^{-3} m and plate area of 6.45×10^{-4} m², both in vacuum and then with a dielectric material placed between the plates. The polarization, P , due to the presence of the dielectric material is 2.22×10^{-7} C/m².

Person 1: Calculate the displacement in vacuum, D_0 , and the capacitance in vacuum, C_0 .

Person 2: Calculate the displacement, D , due to the presence of the dielectric.

Combine your information to calculate the dielectric constant and the capacitance in the presence of the dielectric.

Answers: Eq. (6.32) $D_0 = 8.854 \times 10^{-12} (10/0.002) = 4.427 \times 10^{-8}$ C/m²,
Eq. (6.34) $C_0 = 8.854 \times 10^{-12} (6.45 \times 10^{-4}/0.002) = 2.85 \times 10^{-12}$ F;
Eq. (6.36) $D = 8.854 \times 10^{-12} (10/0.002) + 2.22 \times 10^{-7} = 2.66 \times 10^{-7}$ C/m²,
Eq. (6.38) $\epsilon_r = D/D_0 = 6.0$; $C = \epsilon_r C_0 = 1.71 \times 10^{-11}$ F.

Table 6.3 Dielectric Constants of Selected Ceramics and Glasses at 25°C and 10° Hz

Glasses	ϵ_r	Inorganic Crystalline Materials	ϵ_r
Silica glass	3.8	Barium oxide	3.4
Vycor glasses	3.8–3.9	Mica	3.6
Pyrex glasses	4.0–6.0	Potassium chloride	4.75
Soda–lime–silica glass	6.9	Potassium bromide	4.9
High-lead glass	19.0	Cordierite ceramics (based on $2\text{MgO} \cdot 2\text{Al}_2\text{O}_3 \cdot 3\text{SiO}_2$)	4.5–5.4
		Diamond	5.5
		Potassium iodide	5.6
		Forsterite (Mg_2SiO_4)	6.22
		Mullite ($3\text{Al}_2\text{O}_3 \cdot 2\text{SiO}_2$)	6.6
		Lithium fluoride	9.0
		Magnesium oxide	9.65

Source: K. M. Ralls, T. H. Courtney, and J. Wulff, *Introduction to Materials Science and Engineering*. Copyright © 1976 by John Wiley & Sons, Inc.

We can further describe the polarization, P , according to the different types of dipoles that either already exist or are induced in the dielectric material. The polarization of a dielectric material may be caused by four major types of polarization: electronic polarization, ionic (atomic) polarization, orientation polarization, and space-charge (interfacial) polarization. Each type of polarization is shown schematically in Figure 6.24 and will be described in succession. In these descriptions, it will be useful to introduce a new term called the *polarizability*, α , which is simply a measure of the ability of a material to undergo the specific type of polarization.

Electronic polarization arises because the center of the electron cloud around a nucleus is displaced under an applied electric field, as shown in Figure 6.24. The resulting polarization, or dipole per unit volume, is

$$P_e = N\alpha_e\mathcal{E}_{\text{loc}} \quad (6.39)$$

where N is the number of atoms or molecules, α_e is the electronic polarizability, and \mathcal{E}_{loc} is the local electric field that an atom or molecule experiences. The local electric field is greater than the average field, \mathcal{E} , because of the polarization of other surrounding atoms.

Ionic polarization occurs in ionic materials because an applied field acts to displace cations in the direction of the applied field while displacing anions in a direction opposite to the applied field. This gives rise to a net dipole moment per formula unit. For an ionic solid, the atomic polarization is given by

$$P_i = N\alpha_i\mathcal{E}_{\text{loc}} \quad (6.40)$$

where N is the number of formula units per unit volume, and α_i is the ionic polarizability. Both ionic and electronic polarization contribute to the formation of induced dipoles.

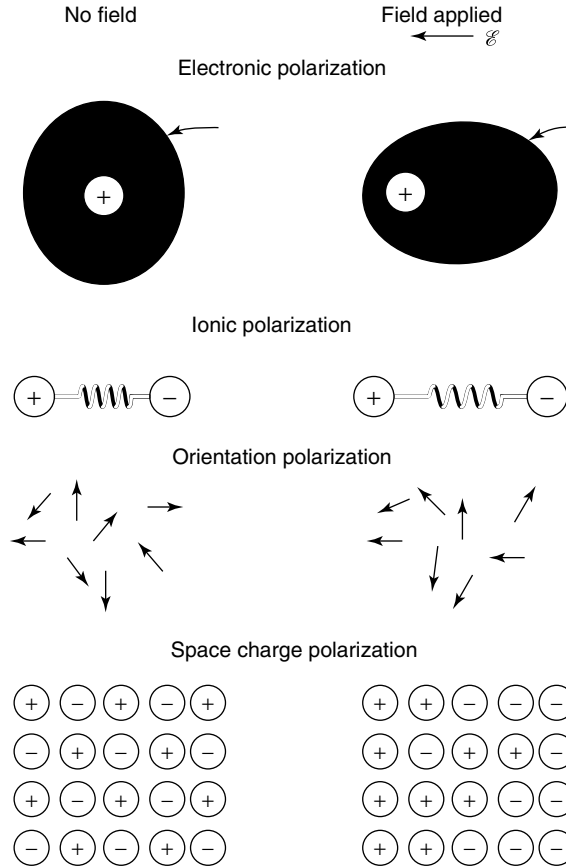


Figure 6.24 Schematic illustration of different types of polarization. From W. D. Kingery, H. K. Bowen and D. R. Uhlmann, *Introduction to Ceramics*. Copyright © 1976 by John Wiley & Sons, Inc. This material is used by permission of John Wiley & Sons, Inc.

Orientation polarization can occur in materials composed of molecules that have permanent electric dipole moments. The permanent dipoles tend to become aligned with the applied electric field, but entropy and thermal effects tend to counter this alignment. Thus, orientation polarization is highly temperature-dependent, unlike the forms of induced polarization which are nearly temperature-independent. In electric fields of moderate intensity, the orientation polarization is proportional to the local electric field, as for the other forms of polarization

$$P_o = N\alpha_o\mathcal{E}_{\text{loc}} \quad (6.41)$$

but in strong electric fields this proportionality is not maintained since saturation must occur when all the permanent dipoles are aligned. Orientation polarization occurs mostly in gases and liquids where molecules are free to rotate. In some solids the rotation of polar molecules may be restricted by lattice forces, which can reduce orientation polarization. For example, the dielectric constant of water is about 82, while that of ice is about 10. The orientation polarizability, α_o , can be further elaborated

upon, since the permanent electric dipole moment per molecule, p_e , is a measurable quantity. The two quantities are related by a relationship similar to the Curie Law, which we shall elaborate upon in Section 6.2:

$$\alpha_o = \frac{p_e^2}{3k_B T} \quad (6.42)$$

where k_B is Boltzmann's constant and T is absolute temperature. A list of permanent dipole moments for selected polar molecules is given in Table 6.4.

The final type of polarization is *space-charge polarization*, sometimes called *interfacial polarization*, and results from the accumulation of charge at structural interfaces in heterogeneous materials. Such polarization occurs when one of the phases has a much higher resistivity than the other, and it is found in a variety of ceramic materials, especially at elevated temperatures. The space-charge polarization, P_{sc} , has a corresponding space-charge polarizability, α_{sc} . The two are related via a relationship of the form for the other types of polarization.

The total polarization, then, is the sum of all the contributions from the different types of polarization:

$$P = P_e + P_i + P_o + P_{sc} \quad (6.43)$$

Table 6.4 Permanent Dipole Moments of Some Polar Molecules in the Gaseous Phase

Molecule	$10^{30} \times \text{Dipole Moment}(\text{C} \cdot \text{m})$
AgCl	19.1
LiCl	23.78
NaCl	30.0
KCl	34.26
CsCl	34.76
LiF	21.1
NaF	27.2
KF	28.7
RbF	27.5
CsF	26.3
HF	6.07
HCl	3.60
HBr	2.74
HI	1.47
HNO ₃	7.24
H ₂ O	6.17
NH ₃	4.90
CH ₃ Cl	6.24
CH ₂ Cl ₂	5.34
CHCl ₃	3.37
C ₂ H ₅ OH	5.64
C ₆ H ₅ NO ₂	14.1

Source: K. M. Ralls, T. H. Courtney, and J. Wulff, *Introduction to Materials Science and Engineering*. Copyright © 1976 by John Wiley & Sons, Inc.

With appropriate substitution of the expressions for the various types of polarization, it is easy to show that the total polarizability, α , is also the sum of the various types of polarizability:

$$\alpha = \alpha_e + \alpha_i + \alpha_o + \alpha_{sc} \quad (6.44)$$

The total polarization, P , and hence the dielectric constant, ϵ_r , subjected to an alternating electric field depend upon the ease with which the permanent or induced dipoles can reverse their alignment with each reversal of the applied field. The time required for dipole reversal is called the *relaxation time*, and its reciprocal is called the *relaxation frequency*. When the time duration per cycle of the applied field is much less than the relaxation time of a particular polarization process, the dipoles cannot change their orientation rapidly enough to remain oriented in the applied field, and they “freeze” their reorientation process. This particular polarization process will not contribute to the total polarization. The order in which the polarization processes cease to contribute to the total polarization is related to their relative size scales. Obviously, electronic polarization is the smallest since it deals with electron density. Ionic polarization is next in size scale, since it deals with the separation of ions, followed by orientation polarization, which is on the order of molecular dimensions and can sometimes be large. Finally, space-charge polarization, if it exists at all, is on the scale of interfacial dimensions. The larger the size scale, the more difficult it is for that type of polarization to respond to an alternating electric field. Thus, we would expect space charge to “freeze” up first with increasing electric field, followed by orientation, ionic, and electronic polarization, respectively. This process is shown in a plot of polarizability (which recall is proportional to polarization) versus the logarithm of the alternating electric field frequency in Figure 6.25a.

As the frequency of the applied field approaches the relaxation frequency, the polarization response increasingly lags behind the applied field. The reorientation of each type of dipole is opposed by internal friction, which leads to heating in the sample and power loss. The *power loss* depends on the degree to which the polarization lags behind the electric field. This lag can be quantified by measurement of the displacement–field relationship in a sinusoidally varying field. It is found that if the alternating field is given by

$$\mathcal{E} = \mathcal{E}_0 \sin(\omega t) \quad (6.45)$$

then the polarizability, P , is given by

$$P = P_0 \sin(\omega t - \delta) \quad (6.46)$$

where δ is the phase angle that the polarization lags behind the field, and ω is the angular frequency of the field. It can be shown that the power loss is related to the phase angle and the applied field:

$$\text{Power loss} = 2\pi \mathcal{E}^2 \omega \epsilon_0 \tan \delta \quad (6.47)$$

where $\tan \delta$ is called the *loss tangent*. For small phase angles, $\tan \delta \approx \delta$. As shown in Figure 6.25b, the power loss for a particular polarization type increases as that process becomes slower to respond to frequency changes, reaches a maximum as the electric field frequency reaches the relaxation frequency, and decreases after that polarization type has reached its relaxation frequency.

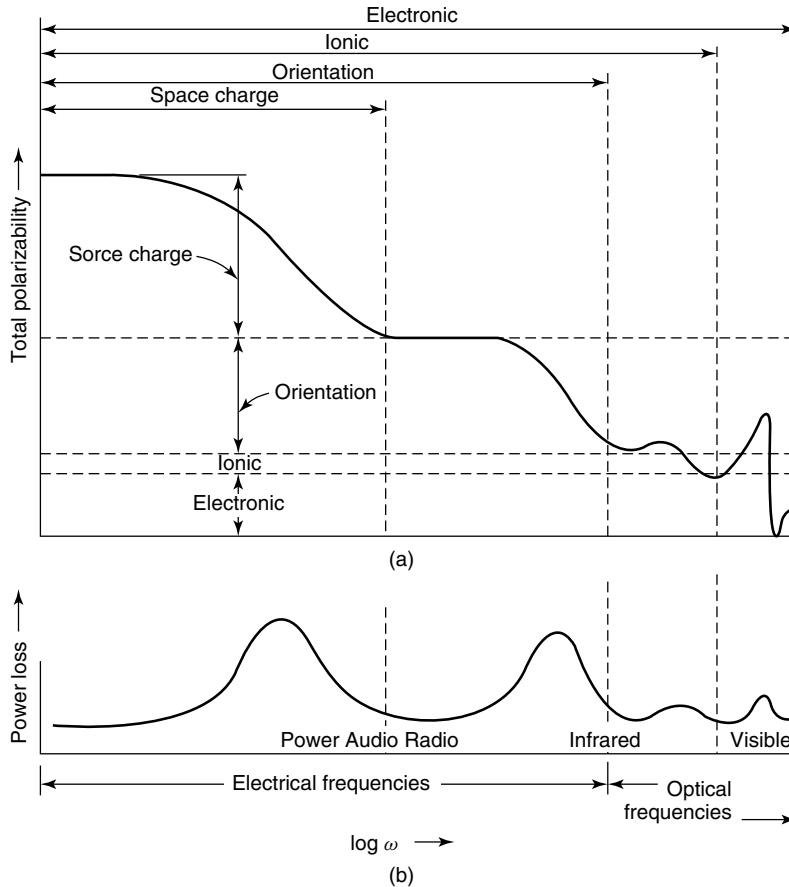


Figure 6.25 Frequency dependence of (a) total polarizability and (b) power loss. From K. M. Ralls, T. H. Courtney, and J. Wulff, *Introduction to Materials Science and Engineering*. Copyright © 1976 by John Wiley & Sons, Inc. This material is used by permission John Wiley & Sons, Inc.

The loss tangent is an important quantity. The product of the loss tangent and the dielectric constant, $\epsilon_r \tan \delta$, is called the *loss factor* and is the primary criterion for judging the usefulness of a dielectric as an insulator material. For this purpose, it is desirable to have a low dielectric constant and a small loss angle. For applications in which it is desirable to obtain a high capacitance in the smallest physical space, a high dielectric constant must be used, and a low value of the loss angle is needed.

At high enough frequencies, the dielectric will experience electrical breakdown and the insulator will become a conductor. As in a semiconductor, breakdown is initiated by the field-induced excitation of a number of electrons to the conduction band with sufficient kinetic energy to knock other electrons into the conduction band. The result is the avalanche effect described earlier. The magnitude of the electric field required to cause dielectric breakdown is called the *dielectric strength*, or *breakdown strength*. The dielectric strength for oxide ceramic insulators lies in the range 1–20 kV/mm, with the value of 9 kV/mm for Al_2O_3 being typical.

The temperature dependence of the dielectric constant is highly dependent upon molecular structure, as well as the predominant polarization mechanism. For large molecules, orientation polarization is difficult below the material melting point, whereas orientation polarization can persist below the melting point in smaller molecules. Some substances undergo structural transformations in the solid state from higher- to lower-ordered structures which can restrict molecular rotation. The effects of temperature and frequency on the dielectric constant are not entirely independent. For example, the frequency effect on electronic and ionic polarization is negligible at frequencies up to about 10^{10} Hz, which is the limit of normal use. Similarly, the effect of temperature on electronic and ionic polarization is small. At higher temperatures, however, there is an increasing contribution resulting from ion mobility and crystal imperfection mobility. The combined effect is to give a sharp rise in the apparent dielectric constant at low frequencies with increasing temperature, as illustrated for alumina porcelain, whose primary component is Al_2O_3 , in Figure 6.26. The loss tangent is also shown

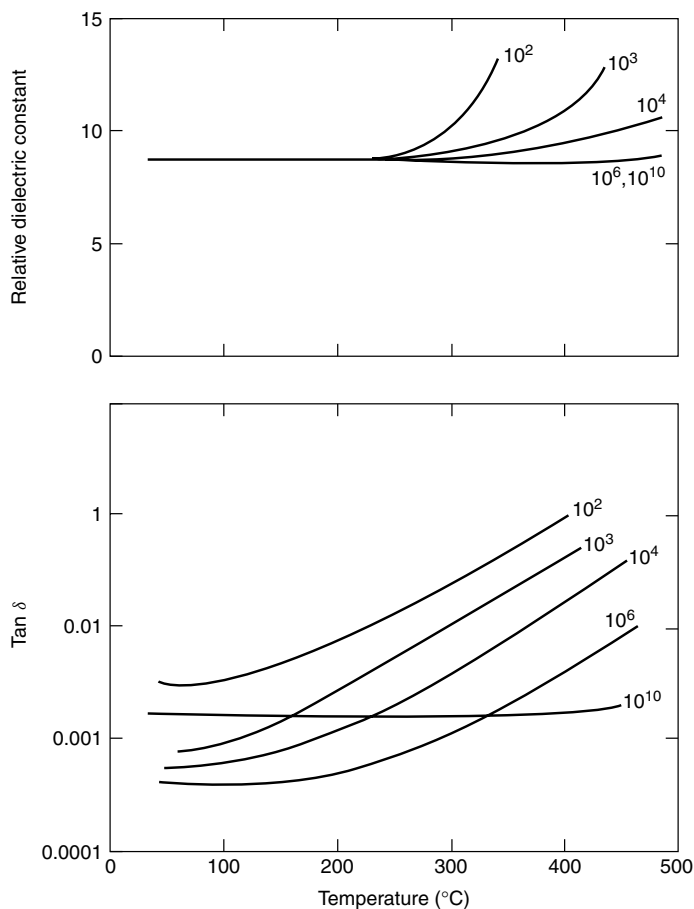


Figure 6.26 Frequency and temperature dependence of dielectric constant and $\tan \delta$ for alumina porcelain. From W. D. Kingery, H. K. Bowen, and D. R. Uhlmann, *Introduction to Ceramics*. Copyright © 1976 by John Wiley & Sons, Inc. This material is used by permission of John Wiley & Sons, Inc.

in Figure 6.26 for reference. Alumina is an important component of most ceramic dielectrics. The other base components are silica, SiO_2 , and magnesia, MgO .

Two phenomena related to the electric dipoles in a material are *ferroelectricity* and *piezoelectricity*. Ferroelectricity is defined as the spontaneous alignment of electric dipoles by their mutual interaction in the absence of an applied electric field. The source of ferroelectricity arises from the fact that the local field increases in proportion to the polarization. Thus, ferroelectric materials must possess permanent dipoles. One of the most important ferroelectric materials is barium titanate, BaTiO_3 . The spontaneous polarization of BaTiO_3 is related directly to the positions of the ions within the tetragonal unit cell, as shown in Figure 6.27a. Divalent barium ions occupy each corner position, with the tetravalent titanium ion near, but just above, the center of the cell. The oxygen ions are located below the center of the (001) plane and just below the centers of the (100) and (010) planes, as illustrated in Figure 6.27b. Consequently, per unit cell, the centers of positive and negative charge do not coincide, and there is spontaneous polarization. At a certain temperature called the *ferroelectric Curie temperature* (120°C for barium titanate), barium titanate becomes cubic with Ti^{4+} ions located at the center of the unit cell and O^{2-} ions occupying face-centered positions, and it loses its spontaneous polarization. Ferroelectric materials have extremely high dielectric constants at relatively low applied field frequencies. Consequently, capacitors made from these materials can be significantly smaller than capacitors made from other dielectric materials.

Closely related to ferroelectricity is *piezoelectricity* in which polarization is induced and an electric field is established across a specimen by the application of external force (see Figure 6.28a,b). Reversing the direction of the external force, as from tension to compression, reverses the direction of the field. Alternatively, the application of an external electric field alters the net dipole length and causes a dimensional change, as in Figure 6.28c. Piezoelectric materials can be used as transducers—devices that

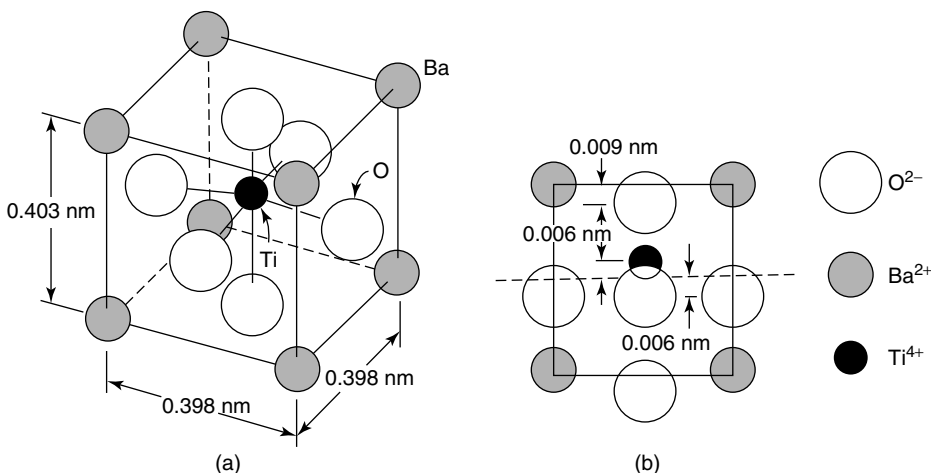


Figure 6.27 View of (a) the tetragonal unit cell of BaTiO_3 and (b) the ionic positions projected in a [100] direction onto a (100) face. From K. M. Ralls, T. H. Courtney, and J. Wulff, *Introduction to Materials Science and Engineering*. Copyright © 1976 by John Wiley & Sons, Inc. This material is used by permission John Wiley & Sons, Inc.

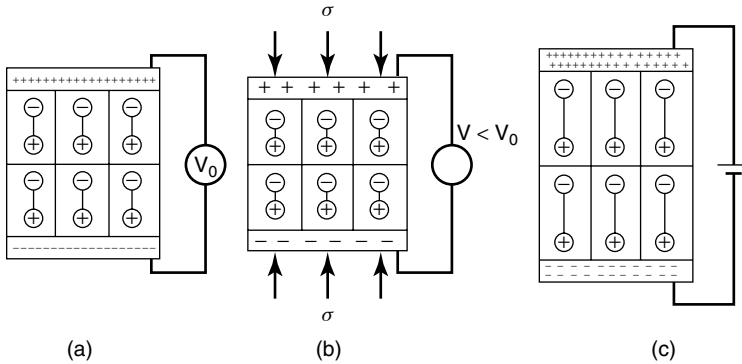


Figure 6.28 Schematic illustration of the piezoelectric effect that occurs in (a) an unstressed and (b) stressed piezoelectric material. Mechanical deformation can also occur when (c) a voltage is applied to a piezoelectric material. From K. M. Ralls, T. H. Courtney, and J. Wulff, *Introduction to Materials Science and Engineering*. Copyright © 1976 by John Wiley & Sons, Inc. This material is used by permission John Wiley & Sons, Inc.

convert mechanical stress into electrical energy and vice versa. Such devices are used in microphones and mechanical strain gauges. Barium titanate is also a piezoelectric material.

Before proceeding, it may be useful to summarize some of the myriad of terms and symbols that have been used to this point. Such a summary is presented in Table 6.5. With the exception of a few more terms dealing with superconductivity, we have introduced all the variables we will need to describe the electrical properties of materials.

6.1.2.3 Ion-Conducting Ceramics and Glasses. In addition to the conduction of charge via electrons, charge can be conducted via ions. Ions are present in most crystalline ceramic materials such as oxides and halides. This process is termed *ionic conduction* and may occur either in conjunction with or separately from electronic conduction. As a result, we must expand our definition of conductivity to include both types of conduction:

$$\sigma = \sigma_{\text{electronic}} + \sigma_{\text{ionic}} \quad (6.48)$$

In a manner analogous to conduction via electrons and holes, the ionic conductivity can be related to the charge carrier density, n_i , charge carrier mobility, μ_i , and carrier charge, q_e , as originally given in Eq. (6.9) for electronic conduction, except that the charge carriers are now ions, which have multiple charges, or valences, z_i , so that Eq. (6.9) must be modified slightly:

$$\sigma_{\text{ionic}} = f n_i (z_i q_e) \mu_i \quad (6.49)$$

An additional factor, f , has been included to account for the number of equivalent sites to which an ion may transfer in a particular crystal structure; for example $f = 4$ for an ion vacancy in the cubic crystal structure.

For an ion to move through the lattice under an electric field driving force, it must have sufficient thermal energy to pass over an energy barrier, which in this case is

Table 6.5 Electrical Symbols, Terms, and SI Units

Quantity	Symbol	SI Units	
		Primary	Derived
Electric charge	q	coulomb, C	(none)
Electric potential	V	$\text{kg} \cdot \text{m}^2/\text{s}^2 \cdot \text{C}$	volt, V
Electric current	I	C/s	ampere, amp, A
Electric field strength	ε	$\text{kg} \cdot \text{m}/\text{s}^2 \cdot \text{C}$	V/m
Resistance	R	$\text{kg} \cdot \text{m}^2/\text{s} \cdot \text{C}^2$	ohm, Ω
Resistivity	ρ	$\text{kg} \cdot \text{m}^3/\text{s} \cdot \text{C}^2$	$\Omega \cdot \text{m}$
Conductance	G	$\text{s} \cdot \text{C}^2/\text{kg} \cdot \text{m}^2$	Ω^{-1}
Conductivity	σ	$\text{s} \cdot \text{C}^2/\text{kg} \cdot \text{m}^3$	$(\Omega \cdot \text{m})^{-1}$
Electrical capacitance	C	$\text{s}^2 \cdot \text{C}^2/\text{kg} \cdot \text{m}^2$	farad, F
Permittivity	ε	$\text{s}^2 \cdot \text{C}^2/\text{kg} \cdot \text{m}^3$	F/m
Dielectric Constant (Relative Permittivity)	ε_r	(dimensionless)	(dimensionless)
Dielectric displacement	D	C/m ²	F · V/m ²
Electric polarization	P	C/m ²	F · V/m ²
Polarizability	α	$\text{s}^2 \cdot \text{C}^2/\text{kg}$	F · m²
Permanent Dipole Moment	p	C · m	debeye, D
Dielectric loss angle	δ	(none)	(none)
Charge carrier mobility	μ	s · C/kg	m ² /V · s
Charge carrier density	n	m ⁻³	(none)
Magnetic field strength	H	C/m · s	A/m

Items in boldface are material properties.

an intermediate position between lattice sites. This activation energy barrier to motion has already been described in Section 4.3.2.1 for diffusion in crystalline solids, so it will not be described here. It makes sense, though, that the ion mobility, μ_i , should be related to the ion diffusivity (diffusion coefficient), D_i , and can be derived from Eq. (6.14) presented earlier:

$$\mu_i = \frac{z_i q_e D_i}{k_B T} \quad (6.50)$$

where z_i is the valence of the ion, q_e is the electronic charge, and k_B and T are Boltzmann's constant and absolute temperature, as before. Substitution of Eq. (6.50) into Eq. (6.49) gives a relationship for the ionic conductivity:

$$\sigma_{ionic} = \frac{f n_i (z_i q_e)^2 D_i}{k_B T} \quad (6.51)$$

Typically, there is a predominate charge carrier in ionic solids. For example, in sodium chloride, the mobility of sodium ions is much larger than the mobility of chloride ions. This phenomenon can be temperature-dependent, however. As shown in Table 6.6, the fraction of total conductivity attributable to positive ions (K^+) in

Table 6.6 Ionic and Electronic Contributions to Total Electrical Conductivity for Some Selected Compounds and Glasses

Compound	Temperature (°C)	Cationic Conductivity ($\sigma_{ionic}^+/\sigma_{total}$)	Anionic Conductivity ($\sigma_{ionic}^-/\sigma_{total}$)	Electronic Conductivity ($\sigma_{e,h}/\sigma_{total}$)
NaCl	400	1.00	—	—
	600	0.95	0.05	—
KCl	435	0.96	0.04	—
	600	0.88	0.12	—
KCl + 0.02% CaCl ₂	430	0.99	0.01	—
	600	0.99	0.01	—
AgCl	20–350	1.00	—	—
AgBr	20–300	1.00	—	—
BaF ₂	500	—	1.00	—
PbF ₂	200	—	1.00	—
CuCl	20	—	—	1.00
	366	1.00	—	—
ZrO ₂ + 7% CaO	>700	—	1.00	10 ⁻⁴
Na ₂ O · 11Al ₂ O ₃	<800	1.00(Na ⁺)	—	< 10 ⁻⁶
FeO	800	—	—	1.00
ZrO ₂ + 18% CeO ₂	1500	—	0.52	0.48
ZrO ₂ + 50% CeO ₂	1500	—	0.15	0.85
Na ₂ O · CaO · SiO ₂ glass	—	1.00(Na ⁺)	—	—
15%(FeO · Fe ₂ O ₃) · CaO ·	1500	0.1(Ca ⁺)	—	0.9
SiO ₂ · Al ₂ O ₃ glass				

Source: W. D. Kingery, H. K. Bowen, and D. R. Uhlmann, *Introduction to Ceramics*. Copyright © 1976 by John Wiley & Sons, Inc.

KCl drops from 0.96 at 435°C to 0.88 at 600°C. Similarly, the conductivity of CuCl is wholly attributable to electronic conduction at room temperature, but completely due to ionic conduction at 366°C. This temperature dependence is illustrated further for NaCl in Figure 6.29. At high temperatures (to the left in Figure 6.29), the number of sodium ion vacancies [n_i in Eq. (6.51)] is a thermodynamic property, and the conductivity varies with temperature as the product of the vacancy concentration and the diffusion coefficient, each of which has an exponential temperature dependence. This is the intrinsic range. At lower temperatures (to the right in Figure 6.29), the concentration of sodium ions is not in thermal equilibrium but is determined by minor solutes. As a result, this is the extrinsic region, and the temperature dependence of conductivity depends only on the diffusion coefficient. The activation energy for mobility can be determined from the data in Figure 6.29 for this region, but the slope of the curve in the intrinsic region gives the sum of the activation energy for mobility and lattice-defect formation.

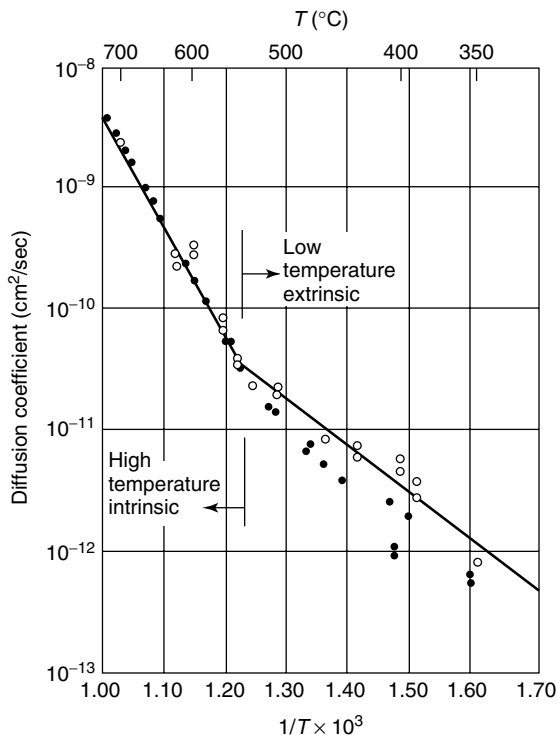


Figure 6.29 Diffusion coefficient measured directly (open circles) and calculated from electrical conductivity data (closed circles) for Na^+ in sodium chloride. From W. D. Kingery, H. K. Bowen, and D. R. Uhlmann, *Introduction to Ceramics*. Copyright © 1976 by John Wiley & Sons, Inc. This material is used by permission of John Wiley & Sons, Inc.

Several types of compounds show exceptionally high ionic conductivity. Such phases fall into three broad categories: halides and *chalcogenides* of silver and copper, in which the metal atom is disordered over several alternative sites; oxides with the β -alumina structure, in which a monovalent cation is mobile; and oxides of fluorite structure, with large concentrations of defects caused either by a variable valence cation or solid solution with a second cation of lower valence. Chalcogenide are chiefly based on the elements of Group VI—that is, S, Se, and Te. The silver and copper halides and chalcogenides often have simple arrays of anions. The cations occur in disorder in the interstices among the anions. The number of available sites is larger than the number of cations. In the highly conductive phases, the energy barrier between neighboring sites is very small, and channels are provided along which cations are free to move. The β -aluminas are hexagonal structures with approximate composition $\text{AM}_{11}\text{O}_{17}$. The mobile ion A is a monovalent species such as Na, K, Rb, Ag, Te, or Li, and M is a trivalent ion, Al, Fe, or Ga. The conductivities for several β -aluminas are plotted as a function of temperature in Figure 6.30. The crystal structure consists of planes of atoms parallel to the basal plane. Four planes of oxygens in a cubic close-packed sequence comprise a slab within which aluminum atoms occupy octahedral and tetrahedral sites as in spinel. The spinel blocks are bound together by a rather open layer of the monovalent ion and oxygen. This loosely bound layer is thought to be disordered

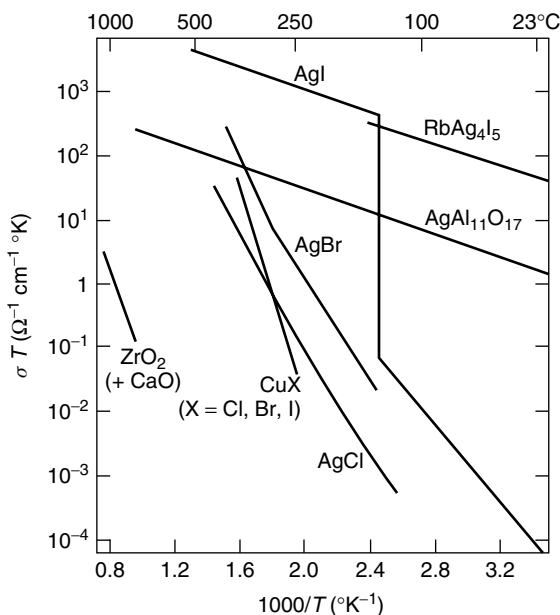


Figure 6.30 Conductivity of some highly conducting solid electrolytes. From W. D. Kingery, H. K. Bowen, and D. R. Uhlmann, *Introduction to Ceramics*. Copyright © 1976 by John Wiley & Sons, Inc. This material is used by permission of John Wiley & Sons, Inc.

and provide a two-dimensional channel for atom motion. Finally, the high dopant levels in the fluorite-type solid solutions leads to large defect concentrations and vacancy ordering. In such materials rapid oxygen migration occurs. This is believed to be due to the high concentration of vacancies. The effect of structure on the ionic conductivity of ceramics leads us naturally into one of the most exciting technological developments of recent decades: high-temperature superconductors.

6.1.2.4 Oxide Superconductors. In Section 6.1.1.3, we learned that some metals can lose all of their residual resistivity near absolute zero and become what are called superconductors. We also learned that for many years, there was believed to be an upper temperature limit of 30 K for the critical transition temperature, T_c , below which a substance begins to superconduct. In 1986, however, the first indication of superconductivity above 30 K was found in barium-doped La_2CuO_4 . Then researchers found that high pressure could increase T_c to 50 K. Work began to find combinations of atoms of different sizes and valences that could simulate the pressure effect through chemical substitution. One of the variations was to substitute yttrium into the perovskite structure of BaCuO_3 . Of these so-called YBC compounds, $\text{YBa}_2\text{Cu}_3\text{O}_7$ (termed 1–2–3 superconductor after the chemical formula) was found to superconduct at 92 K. Why all the fuss over a few tens of degrees? The answer is stated simply with the boiling points of three common gases: $T_b(\text{helium}) = 4.2 \text{ K}$; $T_b(\text{nitrogen}) = 77 \text{ K}$; $T_b(\text{oxygen}) = 90 \text{ K}$. In order to cool the superconductors below T_c , a liquefied gas must be used. It is far less costly to liquefy nitrogen and oxygen (the major components of air) than helium. For any application in which liquid nitrogen can replace liquid helium, the refrigeration

cost is about 1000 times less. In this way, high-temperature superconductors (HTSC), with $T_c > 77$ K, are of great technological interest.

Another striking difference the HTSC compounds exhibited was the anomalous behavior when placed in a magnetic field. Recall from Section 6.1.1.3 that there is also a critical magnetic field, H_c , above which the superconductor loses its superconductivity, and that this critical field is a function of temperature. In the metal and compound-based superconductors of Section 6.1.1.3, the transition from superconducting to nonsuperconducting at a specified temperature is a relatively sharp one as the critical field is reached. This relationship was illustrated in Figure 6.10 and Eq. (6.19). When compounds belonging to the new class of HTSC are placed in a magnetic field, however, the temperature region for the superconducting–nonsuperconducting transition broadens as the field is increased, as illustrated for $\text{YBa}_2\text{Cu}_3\text{O}_7$ in Figure 6.31. At low fields the resistivity drops sharply over a very narrow temperature range, whereas at high fields the transition range is quite large—nearly 15 K. Compare this resistivity–temperature behavior with that of Pb in Figure 6.6. Thus, two classes of superconductors are defined: Type I, also called “hard” superconductors, which exhibit a sharp transition; and Type II, also known as “soft” superconductors, which have a range of transition values. In Type II superconductors, the magnetic field starts penetrating into the material at a *lower critical field*, H_{c1} . Penetration increases until at the *upper critical field*, H_{c2} , the material is fully penetrated and the normal state is restored.

In addition to a critical temperature and critical field, all superconductors have a *critical current density*, J_c , above which they will no longer superconduct. This limitation has important consequences. A logical application of superconductors is as current-carrying media. However, there is a limit, often a low one, to how much current they can carry before losing their superconducting capabilities. The relationship between J_c , H_c , and T_c for a Type II superconductor is shown in Figure 6.32. Notice that the H_c – T_c portion of this plot has already been presented in Figure 6.10 for a Type I superconductor.

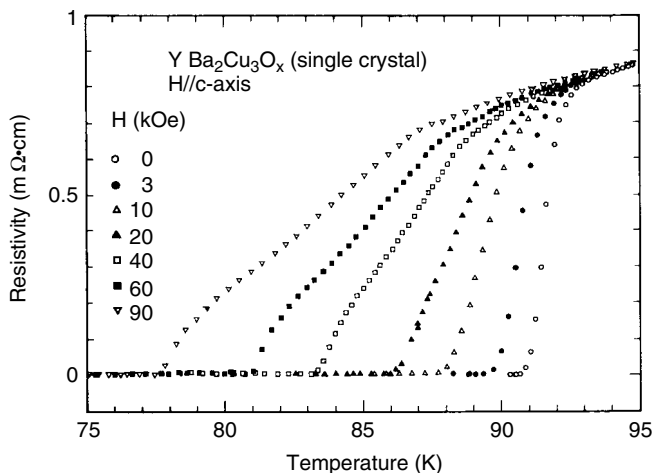


Figure 6.31 Variation of superconducting transition range in a magnetic field. Reprinted, by permission, from T. P. Sheahan, *Introduction to High-Temperature Superconductivity*, p. 121. Copyright © 1994 by Plenum Press.

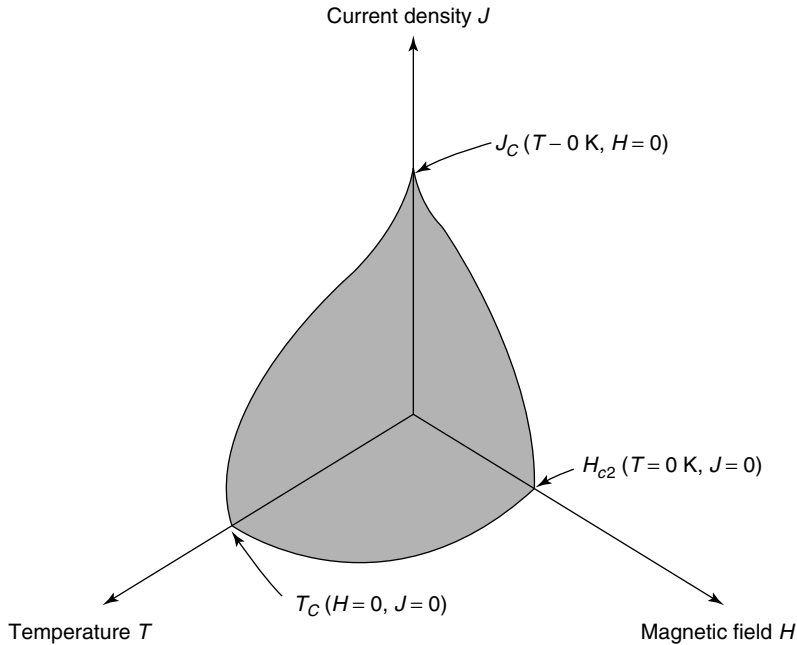


Figure 6.32 The relationship between temperature, magnetic field and current density in a Type II superconductor. Reprinted, by permission, from W. Callister, *Materials Science and Engineering: An Introduction*, 5th ed., p. 699. Copyright © 2000 by John Wiley & Sons, Inc.

Table 6.7 Some HTSC Materials Based on the Copper Oxide Lattice

Compound	T_c (K)
$\text{YBa}_2\text{Cu}_3\text{O}_7$	92
$(\text{BiPb})_2\text{Sr}_2\text{Ca}_2\text{Cu}_3\text{O}_x$	105
$\text{TlBa}_2\text{Ca}_2\text{Cu}_3\text{O}_y$	115
$\text{HgBa}_2\text{Ca}_2\text{Cu}_3\text{O}_y$	135

Most of the oxide Type II HTSC are based upon the copper oxide lattice. Some examples and their transition temperatures are given in Table 6.7. In all cases, the structure is essentially a laminar one, with planes of copper oxide in the center (see Figure 6.33), through which the superconducting current flows. These materials are thus highly anisotropic—very little current can flow perpendicular to the copper oxide planes. As a result, great pains are taken to produce these materials in a highly oriented manner and to use them such that current flows parallel to the copper oxide planes. The role of the elements other than copper and oxygen is secondary. In YBCO, yttrium is only a spacer and a contributor of charge carriers. Nearly any of the rare earth elements (holmium, erbium, dysprosium, etc.) can be substituted for yttrium without significantly changing T_c .

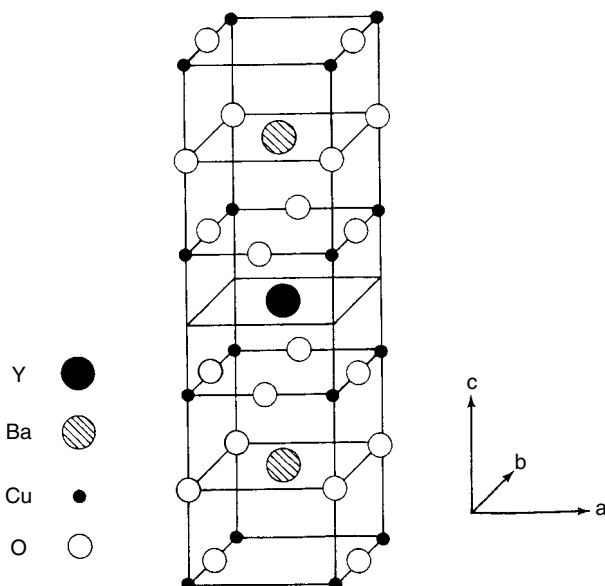


Figure 6.33 Unit cell structure of YBa₂Cu₃O₇ superconductor. Reprinted, by permission, from Sheahan, T. P., *Introduction to High-Temperature Superconductivity*, p. 5. Copyright © 1993 by Plenum Press.

It is beyond the scope of this text to describe the mechanism for charge transfer in the high-temperature superconductors. While there is still a great deal of discussion on the applicability of BCS theory (cf. Section 6.1.1.3) to HTSC materials, it is safe to say that many of the principles still apply—for example, density of states at the Fermi level. The interested reader should refer to existing literature [3,4] for more information on the structure and theory of copper oxide superconductors.

Finally, it would be misleading to suggest that these materials are the technological revolution they were first imagined to be. Like most other oxide ceramics, these materials are very brittle, and attempts to fabricate them in useful forms, such as wire, have proved problematic. The additional difficulty is with current density, as described earlier. For large-scale applications such as particle accelerator magnets, current densities on the order of 10^{10} A/m² are required. A high critical magnetic field would also be beneficial for some applications, where magnetic fields of 30 tesla (30,000 gauss) are required. Oxide superconductors meet neither of these requirements. As a result, the metallic superconductors are still the materials of choice for these high-end applications, since they are more easily formed into wires, and have higher J_c and H_c values, even though their T_c is low. Metallic superconductors of the niobium family are particularly useful in these regards and include NbTi, Nb₃Sn, NbZr, Nb₃Al, and Nb₃Ge.

6.1.2.5 Compound Semiconductors. The niobium-based superconducting compounds lead us naturally into another use for intermetallics—namely, semiconductors. This topic, too, was introduced earlier in this chapter (cf. Section 6.1.1.4 and 6.1.1.5), and we shall build upon those principles here to describe the semiconducting properties of compounds, ceramics, and glasses. The classification of intermetallics as ceramics

may be confusing at this point, but we do so due to the strong covalent nature of their bonds that are more similar to oxide ceramics than to the metallic bond of elemental semiconductors. It is this bond structure that influences the electrical properties; hence, we discuss them together in this section.

Recall that elemental semiconductors such as silicon, germanium, tin, and diamond belong to group IV in the periodic table. They are characterized by four valency electrons, resulting in a tetrahedral arrangement of atoms in a diamond-like structure (cf. Figure 1.40). A large number of compounds possess structural and electrical characteristics that are similar to those of elemental semiconductors, many of which are compounds formed between elements of groups III and V of the periodic table, termed III–V compounds. In these cases, slight deviations from stoichiometry can lead to extrinsic conduction. One of the more successful examples is gallium arsenide, GaAs. Gallium is a group III element and arsenic a group V element, and the resulting average valency in a 50–50 compound is four, just as for a group IV element. However, since the elemental substances have different electronegativities (cf. Table 1.4), the bond will be partly ionic in nature and the band gap will be higher than in the corresponding elemental semiconductor, Ge (see Table 6.8; some values may differ slightly from Table 6.2). These larger band gaps extend the useful range of conduction since intrinsic conduction becomes important only at correspondingly higher temperatures. The general decrease in band gap with increasing atomic number of the II–V compounds is a result of an increasing tendency toward metallic bonding.

Some semiconducting compounds can be of the II–VI type, which also has an average valence of four, but these have much more ionic character than III–V compounds. Their band gaps are thus larger, and in some cases they may even be viewed as insulators. For example, ZnS, with a band-gap energy of 3.6 eV, is an insulator, whereas ZnSe has an band gap of 2.8 eV, which is closer to a semiconductor. A wide variety of

Table 6.8 Electronic Properties of Some Elemental and Compound Semiconductors at Room Temperature

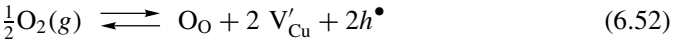
Material	Energy Gap (eV)	Mobility, μ $\frac{m^2}{V \cdot s}$		Effective Mass, m^*/m_0		Dielectric Constant
		Electrons	Holes	Electrons	Holes	
Silicon (Si)	1.1	0.135	0.048	0.97	0.5	11.7
Ge	0.67	0.390	0.190	1.60	0.3	16.3
Sn (gray)	0.08	0.200	0.100			
GaAs	1.40	0.800	0.025	0.072	0.5	12.5
GaSb	0.77	0.400	0.140	0.047	0.5	15.0
GaP	2.24	0.050	0.002			10.0
InSb	0.16	7.800	0.075	0.013	0.60	17.0
InAs	0.33	3.300	0.040	0.02	0.41	14.5
InP	1.29	0.460	0.015	0.07	0.40	14.0
PbS	0.40	0.060	0.020			

Source: Z. Jastrzebski, *The Nature and Properties of Engineering Materials*, 2nd ed. Copyright © 1976 by John Wiley & Sons, Inc.

compounds between transition metals and nonmetals also exhibit semiconductivity, but these materials are used infrequently because impurity control is much more difficult to achieve.

For nonstoichiometric compounds, the general rule is that when there is an excess of cations or a deficiency of anions, the compound is an *n*-type semiconductor. Conversely, an excess of anions or deficiency of cations creates a *p*-type semiconductor. There are some compounds that may exhibit either *p*- or *n*-type behavior, depending on what kind of ions are in excess. Lead sulfide, PbS, is an example. An excess of Pb²⁺ ions creates an *n*-type semiconductor, whereas an excess of S²⁻ ion creates a *p*-type semiconductor. Similarly, many binary oxide ceramics owe their electronic conductivity to deviations from stoichiometric compositions. For example, Cu₂O is a well-known *p*-type semiconductor, whereas ZnO with an excess of cations as interstitial atoms is an *n*-type semiconductor. A partial list of some impurity-controlled compound semiconductors is given in Table 6.9.

The conductivity of these materials can be controlled by the number of defects. In a *p*-type semiconductor such as Cu₂O, in which vacancies are formed in the cation lattice when the oxygen partial pressure is increased, we can develop relationships between conductivity and oxygen partial pressure. The overall reaction for the formation of vacancies and electron holes can be written in Kroger–Vink notation (cf. Section 1.2.6.1) as



From this reaction, we can then write a mass-action relation [cf. Eq. (3.1)] that is a function of temperature:

$$K(T) = \frac{[\text{V}'_{\text{Cu}}]^2 [h^\bullet]^2}{P_{\text{O}_2}^{1/2}} \quad (6.53)$$

Table 6.9 Some Impurity Compound Semiconductors

<i>n</i> -Type					
TiO ₂	Nb ₂ O ₅	CdS	Cs ₂ Se	BaTiO ₃	Hg ₂ S
V ₂ O ₅	MoO ₂	CdSe	BaO	PbCrO ₄	ZnF ₂
U ₃ O ₈	CdO	SnO ₂	Ta ₂ O ₅	Fe ₃ O ₄	
ZnO	Ag ₂ S	Cs ₂ S	WO ₃		
<i>p</i> -Type					
Ag ₂ O	CoO	Cu ₂ O	SnS	Bi ₂ Te ₃	MoO ₂
Cr ₂ O ₃	SnO	Cu ₂ S	Sb ₂ S ₃		Hg ₂ O
MnO	NiO	Pr ₂ O ₃	CuI		
<i>Amphoteric</i>					
Al ₂ O ₃	SiC	PbTe		Ti ₂ S	
Mn ₃ O ₄	PbS	UO ₂			
Co ₃ O ₄	PbSe	IrO ₂			

If the concentration of vacancies is largely determined by reaction with the atmosphere, then the conductivity should be proportional to the concentration of holes [which is equivalent to the concentration of vacancies according to Eq. (6.52)], and we obtain a relationship:

$$\sigma \propto [h^\bullet] = K(T)^{1/4} P_{O_2}^{1/8} \quad (6.54)$$

Experimentally, as illustrated in Figure 6.34, the electrical conductivity of Cu_2O is found to be proportional to $P_{O_2}^{1/7}$, which is in reasonable agreement with the prediction of Eq. (6.54). The variation of another oxide semiconductor, CdO , with temperature is also shown in Figure 6.34 for comparison.

As a final example of oxide-based semiconductors, recall from Section 6.1.2.3 that some chalcogenides exhibit high ionic conductivities. Chalcogenides also play a role in the high conductivities found in some glasses (see Figure 6.35). In addition to the group VI elements, chalcogenide glasses sometimes contain elements of Group V, such as P, As, Sb, and Bi, as well as other ingredients like Ge or the halides. These conductivities are electronic, and not ionic, in nature. Their melting points are low, sometimes below 100°C , and they are quite sensitive to corrosion. The conductivity in these glasses can be explained in terms of a special type of glass structure defects around which pairs of positive and negative centers are present, and with which electrons couple. In addition to their semiconductivity, these glasses have a unique *switching behavior*. If a voltage is applied at the normal high-resistivity state, called the “off state,” a critical current–voltage pair of values is eventually achieved at which point the glass suddenly switches into a low-resistivity state, called the “on state.” Each state is stable, and the process is reversible. This is a type of storage, or memory, effect.

6.1.2.6 MOSFETs. A type of semiconductor device that utilizes oxide ceramics is a *metal-oxide-semiconductor field-effect transistor*, abbreviated as MOSFET. Just like the semiconductor junction devices of Section 6.1.1.6, the MOSFET is composed of *n*- and *p*-type semiconductor regions within a single device, as illustrated in Figure 6.36.

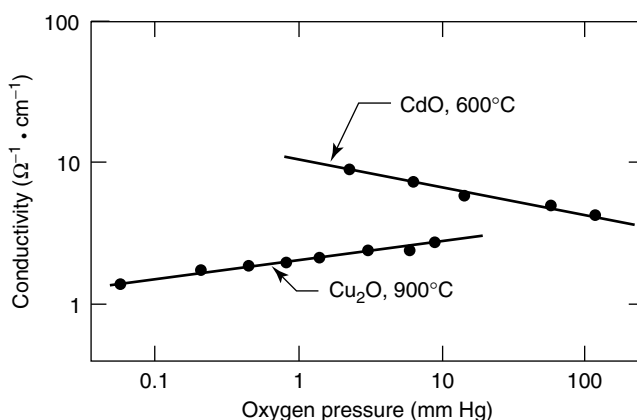


Figure 6.34 Electrical conductivity of two oxide semiconductors as a function of oxygen partial pressure. From W. D. Kingery, H. K. Bowen, and D. R. Uhlmann, *Introduction to Ceramics*. Copyright © 1976 by John Wiley & Sons, Inc. This material is used by permission of John Wiley & Sons, Inc.

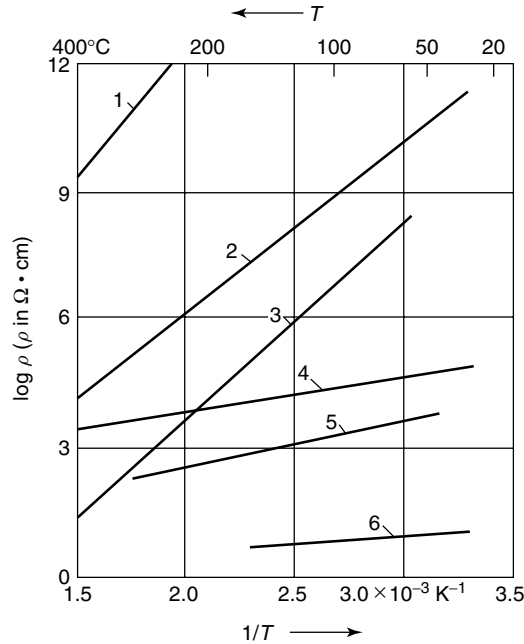


Figure 6.35 Temperature dependence of resistivity for some semiconducting glasses: (1) vitreous silica; (2) soda-lime silicate glass; (3) AsSeTe chalcogenide glass; (4) silicate glass with 18 mol% ($\text{Fe}_3\text{O}_4 + \text{MnO}$); and (6) borosilicate glass with 45 mol% ($\text{Fe}_3\text{O}_4 + \text{MnO}$). Reprinted, by permission, from H. Scholze, *Glass*, p. 312. Copyright © 1991 by Springer-Verlag.

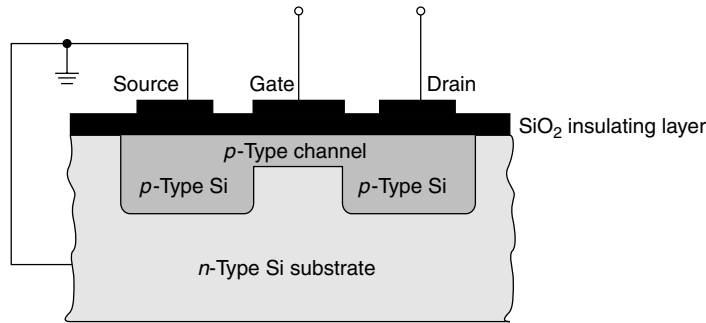


Figure 6.36 Schematic cross-sectional view of a MOSFET transistor. Reprinted, by permission, from W. Callister, *Materials Science and Engineering: An Introduction*, 5th ed., p. 634. Copyright © 2000 by John Wiley & Sons, Inc.

One such device consists of two small islands of *p*-type semiconductor with an *n*-type silicon substrate. The islands are joined by a narrow *p*-type channel. The oxide portion of the MOSFET is an insulating layer of silicon dioxide that is formed by surface oxidation of the silicon. Gate, drain, and source connectors are attached. The MOSFET differs from the junction transistor in that a single type of charge carrier, either an electron or a hole, is utilized, instead of both. The conductivity of the channel

is varied by the presence of an electric field imposed on the gate. For example, a positive field on the gate will drive holes out of the channel, thereby reducing the electrical conductivity. Thus, a small alteration in the field at the gate will produce a relatively large variation in current between the source and the drain. In this respect, the MOSFET is similar to the junction transistor, insofar as both create a signal amplification. The primary difference is that the gate current is exceedingly small in comparison to the base current of the junction transistor. As a result, MOSFETs are used where signal sources to be amplified cannot sustain an appreciable current.

6.1.3 Electrical Properties of Polymers

In this section, we consider the insulating properties of polymers as dielectrics, and we also describe their electrical- and ion-conducting capabilities. Given the highly insulative nature of most polymers, we begin with dielectric properties and then describe special types of polymers that conduct either electrons or ions.

6.1.3.1 Dielectric Polymers. Nonpolar polymers generally have dielectric constants in the 2–3 range while polar polymers can have values up to 7. Typical dielectric strengths of polymers are in the range of 20–50 kV/mm, which are approximately 2–10 times higher than ceramics and glasses and are hundreds of times higher than conducting metals and alloys.

Data from mechanical and dielectric measurements can be related in a qualitative, if not quantitative, manner. Formally, the dielectric constant can be regarded as the equivalent of the mechanical compliance. This highlights the fact that the dynamic mechanical techniques of Section 5.3 measure the ability of a polymer to resist movement, whereas the dielectric technique measures the ability of the system to move, at least the dipolar portions. Interestingly, the dielectric loss appears to match the loss modulus more closely than the loss compliance when the data are compared for the same system. Both techniques respond in a similar fashion to a change in the frequency of the measurement. When the frequency is increased, the transitions and relaxations that are observed in a sample appear at higher temperatures. We expect maximum losses at transition temperatures for both electrical and mechanical deformation, as illustrated for poly(chlorotrifluoroethylene) in Figure 6.37. Just as mechanical fatigue after many alternating cycles can cause a polymer to fail at a lower stress, so dielectric insulation can fatigue under electrical stresses.

6.1.3.2 Electrically Conducting Polymers. High values of resistivity are common for organic polymers, with 10^{12} to $10^{18} \Omega \cdot \text{cm}$ being typical. Electrical resistance can be lowered markedly by the addition of conductive fillers, such as carbon black or metal fillers, but the conductivity is due to the filler in this case. When we consider electronic conduction solely in homogeneous polymers, band theory is not totally suitable because the atoms are covalently bonded to one another, forming polymeric chains that experience weak intermolecular interactions. Thus, macroscopic conduction will require electron movement, not only along chains but also from one chain to another.

Polymers that display electronic conductivity are usually insulators in the pure state but, when reacted with an oxidizing or reducing agent, can be converted into polymer salts with electrical conductivities comparable to metals. Some of these polymers are listed in Figure 6.38, along with the conductivities of metals and ceramics for

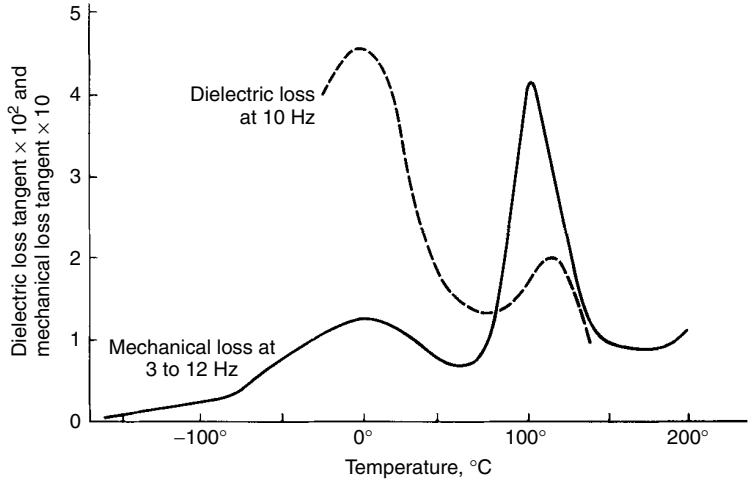


Figure 6.37 Mechanical and dielectric loss tangents for poly (chlorotrifluoroethylene). Reprinted, by permission, from F. Rodriguez, *Principles of Polymer Systems*, 2nd ed., p. 271. Copyright © 1982 by Hemisphere Publishing Corporation.

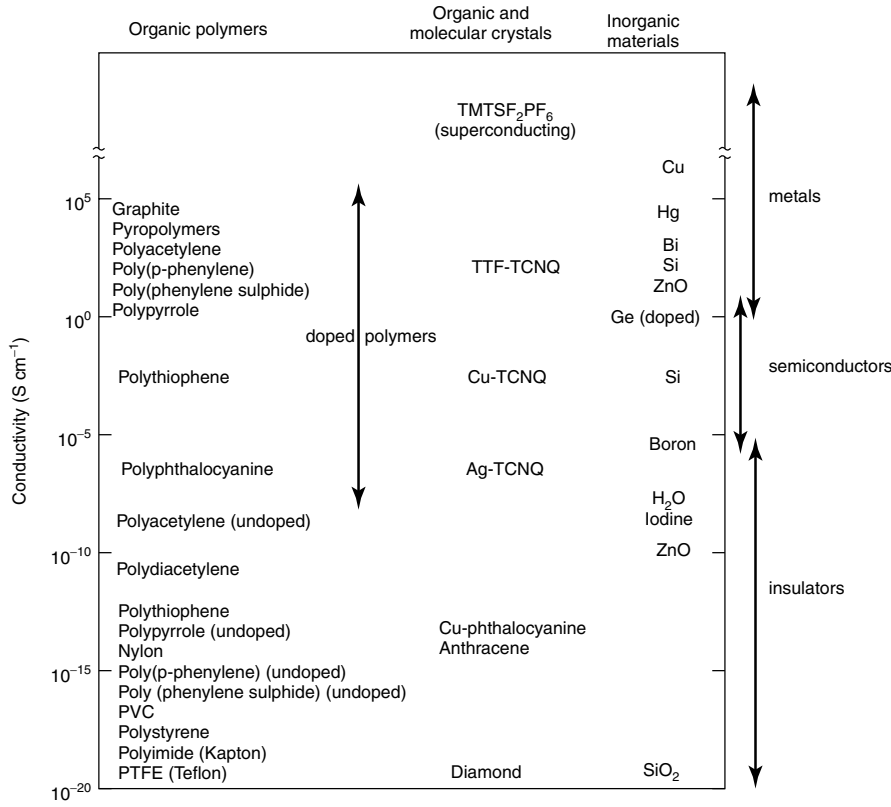
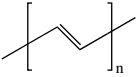
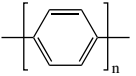
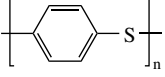
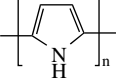
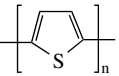
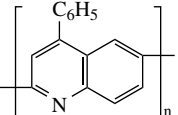


Figure 6.38 Conductivity ranges for doped and undoped polymers, inorganic materials and molecular crystals. One siemen (S) = 1 Ω⁻¹. Reprinted, by permission, from J. M. G. Cowie, *Polymers: Chemistry & Physics of Modern Materials*, 2nd ed., p. 411. Copyright © 1991 by J.M.G. Cowie.

comparison. The preparation and mechanism of conductivity in a few of these polymers will be elaborated upon.

One of the first polymers to exhibit electrical conductivity was polyacetylene. Normally a very poor conductor in the pure state, it was found that a highly conductive polymer could be formed by reacting it with I_2 . The result is a dramatic increase of over 10^{10} in conductivity. Polyacetylene is a *polyconjugated polymer*, the structure of which is shown in Table 6.10. Polyconjugation refers to the existence of multiple C–C bonds in the polymer, typically along the backbone. In a polyconjugated system, the π orbitals (cf. Section 1.0.4.2) are assumed to overlap, and they form a valance and a conduction band as predicted by band theory. If all the bond lengths were equal—that is, delocalization that led to each bond having equal double bond character—then the bands would overlap and the polymer would behave as a quasi-one-dimensional metal having good conductivity. Experimental evidence has shown that this is an unstable system that will undergo lattice distortion. The alternative is to have single and double bonds alternate along the backbone, which leads to an energy gap between the valence and conduction bands. The *trans* structure of polyacetylene has such an alternating single-bond–double-bond backbone. The *trans* structure of polyacetylene is also unique, because it has a twofold degenerate ground state in which sections A and B in Figure 6.39 are mirror images, and the single and double bonds can be interchanged without changing the energy. Thus, if the *cis* configuration begins to isomerize to the *trans* structure from different locations in a single chain, an

Table 6.10 Structures and Conductivities of Doped Conjugated Polymers

Polymer	Structure	Typical Methods of Doping	Typical Conductivity ($S\ cm^{-1}$) ⁻¹
Polyacetylene		Electrochemical, chemical (AsF_5 , I_2 , Li, K)	$500-1.5 \times 10^5$
Polyphenylene		Chemical (AsF_5 , Li, K)	500
Poly(phenylene sulphide)		Chemical (AsF_5)	1
Polypyrrole		Electrochemical	600
Polythiophene		Electrochemical	100
Poly(phenyl-quinoline)		Electrochemical, chemical (sodium naphthalide)	50

One siemen equals $1\ \Omega^{-1}$. Source: J. M. G. Cowie, *Polymers: Chemistry & Physics of Modern Materials*, 2nd ed. Copyright © 1991 by J.M.G. Cowie.

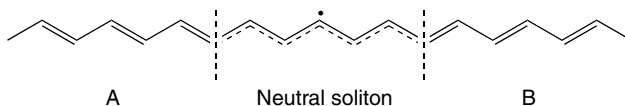


Figure 6.39 Isomerization of *cis* (A) and *trans* (B) sequences in polyacetylene that meet to form a soliton. Reprinted, by permission, from J. M. G. Cowie, *Polymers: Chemistry & Physics of Modern Materials*, 2nd ed., p. 417. Copyright © 1991 by J. M. G. Cowie.

A sequence may form and eventually meet a B sequence, as shown, but in doing so, a free radical, called a *soliton*, is produced. The soliton is a relatively stable electron with an unpaired spin and is located in a nonbonding state in the energy gap, midway between the conduction and valence bands. It is the presence of these neutral solitons which gives *trans*-polyacetylene the characteristics of an intrinsic semiconductor with conductivities of 10^{-7} to $10^{-8}(\Omega \cdot \text{cm})^{-1}$.

The conductivity of polyacetylene can be magnified by doping. Exposure of a polyacetylene film to dry ammonia gas leads to a dramatic increase in conductivity of $10^3(\Omega \cdot \text{cm})^{-1}$. Controlled addition of an acceptor, or *p*-doping, agent such as AsF_5 , I_2 , or HClO_4 removes an electron and creates a positive soliton (or a neutral one if the electron removed is not the free electron). Similarly, a negative soliton can be formed by treating the polymer with a donor, or *n*-doping, agent that adds an electron to the mid-gap energy level. This can be done by an electrochemical method. At high doping levels, the soliton regions tend to overlap and create new mid-gap energy bands that may merge with the valence and conduction bands, allowing freedom for extensive electron flow. Thus, in polyacetylene the charged solitons are responsible for making the polymer a conductor.

Poly(*p*-phenylene) has all the structural characteristics required of a potential polymer conductor. It is an insulator in the pure state, but can be doped using methods similar to those of polyacetylene to form both *n*- and *p*-type semiconductors. However, because poly(*p*-phenylene) has a higher ionization potential, it is more stable to oxidation and requires strong *p*-dopants. Examination of the structure shows that the soliton defect cannot be supported in poly(*p*-phenylene) because there is no degenerate ground state. Instead, it is assumed that conduction occurs because the mean free path of charge carriers extends over a large number of lattice sites and the residence time on any one site is small compared with the time it would take for a carrier to become localized. If, however, a carrier is trapped, it tends to polarize the local environment, which relaxes into a new equilibrium position. This deformed section of the lattice and the charge carrier then form a species called a *polaron*. Unlike the soliton, the polaron cannot move without first overcoming an energy barrier so movement is by a hopping motion. In poly(*p*-phenylene) the solitons are trapped by the changes in polymer structure because of the differences in energy and so a polaron is created which is an isolated charge carrier. A pair of these charges is called a *bipolaron*. In poly(*p*-phenylene) and most other polyconjugated conducting polymers the conduction occurs via the polaron or bipolaron (see Figure 6.40).

There are other types of semiconducting polymers as well, some of the more important of which are listed in Table 6.10. The conduction mechanism in most of these polymers is the polaron model described above. Applications for these polymers are growing and include batteries, electromagnetic screening materials, and electronic devices.

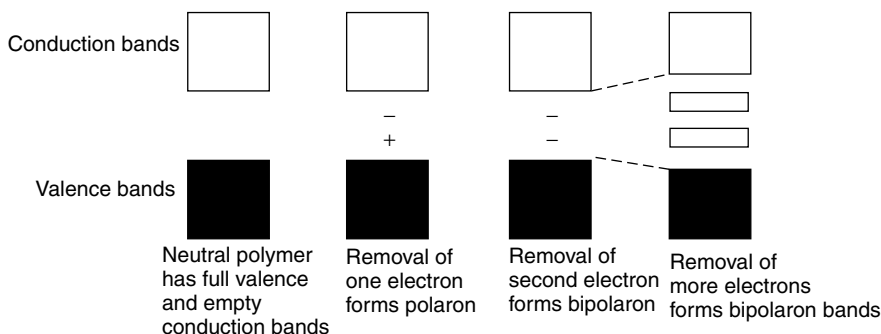


Figure 6.40 Proposed band structure for an oxidized *p*-type semiconducting polymer. Reprinted, by permission, from J. M. G. Cowie, *Polymers: Chemistry & Physics of Modern Materials*, 2nd ed., p. 419. Copyright © 1991 by J. M. G. Cowie.

6.1.3.3 Ion-Conducting Polymers. Recall that electrical conductivity can be the result of electronic conductivity, in which electrons are the charge carriers, ionic conductivity, in which ions are the charges carriers, or a combination of both. In the previous section, we saw how some conjugated polymers can conduct electrons. In this section we concentrate on ion-conducting polymers. There are generally two types of polymers in this category: those that conduct primarily hydrogen ions and those that conduct primarily larger anions. In both cases, the term *polymer electrolyte* is used to describe the type of ion-transporting polymeric material, although it is more commonly used to describe the latter. This should not be confused with the term *ionomer*, which describes polymers that contain ionic groups primarily involved in creating ionic bonds between chains. This is not to say that ionomers are incapable of ionic conductivity—they may well be. It is rather a matter of terminology usage. Ionomers typically have applications other than as ion conductors.

We begin by examining the structure and properties of polymer electrolytes. Initial investigations of ionically conductive polymers were principally focused on poly(ethylene oxide), PEO, when it was discovered that PEO can solvate a wide variety of salts, even at very high concentrations. The solvation occurs through the association of the metallic cations with the oxygen atoms in the polyether backbone (see Figure 6.41). The solvated ions can be quite mobile, and thus give rise to significant bulk ionic conductivities. Pure PEO is a semicrystalline polymer possessing both an amorphous and a crystalline phase at room temperature. Significant ionic transport occurs within the amorphous phase. This explains the dramatic decrease in ionic conductivity seen in many PEO-based systems for temperatures below the melting point of pure crystalline PEO ($T_m = 66^\circ\text{C}$), as shown in Figure 6.42. The crystalline PEO regions are nonconductive and serve to hinder bulk ionic transport.

The mobility of the ions in polymer electrolytes is linked to the local segmental mobility of the polymer chains. Significant ionic conductivity in these systems will occur only above the glass transition temperature of the amorphous phase, T_g . Therefore, one of the requirements for the polymeric solvent is a low glass-transition temperature; for example, $T_g = -67^\circ\text{C}$ for PEO.

One problem associated with polymer electrolytes arises from the opposing effects of increasing the salt concentration. Higher salt concentrations generally imply a higher density of charge carriers, which increases conductivity. However, through their

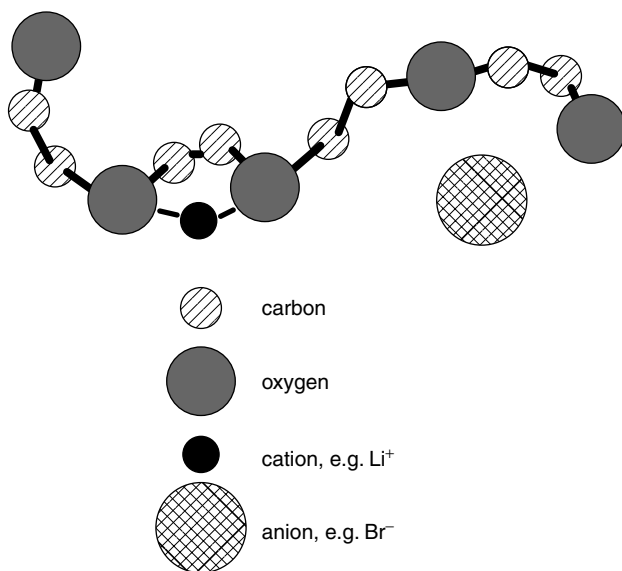


Figure 6.41 Schematic illustration of salt solvation by a PEO chain. Reprinted, by permission, from L. V. Interrante, L. A. Casper, and A. B. Ellis, eds. *Materials Chemistry*, p. 109. Copyright © 1995 by the American Chemical Society.

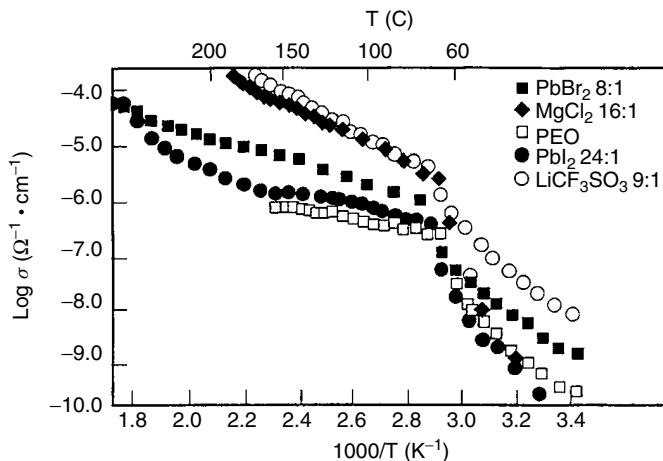


Figure 6.42 Temperature dependence of conductivity for various PEO-based polymer electrolytes containing divalent cations. Reprinted, by permission, from L. V. Interrante, L. A. Casper, and A. B. Ellis, eds., *Materials Chemistry*, p. 110. Copyright © 1995 by the American Chemical Society.

interactions with the polyether chains, inorganic salts increase the T_g as their concentrations increases. This increase in T_g tends to lower the mobility of the ions and thus decreases ionic conductivity. The balance of these two effects leads to a maximum in the conductivity at a specific salt concentration, which varies from system to system.

One method of reducing crystallinity in PEO-based systems is to synthesize polymers in which the lengths of the oxyethylene sequences are relatively short, such as through copolymerization. The most notable linear copolymer of this type is oxymethylene-linked poly(oxyethylene), commonly called amorphous PEO, or aPEO for short. Other notable polymer electrolytes are based upon polysiloxanes and polyphosphazenes. Polymer blends have also been used for these applications, such as PEO and poly(methyl methacrylate), PMMA. The general performance characteristics of the polymer electrolytes are to have ionic conductivities in the range of $10^{-3}(\Omega \cdot \text{cm})^{-1}$ or (S/cm).

Still higher total conductivities are achievable in a special class of hydrogen-ion (proton)-conducting polymers. These polymers are particularly useful for fuel-cell and chlor-alkali processing applications in which the efficient transfer of protons is critical. These polymers are of produced in membrane form and are therefore referred to as *proton-exchange membranes* (PEM).

The most common polymeric proton-exchange membrane is Nafion[®], which is manufactured in various forms by Du Pont. The generalized chemical structure of Nafion[®] is shown in Figure 6.43. It is a perfluorinated polymer, similar to Teflon[®], with small amounts of sulfonic (SO_3^-) or carboxylic functional groups. The microstructure of Nafion[®] is actually quite complex. In general, the models, supported primarily by small-angle X-ray scattering (SAXS) results, predict that the ionic portions of Nafion[®] tend to aggregate due to electrostatic interactions to form ionic clusters. It has been determined that the clusters are on the order of 30–50 Å in size, resulting in (1) a phase-separated polymer with discrete hydrophobic regions formed from the polymer backbone and (2) hydrophilic regions formed from the ionic clusters. These distinct regions are functionally important. Nafion[®] is believed to conduct protons due to extensive hydration that takes place in the ionic clusters. Waters of hydration are necessary, since according to one theory the protons are transported through the polymer in the form of hydronium ions, H_3O^+ [5].

The proton conductivity of Nafion[®] is orders of magnitudes higher than most other proton-conducting polymers (see Table 6.11). The conductivity, however, is

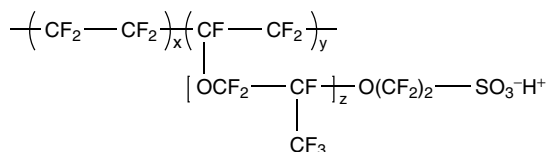


Figure 6.43 The generalized chemical structure of Nafion[®].

Table 6.11 Proton Conductivities of Selected Polymers

Polymer	Conductivity ($\Omega \cdot \text{cm})^{-1}$
Nafion [®]	2.2×10^{-1}
Polybenzimidazole (PBI)	2×10^{-4} – 8×10^{-4}
Poly(vinylidene)fluoride	10^{-2}

highly dependent upon (a) the relative humidity in the membrane and (b) the ability of the membrane to stay hydrated during operation. One particular drawback to all tetrafluoroethylene-based polymers is the inherent difficulty in processing due to limited solubility in most solvents. As a result, only certain types of geometries, such as thick films, are commercially available.

6.1.4 Electrical Properties of Composites

Because electronic and ionic conduction are so structure-sensitive, the simple rule-of-mixtures approach to estimating the conductivity and resistivity of composites is not normally of use. As a result, the conductivity of specific composites for specific applications must be experimentally determined. In the next two sections, we examine two examples of how composites can be used in electrical applications, and we describe the influence of each component on the electrical properties. The first example involves the electrical insulating properties of polymers, and the second one involves enhancing the electrically conducting properties of polymers.

6.1.4.1 Dielectric Properties of Glass-Fiber-Reinforced Polymers. As described in several of the previous sections on composites, the most common type of glass fiber used for reinforcement purposes is E-glass, which was originally developed for electrical insulation purposes, hence its name (“E” stands for “electrical grade”). It is not surprising, then, that when combined with organic resins such as epoxy, a class of materials results which can be readily molded into complex shapes that possess excellent insulating properties and high dielectric strength.

Some electrical properties of reinforcing fibers, composite resins, and the resulting composites are given in Tables 6.12, 6.13, and 6.14, respectively. These values should be taken as approximate only, especially for the composites, since fiber orientation, content, and field strength have an enormous impact on the dielectric properties of these materials. Some of the most widespread electrical applications for glass-fiber-reinforced epoxy systems are in printed circuit boards and electrical housing such as junction boxes.

One interesting application of the dielectric properties of the resins in these composite systems is that it provides an opportunity to monitor the cure characteristics of

Table 6.12 Some Electrical Properties of Selected Reinforcing Glass Fibers

Property	E-Glass	S-Glass	D-Glass
Dielectric constant, 10^6 Hz	5.80	4.53	3.56
Dielectric constant, 10^{10} Hz	6.13	5.21	4.00
Loss tangent, 10^6 Hz	0.001	0.002	0.0005
Loss tangent, 10^{10} Hz	0.0039	0.0068	0.0026

Source: Handbook of Fiberglass and Advanced Plastics Composites, G. Lubin, ed. Copyright © 1969 by Reinhold Book Corporation.

Table 6.13 Some Electrical Properties of Selected Resins

Property	Phenolic	Epoxy	Polyester	Silicone
Resistivity, $\Omega \cdot \text{cm}$	$10^{12} - 10^{13}$	$10^{16} - 10^{17}$	10^{14}	$10^{11} - 10^{13}$
Dielectric strength, $\text{V}/\mu\text{m}$	14–16	16–20	15–20	7.3
Dielectric constant, 60 Hz	6.5–7.5	3.8	3.0–4.4	4.0–5.0

Source: Handbook of Fiberglass and Advanced Plastics Composites, G. Lubin, ed. Copyright © 1969 by Reinhold Book Corporation.

Table 6.14 Some Electrical Properties of Selected Glass-Fiber-Reinforced Resins

Property	GFR Nylon	GFR Polypropylene	GFR Phenolic	GFR (Laminate)	GFR Polyester	GFR Silicone (Laminate)
Resistivity, $\Omega \cdot \text{cm}$	$2.6 - 5.5 \times 10^{15}$	1.7×10^{16}	$10^{10} - 10^{11}$	$6.6 \times 10^7 - 10^9$	$10^{12} - 10^{13}$	$2 - 5 \times 10^{14}$
Dielectric strength, $\text{V}/\mu\text{m}$	16–18	12–19	15–17	26–30	8–16	28.5
Dielectric constant, 60 Hz	4.6–5.6	2.3–2.5	7.1–7.2	4.4	4.6–5.2	3.9–4.2

Source: Shackelford, J. and W. Alexander, *The CRC Materials Science and Engineering Handbook*. Copyright © 1992 by CRC Press.

Cooperative Learning Exercise 6.4

Assume that the conductivity of a unidirectional, continuous fiber-reinforced composite is a summation effect just like elastic modulus and tensile strength; that is, an equation analogous to Eq. (5.88) can be used to describe the conductivity in the axial direction, and one analogous to (5.92) can be used for the transverse direction, where the modulus is replaced with the corresponding conductivity of the fiber and matrix phase. Perform the following calculations for an aluminum matrix composite reinforced with 40 vol% continuous, unidirectional Al_2O_3 fibers. Use average conductivity values from Appendix 8.

Person 1: Calculate the conductivity of the composite in the axial direction.

Person 2: Calculate the conductivity of the composite in the transverse direction.

Compare your answers. How many orders of magnitude difference is there in the two conductivities?

$$\sigma_{\text{axial}} = \sigma_{\text{matrix}} V_f + \sigma_{\text{fiber}} V_m = (10^{-10})(0.4) + (10^{-11})(0.6) = 4 \times 10^{-11} \text{ } \Omega^{-1} \cdot \text{m}^{-1}$$

$$\sigma_{\text{trans}} = \frac{\sigma_{\text{matrix}} \sigma_{\text{fiber}}}{\sigma_{\text{matrix}} V_f + \sigma_{\text{fiber}} V_m} = \frac{(10^{-10})(10^{-11})}{(10^{-10})(0.4) + (10^{-11})(0.6)} = 2.5 \times 10^{-21} \text{ } \Omega^{-1} \cdot \text{m}^{-1}$$

Answers: $\sigma_{\text{axial}} = 4 \times 10^{-11} \text{ } \Omega^{-1} \cdot \text{m}^{-1}$; $\sigma_{\text{trans}} = 2.5 \times 10^{-21} \text{ } \Omega^{-1} \cdot \text{m}^{-1}$. 17 orders.

the resin in the composite. In-process cure monitoring ensures that each molded part has properly cured before the mold is opened. The dielectric loss [see Eq. (6.47)] has been shown to increase rapidly in the beginning of the cure cycle (see Figure 6.44), attain a peak, then reduce to a constant value as the curing reactions are completed. At the beginning of the cure cycle, the resin viscosity in the uncured prepreg is relatively high so that the dipole and ion mobilities are restricted. This results in low loss factors just after the uncured prepreg is placed in the mold. As the temperature of the prepreg increases in the mold, the resin viscosity is reduced and the loss factor increases owing to greater dipole and ion mobilities (see Figure 6.25). As soon as the gel point is reached, the resin viscosity increases rapidly and the loss factor decreases. At a full degree of cure, the loss factor levels off to a constant value.

The technique for monitoring the dielectric loss factor is relatively simple. Two metal electrodes are placed opposite each other at critical locations on opposite sides of the mold. When the sheet molding compound (SMC), is placed between the electrodes, a capacitor is formed. The dielectric power loss is monitored continually throughout the molding cycle, as outlined in Section 6.1.2.2.

6.1.4.2 Metal Oxide-Polymer Thermistors. The variation of electrical properties with temperature heretofore described can be used to tremendous advantage. These so-called thermoelectric effects are commonly used in the operation of electronic temperature measuring devices such as *thermocouples*, *thermistors*, and resistance-temperature detectors (*RTDs*). A thermocouple consists of two dissimilar metals joined at one end. As one end of the thermocouple is heated or cooled, electrons diffuse toward

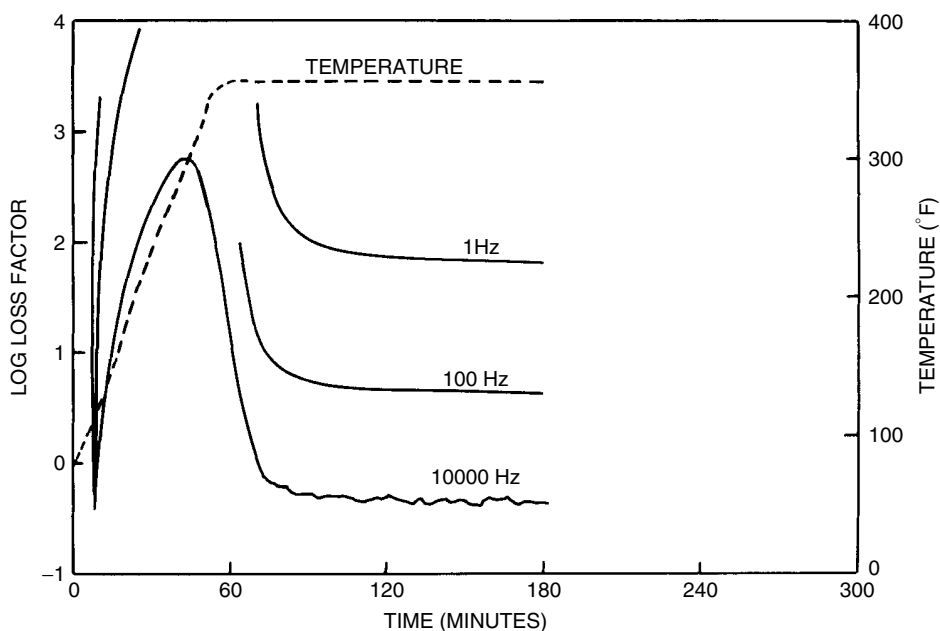


Figure 6.44 Dielectric loss factor as a function of cure time and frequency of the oscillating electric field in a fiber-reinforced polymer. Reprinted, by permission, from P. K. Mallick, *Fiber-Reinforced Composites*, p. 365. Copyright © 1988 by Marcel Dekker, Inc.

the cold end, and a *Seebeck voltage* is produced in each wire. Owing to the intentional dissimilarity between the Seebeck voltage in the two wires that compose the thermocouple, a voltage difference is established between the two wires, which can be measured and calibrated to temperature. A thermistor, on the other hand, directly correlates the change in resistivity of a substance to temperature. Although thermocouples are more widely utilized due to their inherent stability and larger operating temperature range, the thermistor concepts allows us to illustrate a thermoelectric effect that utilizes composite materials.

Thermistors can exhibit two primary resistance effects (see Figure 6.45): the *negative temperature coefficient* (NTC) effect, and the *positive temperature coefficient* (PTC) effect. In composites, these transitions arise from an individual component, such as a semiconductor–metal transition exhibited by V_2O_3 metallic filler, or result from a product property of the composite. Traditionally, PTC thermistors have been prepared from doped-BaTiO₃, such that the grains are semiconducting and the grain boundaries are insulating. The PTC effect occurs during heating through the Curie point, at which point the crystal structure changes from tetragonal to cubic, accompanied by a ferroelectric transition (see Section 6.1.2.2). In the ferroelectric state, the spontaneous polarization compensates for the insulating grain boundaries, resulting in a low resistivity. Although BaTiO₃ thermistors exhibit relatively large (six orders of magnitude) changes in resistivity with temperature, they have high room-temperature resistivities and are expensive to produce.

Composite-based PTC thermistors are potentially more economical. These devices are based on a combination of a conductor in a semicrystalline polymer—for example, carbon black in polyethylene. Other fillers include copper, iron, and silver. Important filler parameters in addition to conductivity include particle size, distribution, morphology, surface energy, oxidation state, and thermal expansion coefficient. Important polymer matrix characteristics in addition to conductivity include the glass transition temperature, T_g , and thermal expansion coefficient. Interfacial effects are extremely important in these materials and can influence the ultimate electrical properties of the composite.

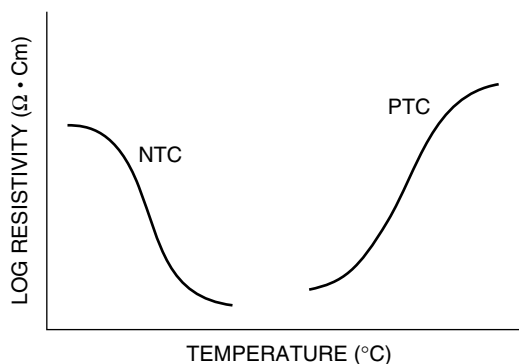


Figure 6.45 Schematic illustration of negative temperature coefficient (NTC) and positive temperature coefficient (PTC) effects. Reprinted, by permission, from D. M. Moffatt, J. Runt, W. Huebner, S. Yoshikawa, and R. Nenham, in *Composite Applications*, T. L. Vigo and B. J. Kinzig, eds., p. 52. Copyright © 1992 by VCH Publishing, Inc.

There is a relatively sharp increase in resistivity near the melting temperature of the polymer, T_m , at which point a discontinuous change in specific volume occurs. The PTC phenomenon in these composites is believed to be the result of a separation of the conducting particles due to the thermal expansion of the polymer. Because the transition occurs at the melting point, one may control the PTC transition by utilizing a different polymer matrix. Composites prepared with crystalline polymers can also exhibit dramatic NTC effects just above the melting point, due to the relaxation of the polymer structure. This effect may be eliminated by crosslinking the polymer or adding a third filler to stabilize the matrix.

Although a majority of these composite thermistors are based upon carbon black as the conductive filler, it is difficult to control in terms of particle size, distribution, and morphology. One alternative is to use transition metal oxides such as TiO , VO_2 , and V_2O_3 as the filler. An advantage of using a ceramic material is that it is possible to easily control critical parameters such as particle size and shape. Typical polymer matrix materials include poly(methyl methacrylate) PMMA, epoxy, silicone elastomer, polyurethane, polycarbonate, and polystyrene.

The resistivity–temperature behavior for a V_2O_3 –PMMA composite is shown in Figure 6.46. When the NTC transition in the V_2O_3 is combined with the PTC effect in the composite, a resistivity–temperature curve with a square-well appearance results. As the amount of V_2O_3 is increased, the PTC effect begins to appear near 50 vol% V_2O_3 . The optimum composition is that which yields the lowest room-temperature resistivity and the largest PTC effect. As the amount of conducting filler is increased, the temperature at which the PTC effect occurs moves to higher temperatures. The PTC exhibited in the composite is related to a phenomenon called *percolation*, which deals with the number and properties of neighboring entities and the existence of a sharp transition at which long-range connectivity in the system appears or disappears. At low

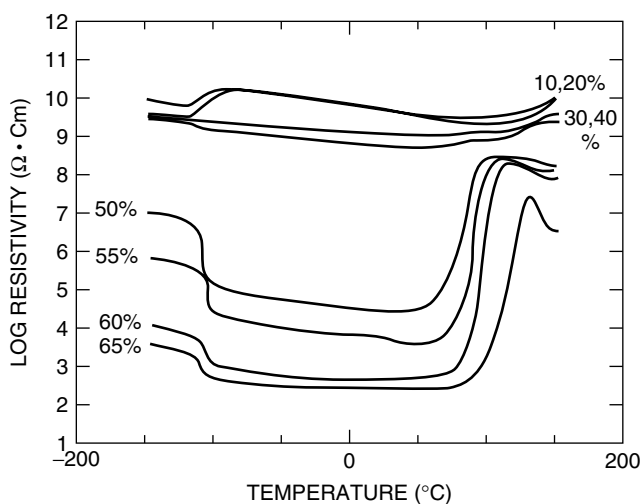


Figure 6.46 Temperature dependence of resistivity for a V_2O_3 –PMMA composite of various volume fractions V_2O_3 at 1 kHz. Reprinted, by permission, from D. M. Moffatt, J. Runt, W. Huebner, S. Yoshikawa, and R. Nenham, in *Composite Applications*, T. L. Vigo and B. J. Kinzig, eds., p. 56. Copyright © 1992 by VCH Publishers, Inc.

filler concentrations, a high resistivity is due to the insulating phase. As the volume fraction is increased, conducting paths start to form, resulting in a decrease in resistivity. This region is known as the *percolation threshold*. At higher filler concentrations, a saturation region is reached wherein the resistivity is relatively constant due to extensive particle contacts and eventually approaches the value of the pure conductor.

6.1.5 Electrical Properties of Biologics

The principles introduced in the previous sections have important applications in the description of many biological processes. Both ionic and electron charge transfer play important roles in bioprocesses such as nerve and muscle cell function. While an understanding of these processes would be a worthwhile academic exercise, there is little new to be learned about the materials involved—that is, structure–property relationships for the biological materials. What would be useful to us is a description of the electrical properties of the biological materials—for example, the electrical conductivity of various tissues, or the ion-conducting capacity of membranes. Unfortunately, while some of this information may indeed exist, it is difficult to find all the necessary information, and it is even more difficult to make generalizations. In other words, the human body, and other biological units like it, are complex chemoelectric devices that are not yet fully understood from a materials standpoint. There are any number of ongoing scientific studies aimed at better understanding these biological processes and utilizing them for the development of biomaterials, such as the stimulation of nerve cell growth using electrically conducting polymers [6], the electrical properties of amphiphilic lipid membranes [7], and the electrical properties of hydroxyapatite thin films [8]. These topics, while fascinating, are much too specific for this introductory text. Instead, let us concentrate on two, more general, classes of artificial biomedical devices that may give us some insight into the electrical processes in biologics: biosensors and bioelectrodes.

6.1.5.1 Biosensors. The term *bioelectrode* is broadly used to denote a class of devices that transmit information into or out of the body as an electrical signal. Those bioelectrodes that transmit information out of the body are generally called *biosensors*. Any type of sensor falls into one of two general categories: physical or chemical. Physical parameters of biological interest include pressure, volume, flow, electrical potential, and temperature. Chemical sensing involves the determination of the concentration of chemical species in a volume of gas, liquid, or tissue. The species can vary in size from a hydrogen ion to a live pathogen. When the species is complex, such as a parasite or a tumor, an interaction with another biological entity is required to recognize it. In this section, we give two examples of chemical biosensors: ion sensors and glucose sensors.

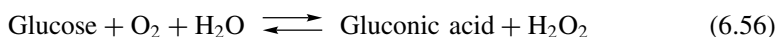
Many simple ions such as K^+ , Na^+ , Cl^- , and Ca^{2+} are normally kept within a narrow range of concentrations in the body, and they must be monitored during critical care. Potentiometric sensors for ion, also called *ion-selective electrodes* or ISEs, utilize a membrane that is primarily semipermeable to one ionic species. The ionic species is used to generate a voltage that generally obeys the Nernst equation [cf. Section 3.1.3.2 and Eq. (3.24)]

$$E = C + \frac{RT}{zF} \ln[a_i + k_{ij}(a_j)^{z/y}] \quad (6.55)$$

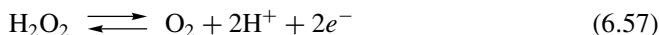
where E is the potential in response to an ion, i , of activity a_i and charge z ; C is a constant; k_{ij} is the selectivity coefficient; and j is any interfering ion of charge y and activity a_j .

Glasses exist that function as selective electrodes for many different monovalent and some divalent cations. Alternatively, a hydrophobic membrane can be made semipermeable if a hydrophobic molecule called an *ionophore* that selectively binds an ion is dissolved in it. The selectivity of the membrane is determined by the structure of the ionophore. Some ionophores are natural products, such as gramicidin, which is highly specific for K^+ , whereas others such as crown ethers and cryptands are synthetic. Ions such as S^{2-} , I^- , Br^- , and NO_3^- can be detected using quaternary ammonium cationic surfactants as a lipid-soluble counterion. ISEs are generally sensitive in the 10^{-1} to 10^{-5} M range, but are not perfectly selective. The most typical membrane material used in ISEs is polyvinyl chloride plasticized with dialkylsebacate or other hydrophobic chemicals.

Biosensors are also available for glucose, lactate, alcohol, sucrose, galactose, uric acid, alpha amylase, choline, and L-lysine. All are amperometric sensors based on O_2 consumption or H_2O_2 production in conjunction with the turnover of an enzyme in the presence of substrate. In the case of glucose oxidase reaction, the normal biological reaction is:



Under many circumstances, the concentration of oxygen is rate-limiting, so the sensor often measures not glucose, but the rate at which oxygen diffuses to the enzyme to reoxidize its cofactor. There are two electrochemical ways to couple the reaction to electrodes: (a) monitor depletion of oxygen by reducing what is left at an electrode or (b) monitoring buildup of H_2O_2 by oxidizing it to O_2 and protons:



An alternative method is to use electrochemical mediators that are at a higher concentration than O_2 and can therefore be shuttled back and forth between the protein and the electrode faster than the enzyme is reduced, so that the arrival of the glucose is always rate-limiting. A typical chemical that works in this way is ferrocene, which is an iron cation between two cyclopentadienyl anions, as shown in Figure 6.47. It exists in neutral and +1 oxidation state that are readily interconvertible at metal or carbon electrodes.

Most of the sensors are macroscopic and are employed in the controlled environment of a clinical chemistry analyzer. However, complete glucose sensors are available that

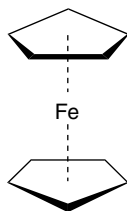


Figure 6.47 The structure of ferrocene.

contain disposable glucose oxidase-based electrodes, power supply, electronics, and readout in a housing the size of a ballpoint pen. The ultimate goal is an implantable glucose sensor, toward which much progress is being made.

6.1.5.2 Electrical Stimulation Devices. Bioelectrodes that transmit electrical signals into the body are generally known as *electrical stimulation* devices, examples of which include cardiac pacemakers, transcutaneous electronic nerve stimulators (TENS) for pain suppression, and neural prostheses such as auditory stimulation systems for the deaf and phrenic nerve stimulators for artificial respiratory control. In these, and other similar devices, electrodes transmit current to appropriate areas of the body for direct control of, or indirect influence over, target cells.

Electrically excitable cells, such as those of the nervous system or heart, possess a potential difference across their membranes of approximately 60–90 mV. The inside of the cell is negative with respect to the outside. Such cells are capable of transmitting electrical signals, called *action potentials*, along their lengths. During an action potential, the cellular membrane (cf. Figure 1.89) changes polarity for a duration of about 1 ms, so that the inside of the cell becomes positive with respect to the outside. Excitable cells can be artificially stimulated by electrodes that introduce a transient electric field of proper magnitude and distribution. In general, the field generated near a cathodically driven electrode can be used to depolarize most efficiently an adjacent excitable cell's axonal process above a threshold value at which an artificially generated action potential results. Cathodes will tend to draw current outward through nearby cell membranes. In their passive state, such membranes can be electrically modeled as parallel arrangements of resistors and capacitors. Outward current therefore elicits depolarizing resistive potential drops and capacitive charging. Depending upon the specific application and electrode properties, a single action potential in a nerve cell might be elicited using currents on the order of a few microamps to a few milliamps, for durations of micro- to milliseconds.

The materials used in bioelectrodes for electrical stimulation vary, depending upon the specific application. For example, intramuscular stimulation requires an electrode with excellent long-term strength and flexibility, but not very high stimulation charge densities. Stimulation of the visual cortex through placement of electrodes on the cortical surface, however, requires little mechanical flexibility in an electrode material with relatively moderate charge needs. Intracortical stimulation electrodes must be fabricated on a very small scale and must be capable of injecting very high charge densities. In all instances, the device must be biocompatible. In most neural control devices, the surface area of the exposed material is relatively small ($< 1 \text{ cm}^2$) so that problems associated with passive biocompatibility are minor. The noble metals such as platinum, iridium, rhodium, gold, and palladium are generally preferred for the conductor material due to their low chemical reactivity and high resistance to corrosion. The insulating materials around the conductive electrodes, however, have a much higher volume and surface area, and they represent the largest problems associated with biocompatibility. Thin layers of medical-grade silicone rubber, poly(tetrafluoroethylene), polyimide, or epoxy are typically used for this purpose. Other devices are fabricated using lithography and thin-film technology that are typically insulated with ceramics such as SiO_2 and Si_3N_4 . These insulating materials must be carefully selected to provide pinhole-free coatings, good adhesion to the conductors, and biocompatibility with the tissue.

Once inserted, charge transfer between the metal electrode and biological tissue requires a change in charge carriers from electrons in the metal to ions in the tissue

fluid. This change in charge carriers occurs by one of two mechanisms. The first is a capacitive mechanism involving only the alignment of charged species at the electrode–tissue interface, in which charging and discharging occurs at the electrode double layer. This mechanism is preferred because no chemical change occurs in either the tissue or the electrode. The amount of charge that can be transferred solely by capacitive charging is only about $20 \mu\text{C}/\text{cm}^2$ of “real” electrode surface area, which is the actual area of the electrode–tissue interface. The second mechanism involves the exchange of electrons across the electrode–tissue interface and therefore requires that some chemical species be oxidized or reduced. Metal electrodes almost always inject charge by this so-called *faradaic charge transfer process*, because the amount of charge required greatly exceeds that available from the capacitive mechanism alone. The types of reactions that occur at the electrode–tissue interface include monolayer oxide formation and reduction, the electrolysis of water, or the oxidation of chloride ions.

Capacitor electrodes are considered the ideal type of stimulation electrode because the introduction of a dielectric at the electrode–tissue interface allows charge flow completely by charging and discharging of the dielectric film. The oxide film that is produced on tantalum by anodic polarization withstands substantial voltage without significant current leakage and permits charge flow without the risk of faradaic charge transfer reactions. Anodized titanium has higher dielectric strength than anodized tantalum, but its current leakage is too high for electrode applications. Capacitor electrodes based on tantalum–tantalum pentoxide have a charge storage capacity of about $100\text{--}150 \mu\text{C}/\text{cm}^2$. Their use is limited to neural prosthesis applications having electrodes about 0.05 cm^2 or larger in surface area, such as peripheral nerve stimulators. It is not possible to obtain adequate charge storage capacity in electrodes smaller than 10^{-3} cm^2 .

6.2 MAGNETIC PROPERTIES OF MATERIALS

Just as materials have a response when placed in an electric field, they can have a response when placed in a magnetic field. We will see in this section that many of the concepts of permanent dipoles and dipole alignment in response to an applied field that were described in the context of electrical fields apply to magnetic fields as well. There are a few differences, however, and we will also see that there are fewer materials with specialized magnetic properties than there were with specialized electrical and electronic properties. The magnetic properties of materials are nonetheless important, and they are applied in a number of technologically important areas.

6.2.1 Magnetic Properties of Metals and Alloys

6.2.1.1 The Molecular Origins of Magnetism. Recall from Section 1.0.3.2 that charge separation in a molecule leads to an electric dipole, and also recall that this dipole can be either permanent (intrinsic) or induced. And just as the magnitude of the electric dipole moment, p_e , was proportional to the charge and separation distance, so is the magnitude of the *magnetic dipole moment*, p_m , proportional to the pole strength, m , and the separation distance, a :

$$p_m = m \cdot a \quad (6.58)$$

Intrinsic magnetic dipole moments arise from two sources: (a) the orbital motion of electrons about the nucleus and (b) the net spin of unpaired electrons. In the first case, the intrinsic magnetic dipole is not observed until acted on by an external field. In the presence of an external magnetic field, the component of the magnetic moment that is parallel to the applied field is given by $m_l(eh/4\pi m_e)$, where m_l is the magnetic quantum number, e and m_e are the magnitude of the electronic charge and mass, respectively, and h is Planck's constant. Any filled shell or subshell contributes nothing to the orbital magnetic moment of an atom, but occupied outer electronic orbitals contribute to a net atomic magnetic moment (parallel to the applied field) if the summation of magnetic quantum numbers is not equal to zero. The quantity $eh/4\pi m_e$ is a fundamental quantity in magnetism called the *Bohr magneton* and is assigned the symbol μ_B . The Bohr magneton has a value of $9.27 \times 10^{-24} \text{ A} \cdot \text{m}^2$. The quantity $h/2\pi$ is the angular momentum of the electron. The second type of intrinsic magnetic dipole moment is associated with the spin of an electron. When the spin quantum number, m_s , is $+1/2$ (spin up), the magnetic moment is $+\mu_B$ (parallel to the magnetic field), and when $m_s = -1/2$ (spin down), the magnetic moment is $-\mu_B$ (antiparallel to the magnetic field). For free atoms like Na and Mg, no permanent magnetic moment exists because there are no unpaired electrons and the individual orbital momentums sum to zero. Free atoms like Na and molecules like O_2 , each of which have unpaired electrons (see Figure 1.7), possess a permanent magnetic dipole moment. When both spin and orbital components of the magnetic dipole moment exist, they are additive, though not in a simple arithmetic manner.

Recall from Section 1.0.4.2 that the pairing of electrons in molecular orbitals of molecules results in two types of magnetism. Diamagnetism is the result of all paired electrons in the molecular orbitals, whereas paramagnetism results from unpaired electrons in the molecular orbitals. Let us now examine how these two types of magnetism behave in the presence of an imposed magnetic field. This can be done by comparing the *magnetic induction*, B , or internal magnetic field strength, within a substance in the presence of an external magnetic field, H , to the induction produced by the field alone in a vacuum, B_0 .

First, consider the case of a field in a vacuum. The field can be created by passing current, I , through a coil of N turns (called a *solenoid*) of total length, l , as shown in Figure 6.48. The field is simply given by:

$$H = \frac{N \cdot I}{l} \quad (6.59)$$

Recall from Eq. (6.2) that the induction and field are related as follows:

$$B_0 = \mu_0 H \quad (6.60)$$

where the subscript “0” has been added to indicate a vacuum, and boldface has been dropped to indicate that the inductance and field—normally vectors—are treated as scalar quantities only. The constant μ_0 is the *magnetic permeability in vacuum* and has a value of $4\pi \times 10^{-7} \text{ Wb/A} \cdot \text{m}$.

If a substance is now placed inside the solenoid, as shown in Figure 6.49, the magnetic field remains the same according to Eq. (6.59) as long as the current remains

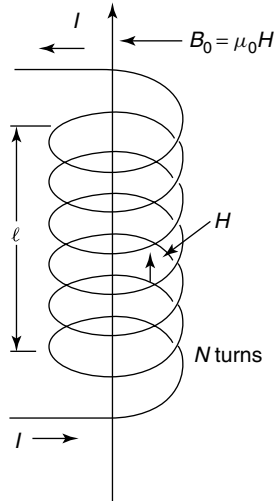


Figure 6.48 Schematic diagram of a solenoid in a vacuum. From K. M. Ralls, T. H. Courtney, and J. Wulff, *Introduction to Materials Science and Engineering*. Copyright © 1976 by John Wiley & Sons, Inc. This material is used by permission John Wiley & Sons, Inc.

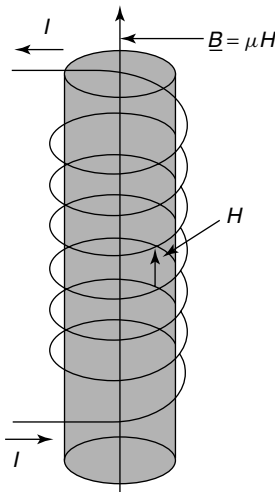


Figure 6.49 Schematic diagram of a substance within a solenoid. From K. M. Ralls, T. H. Courtney, and J. Wulff, *Introduction to Materials Science and Engineering*. Copyright © 1976 by John Wiley & Sons, Inc. This material is used by permission John Wiley & Sons, Inc.

the same, but due to interactions between the field and the substance, the inductance is different (lower or higher), and Eq. (6.60) becomes

$$B = \mu_0 H + \mu_0 M \quad (6.61)$$

where the second term contains the *magnetization*, M , of the substance. Magnetization represents the net magnetic dipole moment per unit volume that is aligned parallel

to the external field. For many substances, a direct proportionality exists between the magnetization and the magnetic field:

$$M = \chi H \quad (6.62)$$

with the dimensionless proportionality constant, χ , called the *magnetic susceptibility*. Do not confuse the magnetic susceptibility with the electronegativity of an element, which is represented by the same variable. The benefit of introducing magnetic susceptibility is that it is a material property, independent of quantity. Even if a direct proportionality does not exist between the magnetization and the magnetic field, Eq. (6.62) still defines the instantaneous magnetic susceptibility and can be substituted into Eq. (6.61) to yield

$$B = \mu_0(1 + \chi)H \quad (6.63)$$

The quantity $(1 + \chi)$ is called the *relative magnetic permeability* (also dimensionless), which is also a material property.

Cooperative Learning Exercise 6.5

A coil of wire 0.20 m long and having 200 turns carries a current of 10 A.

Person 1: Calculate the magnetic field strength in vacuum.

Person 2: Look up the magnetic susceptibility for titanium.

A bar of titanium is now placed in the coil. Combine your information to make the following calculations.

Person 1: Calculate the flux density (magnetic induction) with the titanium bar in the coil.

Person 2: Calculate the flux density (magnetic induction) in vacuum (without the titanium bar).

Compare your answers. Does the titanium bar affect the magnetic induction significantly? Why or why not?

Person 1: What is the relative magnetic permeability of titanium?

Person 2: What is the magnetization of titanium inside the coil?

Answers: Eq. (6.59) $H = (200)(10)/(0.2) = 10,000$ A/m; from Table 6.15 $\chi = 0.182 \times 10^{-3}$, Eq. (6.63) $B = 4\pi \times 10^{-7}(1 + 0.182 \times 10^{-3})(10,000) = 0.0125$ Wb/m²; they are essentially the same due to the small susceptibility of titanium. $(1 + \chi) = 1.000182$; Eq. (6.62) $M = (0.000182)(10,000) = 1.82$ A/m.

With this background on magnetic field production and susceptibility in hand, we can return to our description of diamagnetic and paramagnetic behavior in an applied magnetic field. Substances consisting of atoms or molecules that do not possess permanent magnetic moments exhibit diamagnetism in a magnetic field. That is, they display a negative, but generally quite small, magnetic susceptibility because of the weak, induced opposing magnetic dipole moments. An induced diamagnetic component of magnetization is inherent in all substances, but is often masked by larger intrinsic moments that reinforce an applied field. Inert gases and solids like Bi, Cu, MgO, and

diamond are examples of diamagnetic materials and have typical magnetic susceptibilities on the order of -10^{-5} . The diamagnetic component of susceptibility is independent of temperature and magnetic field. For the most part, diamagnetic materials are of little engineering significance, with the notable exception of superconductors. Type I superconductors (cf. Section 6.1.2.4) can be perfectly diamagnetic ($\chi = -1$ or $B = 0$) up to the critical magnetic field because induced shielding currents persist indefinitely. Type II superconductors exhibit perfect diamagnetism or partial paramagnetism depending on the applied field (cf. Figure 6.31). The strong diamagnetism of superconductors makes it possible to use such materials for magnetic field shielding purposes.

Substances having magnetic susceptibilities in the range from about 10^{-6} to 10^{-2} are called paramagnetic. As described above, paramagnetism results from net intrinsic magnetic moments associated with electronic orbitals and electron spins. For paramagnetic materials, the interactions between atomic moments and an applied field can be described in terms of thermodynamics. When the individual atomic moments are randomly arrayed, the entropy of the material is high. Countering this tendency is the magnetic interaction energy, which is decreased when the moments align with the field. The final degree of moment alignment, therefore, depends on the competing factors of energy and entropy. Thus, the susceptibility, which reflects the degree of alignment, tends to decrease as temperature increases and entropy becomes more dominant. The results of thermodynamic calculations that minimize the free energy as a function of temperature, and they show that the susceptibility decreases with temperature and at intermediate temperatures is given approximately by

$$\chi = \frac{\mu_0 N p_m^2}{3k_B T} \quad (6.64)$$

where p_m is the magnetic dipole moment per atom as given in Eq. (6.58), N is the number of atoms per unit volume, k_B is Boltzmann's constant, T is absolute temperature, and μ_0 is the magnetic permeability in vacuum constant. The dependence of magnetic susceptibility on reciprocal absolute temperature is called the *Curie law*, and it holds for most paramagnetic nonmetallic materials above room temperature. As shown in Figure 6.50, the Curie Law does not hold at low temperatures, and the susceptibility approaches a constant value due to saturation.

In metals, conduction electrons provide both paramagnetic and diamagnetic moments, with a net paramagnetic moment, in addition to the induced diamagnetic moment resulting from core electrons. The paramagnetic component arising from the conduction electrons usually predominates, and most metals have positive susceptibilities. The origin of this paramagnetism can be explained in terms of the conduction electron energy band viewed as two subbands, one containing electrons with spin up and the other containing valence electrons with spin down. With no applied magnetic field, the subbands have equal populations of electrons and there is no net spin. Application of a magnetic field lowers the potential energy for the subband having spins parallel to the field and raises the potential energy of the other subband. Since the Fermi energy must be at the same level in both subbands when equilibrium exists (i.e., the electronic free energy is constant), a greater number of conduction electrons reinforce the field than oppose it, as illustrated in Figure 6.51. Those electrons with moments aligned parallel to the field ($m_s = +1/2$) have a magnetic potential energy $2\mu_0\mu_B H$ lower than those electrons with moments antiparallel ($m_s = -1/2$).

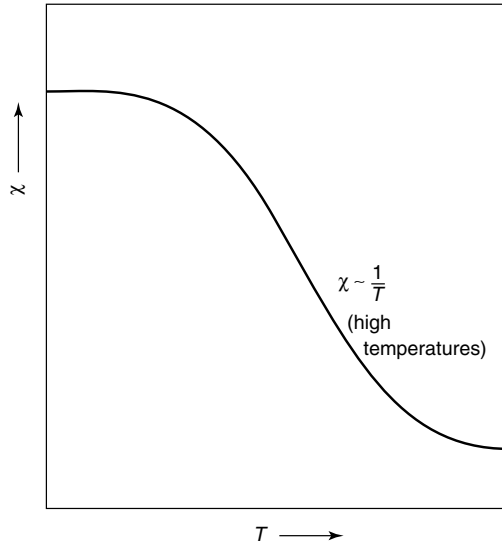


Figure 6.50 Temperature dependence of magnetic susceptibility for a paramagnetic material. From K. M. Ralls, T. H. Courtney, and J. Wulff, *Introduction to Materials Science and Engineering*. Copyright © 1976 by John Wiley & Sons, Inc. This material is used by permission John Wiley & Sons, Inc.

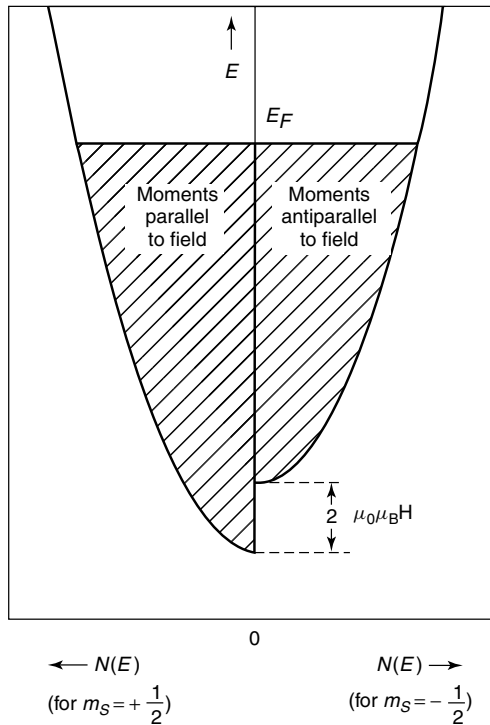


Figure 6.51 Distribution of electrons within the conduction band of a metal in the presence of an applied magnetic field. From K. M. Ralls, T. H. Courtney, and J. Wulff, *Introduction to Materials Science and Engineering*. Copyright © 1976 by John Wiley & Sons, Inc. This material is used by permission John Wiley & Sons, Inc.

Equalization of the Fermi energy within these subbands leads to a greater population of electrons with moments parallel to the field and a resulting net magnetic moment.

It can be shown that the conduction electron net spin susceptibility is proportional to the temperature coefficient of the electronic heat capacity [cf. Eq. (4.42)] and, for free electrons in a single band, having the Fermi energy much lower than any band gap, is given by

$$\chi = \frac{\mu_0 N_v \mu_B^2}{E_F} \quad (6.65)$$

where E_F is the energy of the Fermi level, N_v is the total number of valence electrons per unit volume [see Eq. (6.23)], μ_0 is the magnetic permeability in vacuum constant, and μ_B is the Bohr magneton. Figure 6.51 shows us that only those electrons having energies near the Fermi level are responsible for spin paramagnetism, and this has been accounted for in Eq. (6.65). In general, the spin susceptibility is proportional to the density of states at the Fermi energy, so that transition metals exhibit larger paramagnetic susceptibilities than do nontransition metals (see Table 6.15), just as they exhibit larger electronic heat capacities.

Some metals are diamagnetic because the conduction electron spin susceptibility is smaller than the induced diamagnetic susceptibility component. On the other hand, various rare earth metals display very strong paramagnetism because of unpaired f electrons that remain associated with individual atoms rather than entering into energy bands.

6.2.1.2 Types of Magnetism. In addition to diamagnetic and paramagnetic behavior, there are other types of magnetism which are important. These include *ferromagnetism*, *antiferromagnetism*, and *ferrimagnetism*. The various types of magnetism will be summarized and compared here, and then described in more detail under the appropriate material-related section. In most cases, the different types of magnetism can be differentiated between by their variation of magnetic susceptibility with temperature.

The elements Fe, Co, Ni, Gd, Tb, Dy, Ho, and Tm, as well as a number of alloys and compounds, exhibit very large positive susceptibilities below a critical temperature, θ_c , known as the ferromagnetic *Curie temperature*. (We use the Greek lowercase theta and subscript “c” to designate the Curie temperature to differentiate it from the critical transition temperatures of superconductors, which are designated as T_c .) Such substances display spontaneous magnetization, the origin of which arises from an internal interaction that causes a permanent offset in the electronic subbands. Only certain metals and other solids having partially filled d subshells or partially filled f subshells are capable of ferromagnetism (see Table 6.16). In addition to this necessary, but not sufficient, condition for spontaneous permanent magnetization, the interatomic spacing must be such that an internal interaction, termed the *exchange interaction*, occurs. As shown in Table 6.16, the elements Fe, Co, and Ni are magnetized spontaneously, whereas Cu does not. This is because in Fe, Co, and Ni, the average number of electrons in the d band having spin up is not the same as that having spin down, and the difference between the two gives a net magnetic moment. With increasing temperature, the lowering of internal energy because of the exchange interaction is opposed by a greater entropy that results from the disorder of randomized spins. Ferromagnetic materials become paramagnetic above θ_c ; susceptibilities can be on the order of 250 to 100,000 or more and continue to increase with decreasing temperature

Table 6.15 Magnetic Susceptibilities ($\times 10^3$) of Common Paramagnetic Metals at 20°C

IA	IIA	IIIA	IVA	VA	VIA	VIIA	VIII	IB	IIIB	IIIB	IVB	VB
Li 0.014	Be Dia- magnetic											
Na 0.008	Mg 0.012	Al 0.021										
K 0.006	Ca 0.019	Sc 0.264	Ti 0.182	V 0.375	Cr 0.313	Mn 0.871	Fe Ferro- magnetic	Cu Dia- magnetic	Zn Dia- magnetic	Ga Dia- magnetic		
Rb 0.004	Sr 0.034	Y 0.114	Zr 0.109	Nb 0.226	Mo 0.119	Tc 0.395	Ru 0.066	Ag Dia- magnetic	Cd Dia- magnetic	In Dia- magnetic	Sn 0.002	
Cs 0.005	Ba 0.007	Rare Earths	Hf 0.070	Ta 0.178	W 0.078	Re 0.094	Os 0.015	Au Dia- magnetic	Hg Dia- magnetic	Tl Dia- magnetic	Pb Dia- magnetic	Bi Dia- magnetic

Source: K. M. Ralls, T. H. Courtney, and J. Wulfi, *Introduction to Materials Science and Engineering*. Copyright © 1976 by John Wiley & Sons, Inc.

(see Figure 6.52a). Typically, susceptibilities at $0.9\theta_c$ are approximately half those at absolute zero.

In ferromagnetic materials, the exchange interaction gives rise to a parallel alignment of spins. In some metals like Cr, this exchange interaction, which is extremely sensitive to interatomic spacing and to atomic positions, results in an antiparallel alignment of spins. When the strength of antiparallel spin magnetic moments are equal, no net spin moment exists and the resulting susceptibilities are quite small. Such materials are called antiferromagnetic. The most noticeable characteristic of an antiferromagnetic material is that the susceptibility attains a maximum at a critical temperature, θ_N , called the *Néel temperature*.

The maximum in susceptibility as a function of temperature can be explained using thermodynamic reasoning. At absolute zero, the spin moments are aligned as antiparallel as possible, yielding a small susceptibility. With increasing temperature, the tendency for disorder or more random alignment of spin moments become greater,

Table 6.16 Distribution of Electrons and Electronic Magnetic Moments in Some Transition Metals

Element	Fe	Co	Ni	Cu
Total number ($s + d$) valence electrons	8	9	10	11
Average number of electrons in s band	0.2	0.7	0.6	1.0
Average number of electrons in d band	7.8	8.3	9.4	10.0
Number of d electrons with moments up	5.0	5.0	5.0	5.0
Number of d electrons with moments down	2.8	3.3	4.4	5.0
Net moment per atom (units of Bohr magnetons, μ_B)	2.2	1.7	0.6	0

Source: K. M. Ralls, T. H. Courtney, and J. Wulff, *Introduction to Materials Science and Engineering*. Copyright © 1976 by John Wiley & Sons, Inc.

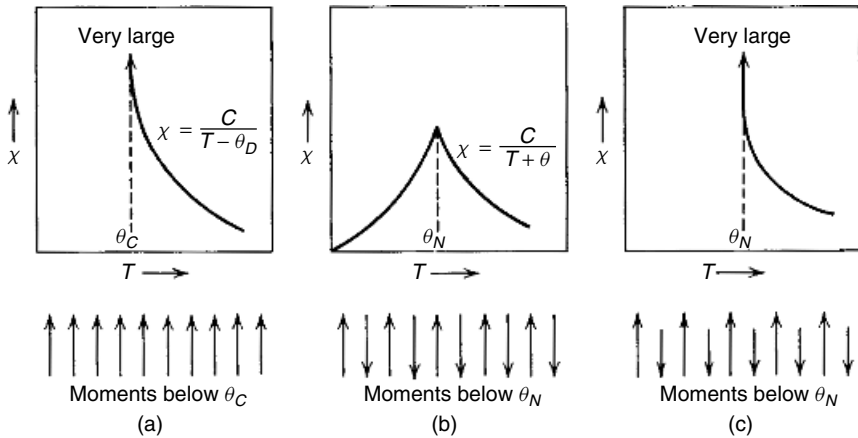


Figure 6.52 The magnetic spin alignments and variation of susceptibility with temperature for (a) ferromagnetic, (b) antiferromagnetic, and (c) ferrimagnetic materials. From K. M. Ralls, T. H. Courtney, and J. Wulff, *Introduction to Materials Science and Engineering*. Copyright © 1976 by John Wiley & Sons, Inc. This material is used by permission John Wiley & Sons, Inc.

and a higher net moment results in the presence of an applied magnetic field. This same process accounts for the decrease in net moment of ferromagnetic materials between absolute zero and θ_c . For antiferromagnetic materials, the spin moments become essentially random at θ_N , and above this temperature, paramagnetic behavior with decreasing χ is observed (see Figure 6.52b). Thus, the Néel temperature of an antiferromagnetic material is analogous to the Curie temperature of a ferromagnetic material. We will discuss antiferromagnetic materials in further detail in a later section.

Ferrimagnetism is similar to antiferromagnetism in that the spins of different atoms or ions tend to line up antiparallel. In ferrimagnetic materials, however, the spins do not cancel each other out, and a net spin moment exists. Below the Néel temperature, therefore, ferrimagnetic materials behave very much like ferromagnetic materials and are paramagnetic above θ_N (see Figure 6.52c). Ferrites, a particularly important class of ferrimagnetic materials, will be described later.

The different types of magnetism described so far are summarized in terms of the sign and magnitude of their susceptibilities in Table 6.17. A summary of the terms, symbols, and units used in magnetism are provided in Table 6.18, in a manner analogous to the electrical terms in Table 6.5.

6.2.1.3 Magnetic Domains and Hysteresis. In addition to susceptibility differences, the different types of magnetism can be distinguished by the structure of the magnetic dipoles in regions called *magnetic domains*. As shown in Figure 6.53, each domain consists of magnetic moments that are aligned, giving rise to a permanent net magnetic moment per domain. The domains are separated by domain boundaries (not the same as the grain boundaries), or domain walls, across which the direction of the spin alignment gradually changes. Typically, the domain wall has a thickness of about 100 nm. This type of arrangement represents the lowest free energy in the absence of an externally applied magnetic field. When the bulk material is unmagnetized, the net magnetization of these domains is zero, because adjacent domains may be oriented randomly in any number of directions, effectively canceling each other out.

Table 6.17 Summary of the Various Types of Magnetism

Type of Magnetic Behavior	Characteristics of Magnetic Susceptibility		Typical Materials
	Sign	Magnitude	
Diamagnetism	Negative	Small ^a $\chi = \text{constant}$	Organic materials, superconducting metals, and other metals (e.g., Bi)
Paramagnetism	Positive	Small $\chi = \text{constant}$	Alkali and transition metals, rare earth elements
Ferromagnetism	Positive	Large $\chi = f(H)$	Some transition metals (Fe, Ni, Co) and rare earth metals (Gd)
Antiferromagnetism	Positive	Small $\chi = \text{constant}$	Salts of transition elements (MnO)
Ferrimagnetism	Positive	Large $\chi = f(H)$	Ferrites (MnFe_2O_4 , ZnFe_2O_4) and chromites

^aDiamagnetic susceptibilities for superconducting metals are large.

Table 6.18 Magnetic Symbols, Terms, and SI Units

Quantity	Symbol	SI Units	
		Primary	Derived
Magnetic field strength	H	$\text{C/m} \cdot \text{s}$	$\text{A/m} = 10^{-3} \text{ oersted (Oe)}^a$
Magnetic induction (magnetic flux density)	B	$\text{kg/s} \cdot \text{C}$	$\text{V} \cdot \text{s/m}^2 = \text{Weber (Wb)/m}^2 = \text{tesla (T)} = 10^4 \text{ gauss (G)}^a$
Magnetic susceptibility	χ	(dimensionless)	(dimensionless)
Magnetization	M	$\text{C/m} \cdot \text{s}$	A/m
Magnetic dipole moment	p_m	$\text{C} \cdot \text{m}^2/\text{s}$	$\text{A} \cdot \text{m}^2$
Remnant induction	B_r	$\text{kg/s} \cdot \text{C}$	$\text{V} \cdot \text{s/m}^2 = \text{weber/m}^2 = \text{tesla (T)} = 10^4 \text{ gauss(G)}^*$
Coercivity (coercive force)	H_c	$\text{C/m} \cdot \text{s}$	$\text{A/m} = 10^{-3} \text{ oersted(Oe)}^*$
Magnetic permeability in vacuum	μ_0	$\text{kg} \cdot \text{m/C}^2$	$\text{Henry/m} = \text{Wb/A} \cdot \text{m}$
Saturation magnetization	M_s	$\text{C/m} \cdot \text{s}$	A/m

^acgs unit; items in boldface are material properties.

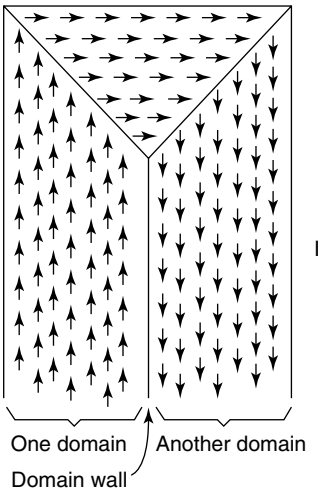


Figure 6.53 Schematic illustration of magnetic domains.

The average magnetic induction of a ferromagnetic material is intimately related to the domain structure. When a magnetic field is applied, the domains most nearly parallel to the direction of the applied field grow in size at the expense of the others. This is called *boundary displacement of domains* or *domain growth*. This process continues until only the most favorably oriented domains remain. The spontaneous moments are aligned naturally with respect to certain crystallographic directions; in the case of iron, they are parallel to the [100] direction. When domain growth is completed, a further increase in the magnetic field causes the domains to rotate and align parallel

to the applied field. The material reaches the point of saturation magnetization, and no further change will take place on increasing the strength of the magnetic field.

This change in magnetization with applied magnetic field is shown schematically in Figure 6.54, in a diagram known as a *hysteresis loop*. Hysteresis is defined as the lag in magnetization change that follows variations in the applied magnetic field. If an unmagnetized specimen, such as iron, is placed in a magnetic field, H , a magnetic induction, B , results, as described earlier. When the field is increased, the magnetic induction will also increase, as shown in curve (a) of Figure 6.54. This is the domain growth region. At sufficiently high magnetic fields, all of the magnetic dipoles become aligned with the external field, and the material becomes magnetically saturated; that is, the magnetization becomes constant and is called the *saturation magnetization*, M_s . There is a corresponding *saturation flux density*, B_s , as the induction reaches a maximum value. Once magnetic saturation has been achieved, a decrease in the applied field back to zero, as illustrated in curve (b) of Figure 6.54, results in a macroscopically permanent induction, called the *remnant induction*, B_r , under which the material is in the magnetized condition, even at zero applied field. At this point, spin orientations within domains have readily rotated back to their favorable crystallographic positions, but the original random domain arrangement is not achieved because domain wall motion is limited and the domain growth process is not entirely reversible. To bring the induction back to zero, a field of magnitude H_c , termed the *coercivity*, must be

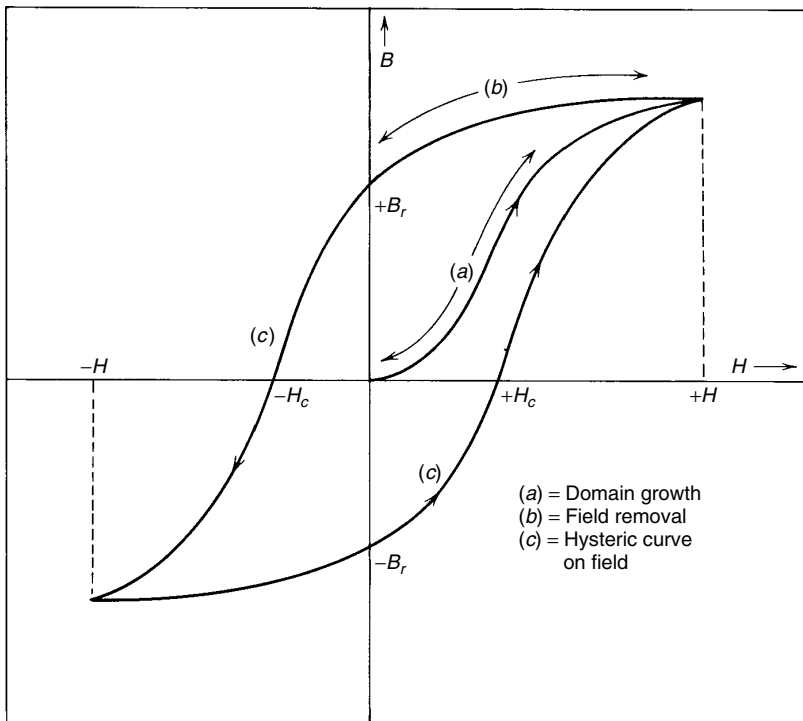


Figure 6.54 A hysteresis loop for a ferromagnetic materials. From K. M. Ralls, T. H. Courtney, and J. Wulff, *Introduction to Materials Science and Engineering*. Copyright © 1976 by John Wiley & Sons, Inc. This material is used by permission John Wiley & Sons, Inc.

applied antiparallel to the original magnetic field, shown as curve (c) in Figure 6.54. A further increase in the magnetic field in the negative direction results in a maximum induction and saturation magnetization, but in the opposite direction of the previous maximum achieved under an applied field in the forward direction. The field can once again be reversed, and the field-induction loop can be closed. The area within the hysteresis loop represents the energy loss per unit volume of material for one cycle and, unless suitable cooling is provided, the material heats up. Smaller hysteresis loops result for cycling between applied fields that do not cause saturation magnetization.

Cooperative Learning Exercise 6.6

Recall that the saturation magnetization, M_s , is the maximum possible magnetization in the material, and is simply the product of the net magnetic moment per atom, P_m , and the number of atoms per unit volume, N . The net magnetic moment, in turn, is related to the electronic structure (paired or unpaired electrons), although a number of other factors come into play. Use this information to calculate the saturation magnetization for nickel.

Person 1: Look up the net magnetic moment of nickel in Table 6.16 and convert it from units of Bohr magnetons to $\text{A} \cdot \text{m}^2$.

Person 2: Look up the density and atomic weight of nickel in Tables 1.11 and 1.3, respectively, and calculate the number of atoms per cubic meter for nickel. (Don't forget Avogadro's number.)

Combine your information to calculate M_s for nickel in units of A/m .

Since the magnetic susceptibilities of ferromagnetic materials are so high, $H \ll M$, and Eq. (6.59) can be simplified. Use this information and your value of M_s to calculate the saturation flux density, B_s .

$$\begin{aligned} \text{Answers: } P_m &= 0.60 \text{ Bohr magnetons} = 0.60(9.27 \times 10^{-24} \text{ A} \cdot \text{m}^2) \\ &= 5.56 \times 10^{-24} \text{ A} \cdot \text{m}^2; N = \rho_{\text{Ni}} N_A / (A \cdot W)_{\text{Ni}} = (8.91)(10^3)(6.02 \times 10^{23}) / (58.71) \\ &= 9.136 \times 10^{28} \text{ atoms/m}^3; M_s = 5.1 \times 10^5 \text{ A/m. Equation (6.61) simplifies to} \\ B_s &= \mu_0 M_s = 0.638 \text{ Wb/m}^2. \end{aligned}$$

When applied magnetic fields cyclically vary at some finite speed, *eddy currents* are formed. Eddy currents are electrical currents that are set up in the material due to the applied field and that lead to additional energy losses. The magnitude of these currents depends on the frequency and flux density imposed by the magnetic field, as well as on the specific resistance and geometry of the material. The effect of eddy currents is to increase the magnetic field, H , for the same induction, causing a much wider hysteresis loop. The sum of the hysteresis loss and eddy current loss is known as the *total core loss*, and it is usually expressed in watts per pound of a standard sample thickness and at a given magnetic induction.

Magnetic materials can be divided into soft and hard magnets, depending on their behavior in the presence of a magnetic field. This is the topic of the next two sections.

6.2.1.4 Soft and Hard Magnets. *Soft magnets*, sometimes called *permeable magnets*, have high magnetic permeabilities and low coercive forces, H_c ; they are easily magnetized and demagnetized. In devices subjected to alternating magnetic fields, such as transformer cores, not only is a high magnetic permeability and high saturation induction desirable, but it is also necessary that the material dissipate as little energy

per cycle as possible. In other words, the core material must have a hysteresis loop of small area, as characterized by a low coercive force, as illustrated in the inner loop of Figure 6.55.

In ferromagnetic materials, the saturation magnetization is primarily a function of composition, but the susceptibility, coercivity, and shape of the hysteresis curve are very sensitive to structure. A low coercivity coincides with easy motion of domain walls. Domain wall motion is restricted to structural defects such as nonmagnetic inclusions, voids, and precipitates of a nonmagnetic phase. Domain walls are pinned by these defects because the wall energy is lowered. Consequently, the number of such defects must be minimized in a soft magnetic material. Impurities and dislocation structures resulting from cold deformation also lead to higher hysteresis.

Energy losses in soft magnetic materials arise due to both hysteresis and eddy currents, as described in the previous section. Eddy current losses can be reduced by increasing the electrical resistivity of the magnetic material. This is one reason why solid-solution iron–silicon alloys ($\sim 4\%$ Si) are used at power frequencies of around 60 Hz and why iron–nickel alloys are used at audio frequencies. Some magnetically soft ferrites (see Section 6.2.2.1) are very nearly electrical insulators and are thus immune to eddy current losses. Some common soft magnetic materials and their properties are listed in Table 6.19. Soft magnetic alloys are described further in Section 6.2.1.6.

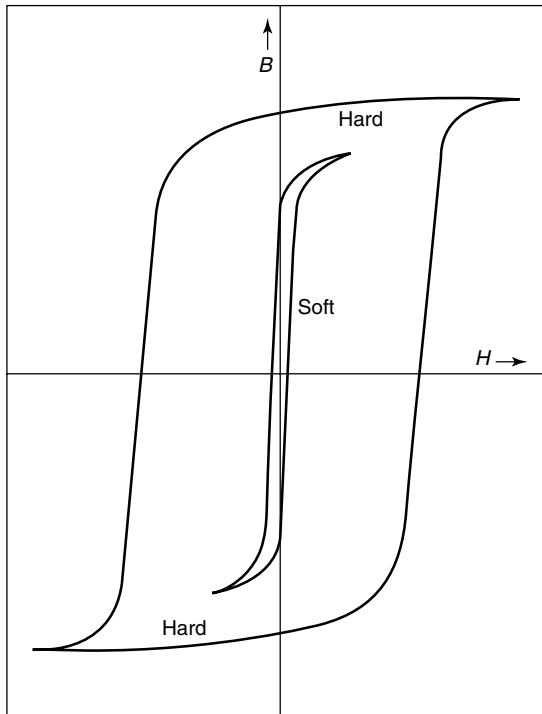


Figure 6.55 Comparison of hysteresis loops for soft and hard magnetic materials. From K. M. Ralls, T. H. Courtney, and J. Wulff, *Introduction to Materials Science and Engineering*. Copyright © 1976 by John Wiley & Sons, Inc. This material is used by permission John Wiley & Sons, Inc.

Table 6.19 Selected Properties of Some Soft Magnetic Materials

Material	Initial Susceptibility (χ at $H \sim 0$)	Hysteresis Loss per Cycle (J/m ³)	Saturation induction (Wb/m ²)
Commercial iron ingot	250	500	2.16
Fe–4% Si, random	500	50–150	1.95
Fe–3% Si, oriented	15,000	35–140	2.0
45 Permalloy (45% Ni–55% Fe)	2,700	120	1.6
Mu metal			
(75% Ni–5% Cu–2% Cr–18% Fe)	30,000	20	0.8
Supermalloy			
(79% Ni–15% Fe–5% Mo–0.5% Mn)	100,000	2	0.79
Ferroxcube A (Mn, Zn)Fe ₂ O ₄	1,200	~40	0.36
Ferroxcube B (Ni, Zn)Fe ₂ O ₄	650	~35	0.29

Source: K. M. Ralls, T. H. Courtney, and J. Wulff, *Introduction to Materials Science and Engineering*. Copyright © 1976 by John Wiley & Sons, Inc.

6.2.1.5 Hard Magnets. Permanent magnets require materials with high remnant inductions and high coercivities. These materials, called *hard magnets*, also generally exhibit large hysteresis losses. A typical hysteresis loop for a hard magnetic material is shown in the outer loop of Figure 6.55, which is shown relative to a soft material for comparison. The term hard magnet, is derived from the mechanical properties of these materials, since increases in mechanical strength in ferromagnetic materials also tend to increase hardness. A relative measure of hardness in magnetic materials is the product of the remnant induction and the coercivity, $B_r \times H_c$, which is roughly twice the energy required to demagnetize a unit volume of material. That is, $(B_r \times H_c)/2$ is roughly twice the area under the B versus H curve between $H = 0$ and $H = -H_c$.

Hard magnetic behavior is intimately related to microstructure. Some permanent magnetic materials, including carbon steel and alloy steels containing combinations of Cr, Co, or W, undergo martensitic transformations upon cooling, resulting in a fine-grained microstructure. Others undergo an order–disorder transformation that results in internal strains. Specific hard magnetic materials will be described further in Sections 6.2.1.6 and 6.2.2.2.

6.2.1.6 Magnetism in Alloys. Recall from Table 6.15 that the transition metal Ni exhibits spontaneous magnetization, whereas Cu does not. The difference in magnetic behavior between these two transition metals can be explained in terms of band theory—specifically, the overlap of the s conduction band with the d band immediately below in energy. In the transition metals, the d band is not normally filled entirely. One exception is copper, Cu, which has a $3d^{10}4s^1$ outer shell configuration (cf. Table 1.3). The filled $3d$ band of copper has two separate subbands of opposite electron spin orientation, each holding five electrons. With both subbands filled, the net spin, and hence the net magnetization, of the d band are zero. Nickel, which has one less electron than copper, is ferromagnetic and has a saturation magnetic moment of $0.60\mu_B$ per atom at absolute zero. After a small correction for orbital electron motion, the result is that Ni at saturation has an excess of 0.54 electrons per atom with spin preferentially oriented

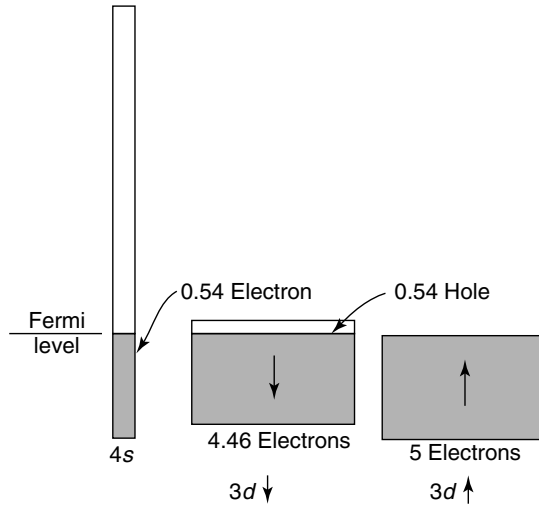


Figure 6.56 Schematic relationship of outer-shell energy bands in nickel at absolute zero.

in one direction. At absolute zero, the electrons are distributed as shown in Figure 6.56. We take one $3d$ subband as filled, and we take the other as filled except for a 0.54 hole. The 0.54 excess electron goes into the $4s$ band as shown, and it creates a net spin in the d -band due to the 0.54 hole in one of its subbands. The separation in energy between the $3d$ subbands is a result of a phenomenon called the *exchange interaction energy*, which is a function of temperature. When Ni is heated above θ_c (631 K), the exchange interaction is dominated by thermal effects, the 0.54 hole distributes itself equally in the two $3d$ subbands as shown in Figure 6.57, and the saturation magnetic moment disappears.

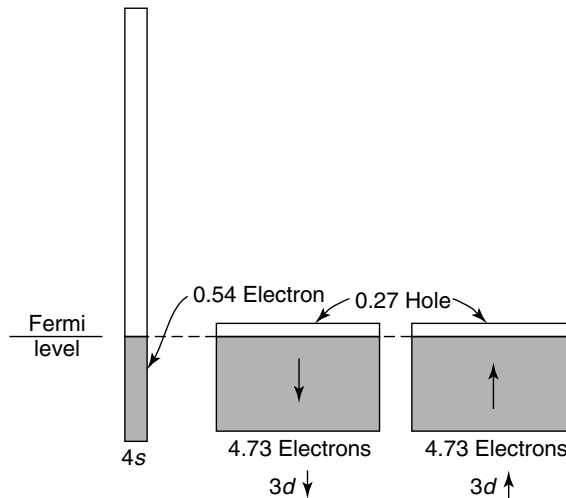


Figure 6.57 Schematic relationship of outer-shell energy bands in nickel over the Curie temperature.

When a series of solid solutions between Cu and Ni is formed, it is observed that the spontaneous magnetization decreases linearly with increasing Cu content until no spontaneous magnetization remains at 60 at % Cu (see Figure 6.58). At this composition, we have added about 0.54 electrons to the d band and about 0.06 electron to the s band. But the 0.54 electron added to the d band in Figure 6.57 will fill both d subbands, and the magnetization will be zero. The 10.6 total valence electrons per atom are now equally divided between spin up and spin down, as shown in Figure 6.59.

This simple band model predicts that an alloying metal with $10 + z$ valence electrons outside a filled p shell (rare gas configuration) is expected to decrease the magnetization of nickel by approximately z Bohr magnetons per solute atom (μ_B). As illustrated in

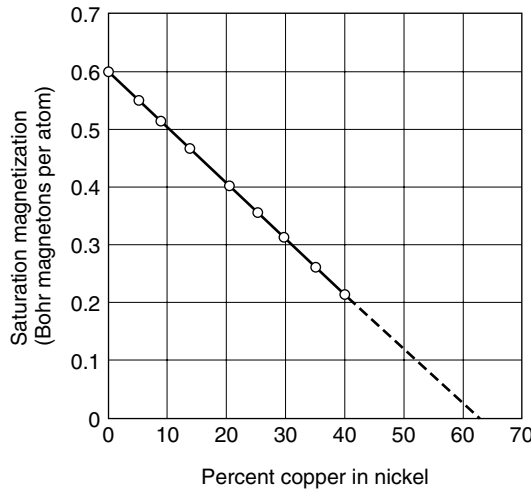


Figure 6.58 Variation in saturation magnetization for a copper–nickel alloy. Reprinted, by permission, from C. Kittel, *Introduction to Solid State Physics*, p. 333. Copyright © 1957 by John Wiley & Sons, Inc.

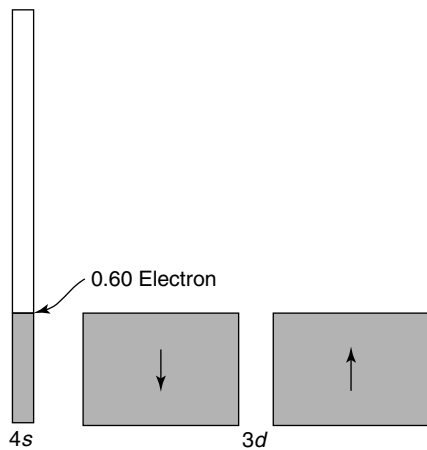


Figure 6.59 Schematic relationship of bands in a 60% Cu, 40% Ni alloy with zero magnetization.

Figure 6.60, this simple relationship is obeyed extraordinarily well for small amounts of such atoms as Sn(+4), Al(+3), Zn(+2), Cu(+1), Co(−1), Fe(−2), and Mn(−3).

It is believed that palladium may have a distribution of electrons similar to that of nickel. At room temperature the picture for palladium is like Figure 6.57 for Ni above the Curie temperature, except that we now have to deal with a $5s$ band instead of $4s$, and $4d$ instead of $3d$. The addition of hydrogen in solution in metallic palladium reduces the susceptibility. The hydrogen is ionized, with the free electrons joining the palladium bands just as the valence electron of copper joins the bands of nickel.

Widely used permanent magnetic materials include low-alloy steels, containing between 0.6% and 1.0% carbon, that are hardened by quenching or precipitation hardening. Another important group is iron–nickel–aluminum alloys with a certain amount of cobalt, known as *Alnico alloys*. The permanent-magnet materials tend to be brittle and difficult to shape, so that they must be cast and finished by grinding. More ductile alloys such as copper–nickel–iron and copper–nickel–cobalt are available that can be cold-worked and machined by ordinary methods. All three types of alloys are subject to precipitation hardening, which can be controlled in such a way as to produce a microscopically heterogeneous structure composed of acicular particles oriented in a required direction. The size of these particles is very small and approaches the dimensions of a magnetic domain (about $1\ \mu\text{m}$). The reversal of magnetization can then occur only by a complete rotation of the magnetic domain in a particle. This, however, would require a very high magnetizing force because of the crystal anisotropy. Consequently, the boundary displacement of the domains is suppressed, resulting in very high coercive forces.

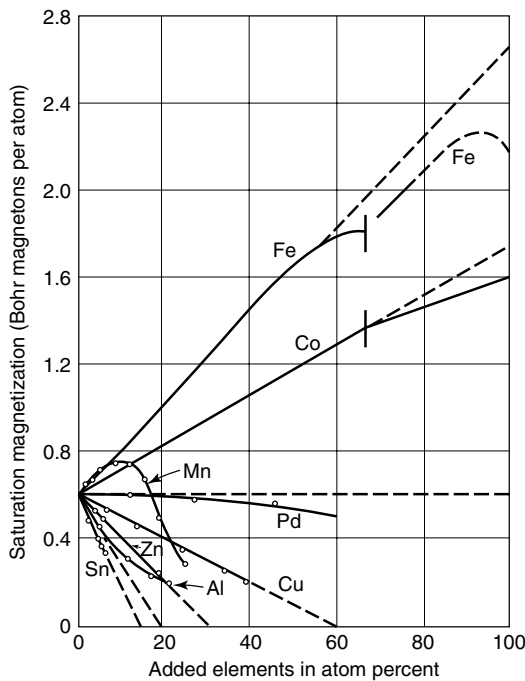


Figure 6.60 Saturation magnetization of some nickel alloys. Reprinted, by permission, from C. Kittel, *Introduction to Solid State Physics*, p. 335. Copyright © 1957 by John Wiley & Sons, Inc.

The same principle has been observed in the production of permanent magnets from powdered materials having particle sizes of colloidal dimensions (0.1 to 0.01 μm). A number of iron-based permanent magnet alloys made from these fine powders have very high coercive forces. For example, a piece of iron has a coercive force of 1 oersted ($\text{Oe} = 1000\text{A}/4\pi\text{m}$), whereas a compact made of a fine iron powder may have a coercive force as great as 500 Oe. Other compact powdered alloys, such as iron–cobalt, exhibit still higher coercive forces reaching thousands of oersteds.

As mentioned in the previous section, the magnetization behavior of a single crystal depends upon its crystallographic orientation relative to the applied magnetic field. For example, the easy magnetization directions are [100] for BCC iron and [111] for FCC nickel since these correspond to the natural spin moment alignments. A crystal oriented in the easy magnetization direction is easier to magnetize, or softer, than one oriented in another direction. Beneficial use of this characteristic is realized in the case of Fe–Si alloys that are formed by rolling into a sheet, with appropriate intermediate annealing treatments. When the thermomechanical processing is carefully controlled, a preferred crystallographic orientation develops within the polycrystalline sheet, such that the direction of easy magnetization is parallel to the rolling direction. Such a textured alloy is readily magnetized, and the hysteresis loop is small.

Magnetically soft Fe–Ni alloys can have their properties altered by heat treatment. The compound Ni_3Fe undergoes an order–disorder transformation at about 500°C . Since the susceptibility of the ordered phase is only about half that of the disordered phase, a higher susceptibility is realized when the alloy is quenched from 600°C , a process that retains the high-temperature, disordered structure. Heat treatment of Fe–Ni alloys in a magnetic field further enhances their magnetic characteristics (see Figure 6.61), and the square hysteresis loop of 65 Permalloy so processed is desirable in many applications. A related alloy called Supermalloy (see Table 6.19) can have an initial susceptibility of approximately one million.

Other alloys undergo an order–disorder transformation that results in internal strains. For example, Co–50 at % Pt transforms from a high-temperature, disordered FCC structure to an ordered body-centered tetragonal structure having Co atoms and Pt atoms on alternating (002) planes. The partially ordered alloy can have coercivities as large as $3.7 \times 10^5 \text{A/m}$. In addition, there are many permanent magnetic materials having two-phase microstructures produced by solid precipitation. Among these are Cu–Ni–Fe alloys (Cunife), Cu–Ni–Co alloys (Cunico), and Fe–Al–Ni–Co–Cu alloys (Alnico). Selected hard magnetic alloys are listed in Table 6.20.

The Alnico-type alloys are commercially very important. At high temperatures, these alloys exist as a homogeneous solid solution which, below a miscibility gap (cf. Section 2.3.1), decomposes into a fine two-phase mixture consisting of FeCo-rich particles within an NiAl-rich matrix. Both product phases tend to be ordered with the CsCl structure. A suitable phase decomposition heat treatment yields particles of the strongly magnetic FeCo-rich phase that are sufficiently small so that each particle contains a single magnetic domain. This, in combination with the fact that the NiAl-rich phase is only weakly magnetic, leads to a high coercivity. The magnetic properties of Alnico alloys can be enhanced by various processing techniques. For example, directional solidification leads to a preferred crystallographic orientation, and phase decomposition in the presence of an applied magnetic field causes particles of the strongly magnetic phase to be elongated in the field direction.

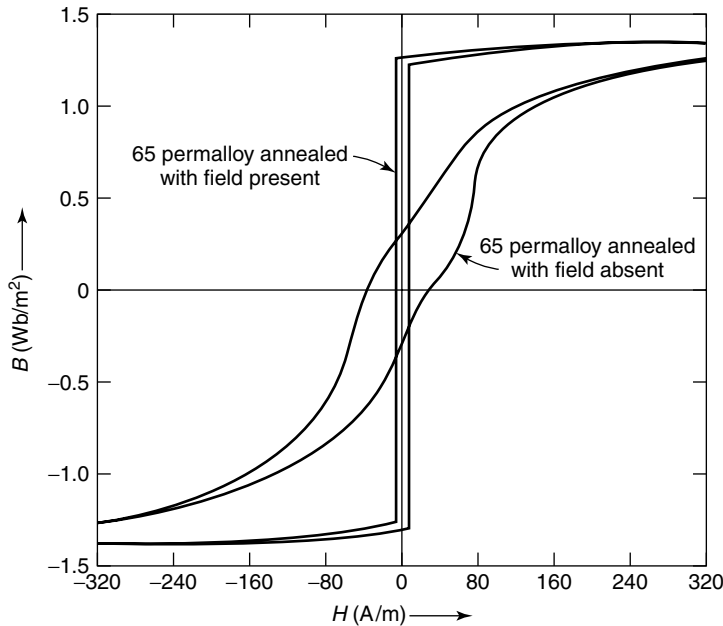


Figure 6.61 Hysteresis loop for Permalloy 65 heat treated with and without an applied magnetic field. From K. M. Ralls, T. H. Courtney, and J. Wulff, *Introduction to Materials Science and Engineering*. Copyright © 1976 by John Wiley & Sons, Inc. This material is used by permission John Wiley & Sons, Inc.

Table 6.20 Some Hard Magnetic Alloys and Their Selected Properties

Material	Composition (wt%)	B_r (Wb/m ²)	H_c (kA/m)	$B_r H_c$ (J/m ³)
Martensitic				
carbon steel	98.1 Fe–1 Mn–0.9 C	0.95	4.0	3.8
Tungsten steel	92.7 Fe–6 W–0.7 C–0.3 Cr–0.3 Mn	1.05	5.6	5.9
Chromium steel	95.3 Fe–3.5 Cr–0.9 C–0.3 Mn	0.97	5.2	5.0
Cobalt steel	71.8 Fe–17 Co–8 W–2.5 Cr–0.7 C	0.95	11.9	11.3
Cunife	60 Cu–20 Ni–20 Fe	0.54	43.8	23.7
Cunico	50 Cu–29 Co–21 Ni	0.34	52.5	17.9
Alni–a	59.5 Fe–24 Ni–13 Al–3.5 Cu	0.62	38.0	23.6
Alnico-I	63 Fe–20 Ni–12 Al–5 Co	0.72	35.0	25.2
Alnico-V	51 Fe–24 Co–14 Ni–8 Al–3 Cu	1.25	43.8	54.8
Alnico-XII	52 Fe–24.5 Co–13.5 Ni–8 Al–2 Nb	1.20	64.0	76.8
Co–Pt	77 Pt–23 Co	0.52	246.8	128.3
Ferroxdur	60.3 Fe–12.4 Ba–27.3 O (BaFe ₁₂ O ₁₉)	0.20	120.0	24.0
Ferroxdur (oriented)		0.39	240.0	93.6

Source: K. M. Ralls, T. H. Courtney, and J. Wulff, *Introduction to Materials Science and Engineering*. Copyright © 1976 by John Wiley & Sons, Inc.

Rare-earth magnets have superior magnetic properties and are particularly suitable for use in compact and lightweight devices due to their coercive forces that are up to 10 times that of ordinary magnets. They are alloys of rare-earth elements, which include elements 57 through 71, so-named because of the inherent difficulty in extracting them from ores, not due to their rarity. The most common rare-earth alloys for magnetic applications are samarium–cobalt (Sm–Co) and neodymium–iron–boron (Nd–Fe–B). Sm–Co *rare-earth magnets*, of which the composition SmCo_5 is the most common, are relatively stable to changes in temperature. Nd–Fe–B rare-earth magnets, such as $\text{Nd}_2\text{Fe}_{14}\text{B}$, have magnetic properties superior to those of Sm–Co. However, the magnetic flux variation is very sensitive to changes in temperature, making it necessary to select a magnetic material with properties suited to meet its specific service conditions.

6.2.2 Magnetic Properties of Ceramics and Glasses

Most of the important magnetic ceramics are of the ferrimagnetic class. However, some ceramics do exhibit other types of magnetic behavior. These ceramic materials will be described first, followed by a more thorough description of an important class of ferrimagnetic ceramics called ferrites. Finally, a topic related to the magnetic properties of ceramic superconductors will be introduced.

6.2.2.1 Diamagnetic, Paramagnetic and Antiferromagnetic Ceramics and Glasses. In general, diamagnetism is associated with all ceramic materials in which the ions have closed electronic shells—that is, no unpaired electrons. This means that ceramics with no transition metal ions or rare-earth ions are generally diamagnetic. We will return to a special class of diamagnetic ceramics in Section 6.2.2.3.

Paramagnetism results from unpaired electrons. As a result, most compounds containing transition, rare-earth, and actinide elements, including oxides, nitrides, carbides, and borides, exhibit paramagnetism. Such ceramics are generally not of importance due to their paramagnetism alone, since they often exhibit other types of magnetism, as well.

Aside from ferrimagnetic ceramics, which is the subject of the next section, the only other type of magnetism exhibited by ceramics is antiferromagnetism. Several of the transition metal monoxides exhibit antiferromagnetic behavior, in which the exchange between the unpaired electrons causes antiparallel spin alignments. These oxides include MnO , FeO , NiO , and CoO , all of which have the rock salt structure. For example, in FeO , the O^{2-} ions possess no net magnetic moment, whereas the Fe^{2+} ions do. Since neutrons have a magnetic moment, neutron diffraction can be employed to determine the spin arrangement, as shown in Figure 6.62. The spins of the d electrons of adjacent iron ions are aligned in opposite directions. Furthermore, any ions in a (111) plane have parallel spins, but ions in adjacent (111) planes have antiparallel spins, as illustrated in Figure 6.62. The aligned moments of the ions in the two directions cancel, and the FeO crystal as a whole has no magnetic moment. The ordering of spins in antiferromagnetic substances often introduces a complexity with respect to viewing their crystal structures. Because of the spin ordering, the magnetic unit cell has twice the lattice parameter of the standard unit cell. Some antiferromagnetic ceramics and their magnetic properties are listed in Table 6.21.

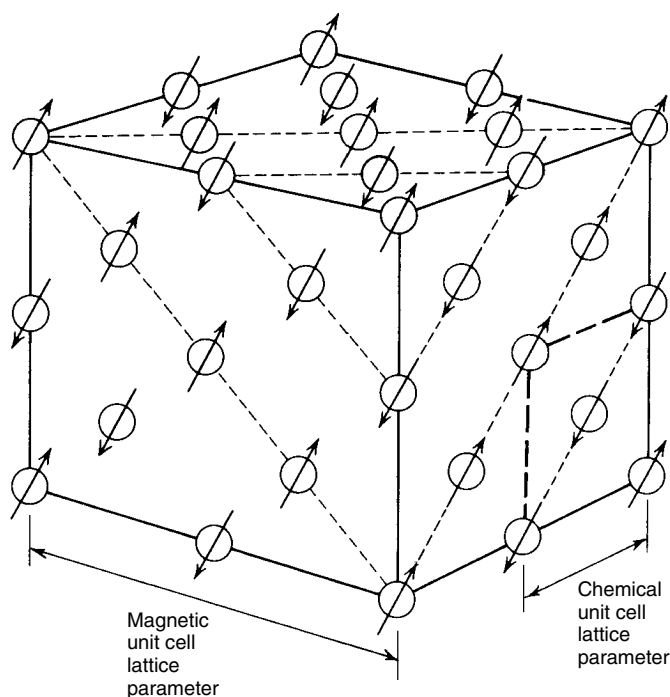


Figure 6.62 Schematic illustration of spin alignments in adjacent (111) planes of FeO. From K. M. Ralls, T. H. Courtney, and J. Wulff, *Introduction to Materials Science and Engineering*. Copyright © 1976 by John Wiley & Sons, Inc. This material is used by permission John Wiley & Sons, Inc.

Table 6.21 Selected Magnetic Properties of Some Antiferromagnetic Ceramics

Substance	Néel Temperature, θ_N , (K)	$\chi(0\text{ K})/\chi(\theta_N)$
MnO	116	0.67
MnS	160	0.82
MnF ₂	67	0.76
FeF ₂	79	0.72
FeO	198	0.80
CrSb	723	~0.25
FeCO ₃	35	~0.25

Source: K. M. Ralls, T. H. Courtney, and J. Wulff, *Introduction to Materials Science and Engineering*. Copyright © 1976 by John Wiley & Sons, Inc.

Before moving on to ferrites, we should at least mention that magnetic glasses do exist, although any further coverage of them is beyond the scope of this text. Not surprisingly, the magnetic glasses are found chiefly in the group of glasses with high contents of transition elements or rare earths, as well as in the corresponding fluoride glasses but especially in the metallic glasses.

Table 6.22 Some Ferrites and their Magnetic Properties

Composition	Saturation Magnetization (A/m)	Curie Temperature (°C)	Crystal Structure
MnFe ₂ O ₄	4.13×10^5	300	Inverse spinel
FeFe ₂ O ₄	4.77×10^5	585	Inverse spinel
NiFe ₂ O ₄	2.71×10^5	590	Inverse spinel
CoFe ₂ O ₄	3.98×10^5	520	Inverse spinel
CuFe ₂ O ₄	1.35×10^5	455	Inverse spinel
BaFe ₁₂ O ₁₉	3.18×10^5	450	Hexagonal
SrFe ₁₂ O ₁₉	3.18×10^5	453	Hexagonal
MgFe ₂ O ₄	1.11×10^5	440	Inverse spinel
Li _{0.5} Fe _{2.5} O ₄	3.10×10^5	670	Inverse spinel
γ - Fe ₂ O ₃	4.13×10^5	575	Inverse spinel
Y ₃ Fe ₅ O ₁₂	1.35×10^5	287	Garnet

Source: S. Somiya, *Advanced Technical Ceramics*. Copyright © 1984 by Academic Press.

6.2.2.2 Ferrites. Ferrites are ceramic materials having the general formula MO · Fe₂O₃, where M is a bivalent element such as Fe, Cu, Mn, Zn, and Ni. The oldest known ferrite with magnetic properties is magnetite (Fe₃O₄), which may be considered a double oxide composed of ferrous and ferric oxides, FeO · Fe₂O₃. Mixed ferrites can also be fabricated in which the divalent cation may be a mixture of ions, such as Mg_{1-x}Mn_xFe₂O₄, so that a wide range of composition and magnetic properties are available. The major ferrite solid solutions are Mn–Zn, Ni–Zn, and Cu–Zn. These, along with the Ba and Sr ferrites, form the mainstream of magnetic materials for electronic applications. Table 6.22 presents the most important types of ferrites and their basic properties.

The ferrites generally have one of three crystal structures: inverse spinel, garnet, and hexagonal. The spinel structures (cf. Figure 1.41) have the oxygen ions in a nearly close-packed cubic array. The unit cell contains 32 oxygen ions, with 32 octahedral and 64 tetrahedral sites, of which 16 of the octahedral and 8 of the tetrahedral sites are filled. It is the position of these 24 cations within the unit cell that determines magnetic behavior. The distribution of cations in the sites is specific to the type of cations, and it must be determined experimentally. There are two idealized spinel structures. In the *normal spinel*, all the divalent ions are on the tetrahedral sites, as in ZnFe₂O₄. In the *inverse spinel*, the 8 occupied tetrahedral sites are filled with trivalent ions and the 16 occupied octahedral sites are equally divided between di- and trivalent ions (see Figure 6.63). The prototypical inverse spinel ferrite is magnetite, whose structure consists of an FCC oxygen array with Fe²⁺ and Fe³⁺ ions in the interstices.

HISTORICAL HIGHLIGHT

Lodestone, also known as magnetite, was one of the first known magnetic materials. Its ability to attract iron was known as far back as 600 B.C., and it was used in compasses beginning in the thirteenth century. It was studied by J. L. Snoeck at the Philips Laboratories in Holland in the 1940s, however, that led to the first application of oxide ceramics with strong magnetic properties.

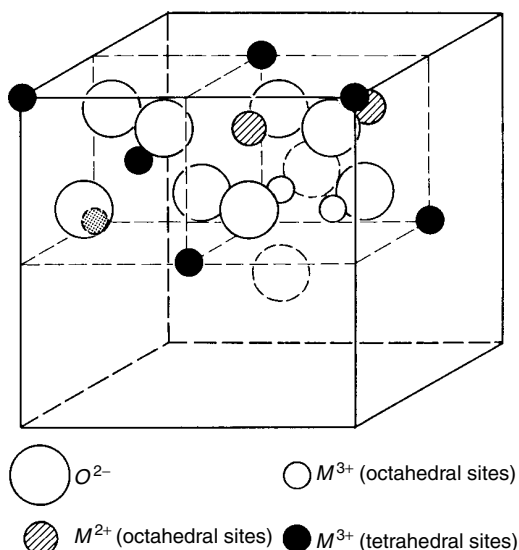


Figure 6.63 A portion of the inverse spinel unit cell found in many ferrites. From K. M. Ralls, T. H. Courtney, and J. Wulff, *Introduction to Materials Science and Engineering*. Copyright © 1976 by John Wiley & Sons, Inc. This material is used by permission John Wiley & Sons, Inc.

Ferrite compounds with the inverse spinel structure are similar to magnetite, with different ions substituting for the iron atoms. As with FeO (cf. Figure 6.62), the oxygen ions have no permanent magnetic moment. Tetrahedral sites in the FCC oxygen array are occupied by half of the trivalent cations, and octahedral sites are occupied equally by divalent cations and the remaining trivalent cations.

The permanent moments of the cations in the octahedral and tetrahedral sites are antiparallel. Thus, the moments of the trivalent cations (Fe^{3+}) cancel out, and the net moment is due to the divalent cations. If the individual divalent cation moments are known, then it is possible to calculate the net moment per formula unit (see Cooperative Learning Exercise 6.7). In a formula unit of magnetite, there is one divalent iron ion that has a total moment of $4\mu_B$ resulting from four unpaired electrons, which is very close to the observed value. Similarly, in $NiFe_2O_4$, the moment per formula unit is $2\mu_B$ identical to that of the divalent nickel ion.

In some systems, and particularly at high temperatures, the cation distribution may be disordered and the cations nearly randomly distributed between tetrahedral and octahedral sites, but generally there is a tendency for individual ions to fit into particular sites so that either the normal or inverse arrangement is preferred. The extent to which inversion of the cations occurs depends on the heat treatment, but, in general, increasing the temperature of a normal spinel causes an excitation of the ions to the inverted position. For example, manganese ferrite is about 80% normal spinel, and this arrangement does not change greatly with heat treatment. Since the Mn^{2+} ion has a moment of $5\mu_B$, the inversion should not affect the net moment of $MnFe_2O_4$. Nickel ferrite has similar properties, and it is 80–90% normal spinel. Magnesium ferrite, however, transforms at high temperature to the normal spinel structure as the divalent magnesium ions are thermally excited onto the tetrahedral sites. In this case, the magnetization is strongly influenced by the cooling rate. Slow cooling allows the inverse spinel structure

Cooperative Learning Exercise 6.7

The number of Bohr magnetons contributed by various divalent transition metal ions are summarized below. Since the trivalent ions are equally distributed between half of the occupied octahedral sites (8) and all the occupied tetrahedral sites (8), their moments cancel out, and the net magnetic moment of a ferrite can be predicted from the moment of the divalent ions that occupy the remainder of the octahedral sites (8).

Magnetic Moment	
Ion	(Bohr magnetons, $\mu_B = 9.27 \times 10^{-24} \text{ A} \cdot \text{m}^2$)
Mn ²⁺	5
Fe ²⁺	4
Co ²⁺	3
Ni ²⁺	2
Cu ²⁺	1

Person 1: Calculate the net magnetic moment per unit cell for copper ferrite. Remember that there is more than one formula unit (CuFe₂O₄) per unit cell in the inverse spinel structure.

Person 2: Calculate the net magnetic moment per unit cell for nickel ferrite. Remember that there is more than one formula unit (NiFe₂O₄) per unit cell in the inverse spinel structure.

Exchange information.

Person 1: Calculate the saturation magnetization, M_s , for nickel ferrite, which has a lattice parameter of $a = 0.833 \text{ nm}$.

Person 2: Calculate the saturation magnetization, M_s , for copper ferrite, which has a lattice parameter of $a = 0.838 \text{ nm}$.

Answers: $p^m(\text{Cu}^{2+}) = 8\mu_B$; $p^m(\text{Ni}^{2+}) = 16\mu_B$; $M_s(\text{NiFe}_2\text{O}_4) = 2.6 \times 10^5 \text{ A/m}$; $M_s(\text{CuFe}_2\text{O}_4) = 1.3 \times 10^5 \text{ A/m}$.

to occur because enough thermal energy and time are available to allow the magnesium ions to migrate to the preferred octahedral sites. The saturation moment for a rapidly quenched sample is $2.23\mu_B$; a slow furnace cool results in $1.28\mu_B$. The Mg^{2+} ion has no net moment so that the inverse spinel should have zero magnetization and the normal spinel $10\mu_B$. Magnesium ferrite has high resistivity and low magnetic and dielectric losses that make it most suitable for microwave applications.

Some ferrimagnetic oxides have the garnet structure, which can accommodate large trivalent rare-earth ions with large magnetic moments. The chemical formula for ferrimagnetic garnets is $\text{M}_3\text{Fe}_5\text{O}_{12}$, where M is a rare-earth ion or a yttrium ion. The garnet $\text{Y}_3\text{Fe}_5\text{O}_{12}$, called yttrium–iron–garnet (YIG), has a high electrical resistivity and, correspondingly, a very low hysteresis loss even at microwave frequencies.

The hexagonal ferrites have a structure related to the spinel structure but with hexagonal close-packed oxygen ions and a unit cell made up of two formulae of $\text{MN}_{12}\text{O}_{19}$, where M is divalent (Ba, Sr, or Pb) and N is trivalent (Al, Ga, Cr, or Fe),

which gives a molecular formula of $M^{2+}O \cdot N_2^{3+}O_3$. The best-known examples are magnetoplumbite, which has a formula $PbFe_{12}O_{19}$, and barium ferrite, $BaFe_{12}O_{19}$. As in the spinel structures, magnetization of these compounds is the result of unpaired electrons, usually in the Fe ions. Hexagonal ferrites are of interest because of their high magnetocrystalline anisotropy and high coercivity, which make them suitable for permanent magnets.

For all the ferrites, a number of other factors influence the magnetic properties beside structure. These include impurities, oxygen partial pressure, grain size, and porosity. For example, nickel ferrite thin films deposited by reaction sputtering at 0°C are noncrystalline, and the magnetic susceptibility shows the material to behave as a paramagnet. If the deposition temperature is raised to 400°C , a micropolycrystalline film results with grain sizes less than 15 nm, and the resulting film shows superparamagnetic behavior. *Superparamagnetism* is the result of clusters of paramagnetism. If there are n clusters, each with N spins, it can be shown that the magnetic susceptibility is now proportional to N^2/n , where in normal paramagnetic materials the Curie Law [Eq. 6.64] tells us that χ is proportional to N . This causes the magnetic moment to increase by orders of magnitude, provided that $N \gg n$. If the size of the clusters get so big as to form magnetic domains, the advantage is lost.

Ferrite can be used as soft magnets, hard magnets, and a class of materials known as *semihard magnets*. Soft magnetic ferrite is used for core materials for coils and transformers. Hard magnetic ferrite is used in making permanent magnets. Semihard magnetic ferrites have properties between those of soft and hard magnetic ferrites. They are comparatively easy to magnetize, can retain magnetization, and can produce changes in the magnetic flux from this state, as needed. The typical application for semihard magnetic ferrites is in memory cores for computers. In general, the Mn–Mg ferrites and the lithium ferrites are useful for semihard applications. There is a growing list of applications for ferrites, including microwave applications that utilize the unique magnetic properties of these materials.

6.2.2.3 The Meissner Effect. In Section 6.1.2.4, we describe the interrelationship between electric current density, magnetic field, and temperature for oxide superconductors, and although a great deal of description was given to upper and lower critical magnetic fields, one particularly important topic related to magnetism was deferred to this section. That topic has to do with an important phenomenon related to superconductivity called the *Meissner effect*. Like superconductivity itself, the Meissner effect is relatively old as far as scientific discoveries go. It was found in 1933 by W. Meissner and colleagues, who determined that a superconducting metal expels any magnetic field when it is cooled below the critical transition temperature, T_c , and becomes superconducting. By expelling the field and thus distorting nearby magnetic field lines, as shown in Figure 6.64b, a superconductor will create a strong enough force field to overcome gravity. This expulsion of the magnetic field is to be distinguished from simply preventing the field lines from penetrating—any metal with infinite conductivity would do the latter. If a magnetic field is already present, and a substance is cooled below T_c to become a superconductor, the magnetic field is expelled. The significance of this difference cannot be explained merely by infinite conductivity.

The ability of the superconductor to overcome gravitational forces has led to the famous demonstration, typically involving an oxide superconductor and a rare-earth magnet, in which the magnet is levitated above the superconductor when it is cooled

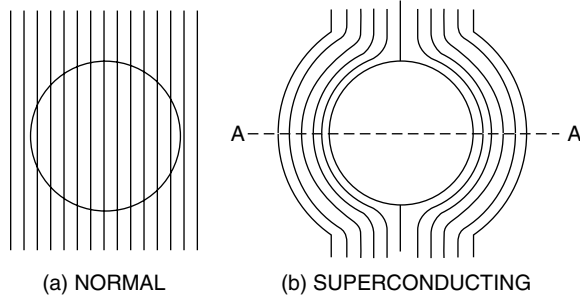


Figure 6.64 Schematic illustration of Meissner effect in which magnetic flux lines that (a) normally penetrate the material are (b) expelled in the superconducting state.

with liquid nitrogen. In this experiment, the magnetic field lines from the strong (but small) magnet penetrate the superconductor to a small depth called the *penetration depth*, λ , which sets up circulating currents—called *eddy currents*—in the superconductor. Typically, the penetration depth is less than $0.05 \mu\text{m}$, so that on a macroscopic scale, the superconductor is said to exclude the magnetic field. In actuality, these eddy currents create their own magnetic field lines that exactly cancel the applied magnetic field from the magnet, thus levitating it.

No superconductor can keep out very strong magnetic fields. As described previously, Type I superconductors have a critical magnetic field, H_c , above which they no longer superconduct. Type II superconductors have a range of critical fields from the upper critical field, H_{c2} , to the lower critical field, H_{c1} . Below these critical fields, the superconductor is perfectly diamagnetic. For a perfect diamagnet, $M = -H$, so that according to Eq. (6.61) the inductance is $B = 0$. Thus, the earlier statement that diamagnetism is not important in ceramic materials must be strongly qualified for the oxide superconductors—diamagnetism is critical to their importance.

At first, the superconducting state was not thought to be a thermodynamic equilibrium state. But, as we know from Chapter 2, any equilibrium state must be the result of a free energy minimization. It can be shown that the superconducting and normal states will be in equilibrium when their free energies are equal, and that the free energy difference between the normal state at zero field, $G_n(H = 0)$, and the superconducting state at zero field, $G_s(H = 0)$, is

$$G_n(H = 0) - G_s(H = 0) = \frac{\mu_0 H_c^2}{2} \quad (6.66)$$

The free energies for the respective states can be determined from heat capacity data, and the thermodynamic critical field can be determined from a plot of free energy versus applied field for the two states, as illustrated in Figure 6.65.

The Meissner effect is a very important characteristic of superconductors. Among the consequences of its linkage to the free energy are the following: (a) The superconducting state is more ordered than the normal state; (b) only a small fraction of the electrons in a solid need participate in superconductivity; (c) the phase transition must be of second order; that is, there is no latent heat of transition in the absence of any applied magnetic field; and (d) superconductivity involves excitations across an energy gap.

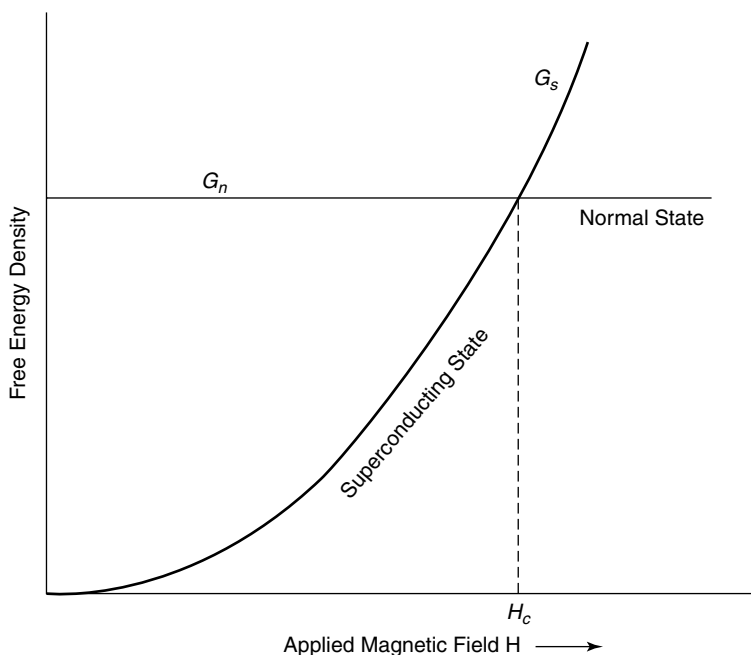


Figure 6.65 Free energy curves for both normal and superconducting states.

6.2.3 Magnetic Properties of Polymers

Much like ceramics, the electrical and magnetic properties of polymers are closely linked. Initially, this statement can be viewed with considerable disappointment, since, with only a few notable exceptions, polymers are poor electrical conductors, and what is known about their potential for magnetization is even less than is known about their electrical conductivity. Nonetheless, there is hope. Just as new classes of polymers are currently being developed with improved electrical conductivities, there is reason to believe that polymers can be developed that will have significant magnetic properties. What a potential benefit this could be for the development of lightweight magnets. We briefly describe here just one topic related to magnetic polymers that is still too “young” in its scientific development to warrant significant coverage in an introductory text: *molecular magnets*. The more common use of polymers in magnetic media, that as a matrix for the support of nonpolymeric magnetic particles, is more appropriately addressed in the section on composites.

6.2.3.1 Molecular Magnets*. Much of the information presented here on molecular magnets is drawn from some excellent, recent review articles [9–12] on this emerging field. Following a brief introduction to the general topic of molecular magnets, a description of organic molecular magnets will be given, with an emphasis on the development of polymeric molecular magnets.

A molecular magnet is a magnet that is molecule-based—that is, composed of molecular or molecular ion entities, and not atoms or atomic ions. This distinction is not new to us, though previously we have not elaborated upon it. Simply compare the crystal structures of such atom-based solids as BaTiO_3 in Figure 1.42, in which the

positions of the atoms determine the crystal structure, with that of a molecule-based solid such as polyethylene in Figure 1.65, in which the positions of the molecules, in this case chains, determine the crystal structure. Think about this distinction for a moment, and you will realize that most molecular materials are organic in nature. The covalent bonds within the molecules are stronger than the noncovalent bonds that draw the organic compounds into a molecular crystal, such as hydrogen bonding and van der Waals interactions. This is different from metallic and ionic solids, in which any Na–Cl interaction, for example, is essentially the same anywhere in the crystal, so that ordering takes place on the atomic scale.

The magnetic materials described so far in this chapter are all atom-based: Their bulk magnetic properties are due to the incorporation of atoms such as Fe or Nd. In these materials, magnetic order arises from cooperative spin–spin interactions between unpaired electrons located in *d* or *f* orbitals of the metal atoms. Molecular-based materials, on the other hand, do not tend to exhibit magnetic properties for some very good reasons. Organic compounds generally have closed-shell structures and are thus diamagnetic. Paramagnetic organic molecules are very rare because the presence of unpaired electrons—which are required for paramagnetism—in the *s* and *p* orbitals gives instability to the molecules, which tend to spontaneously form a covalent bond with another molecule, thus pairing the spins. Even if one or more unpaired electrons are maintained stably in an organic molecule, stabilization of a triplet state (parallel alignment of spins) requires that certain quantum mechanical conditions be met which are difficult to satisfy, such that they prefer to couple in an antiferromagnetic manner with no spontaneous magnetic moment. Thus, the development of ferro- or ferromagnetic organic molecules has been elusive. However, recent advances in synthetic molecular chemistry have made possible the formation of organic molecules with sufficient magnetic function that can serve as building blocks for bulk magnetic behavior. Without delving into the theory of magnetism in these materials, we describe some of these building blocks that may one day be the precursors to polymer magnets.

The typical synthetic approach to designing molecular magnets consists of choosing molecular precursors, each of which contains an unpaired spin, as represented by the arrow in Figure 6.66. The precursors are then assembled in such a way that there is

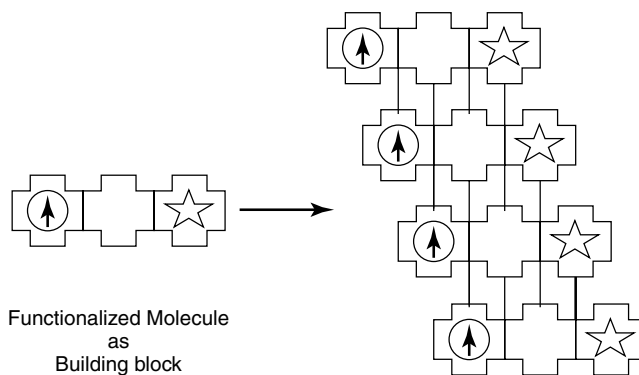


Figure 6.66 Schematic illustration of building blocks used to construct molecular magnets. An arrow indicates an unpaired electron, and a star represents some other desirable functionality. Reprinted, by permission, from J. V. Yakhmi, *Physica B*, **321**, 206. Copyright © 2002 by Elsevier Science B. V.

no compensation of the spins at the crystal lattice scale. In Figure 6.66, the precursors may contain other functional groups, represented by the star, that can assist in self-assembly, or impart some additional property such as chirality or ferroelectricity. The primary criteria for designing a molecular magnet, then, are that (a) all the molecules in the lattice have unpaired electrons, and (b) the unpaired electrons have spins aligned parallel along a given direction. Since magnetism is a cooperative effect, the spin–spin interaction must extend to all three dimensions in the lattice. These criteria are met in molecules such as the nitronyl nitroxide radical, NITR, shown in Figure 6.67a, where R is an alkyl group. Through different substitutions for the alkyl group, the spin delocalization effect can be fine-tuned. An example is when R is a nitrophenyl compound, which results in 4-nitrophenyl nitronyl nitroxide, or *p*-NPNN for short, as shown in Figure 6.67b. Ferromagnetism has been exhibited in this purely organic compound at around 0.6 K. Other similar, organic compounds have Curie temperatures of 16 K and above.

An alternative strategy is to utilize ferrimagnetic chains containing alternating spins of unequal magnitude and assemble them in such a way that there is a net spin. For example, two different spin carriers such as Mn ions, with $m_s = 5/2$, and Cu ions, with $m_s = 1/2$, can be incorporated within the same molecular precursor, as schematically illustrated in Figure 6.68. It is also possible to create different spins using organic radicals instead of metal ions. An example of such a building block is shown in Figure 6.69 for $[\text{Cu}(\text{opba})]^{2-}$, where “opba” stands for ortho-phenylenebis(oxamato). This copper

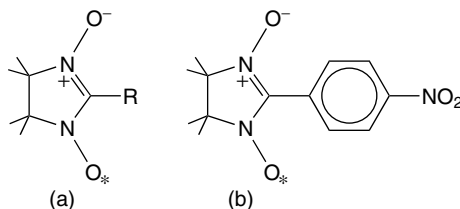


Figure 6.67 Chemical structures of (a) NITR and (b) *p*-NPNN used in molecular magnets. An asterisk, *, indicates an unpaired electron. Reprinted, by permission, from J. V. Yakhmi, *Physica B*, **321**, 206. Copyright © 2002 by Elsevier Science B. V.

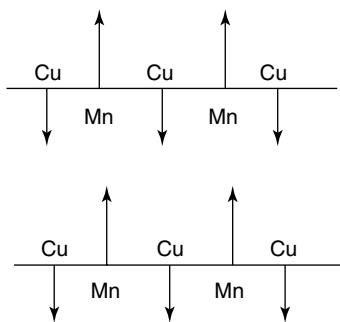


Figure 6.68 Schematic illustration of spin assembly metal-based ferrimagnetic chains. Reprinted, by permission, from J. V. Yakhmi, *Physica B*, **321**, 206. Copyright © 2002 by Elsevier Science B. V.

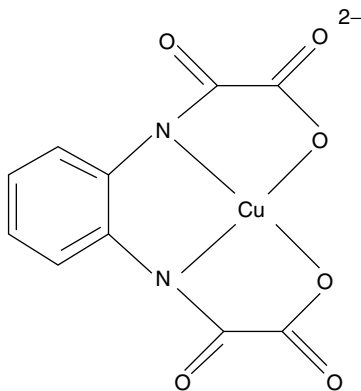


Figure 6.69 Structure of the copper dianion precursor $[\text{Cu}(\text{opba})]^{2-}$. Reprinted, by permission, from J. V. Yakhmi, *Physica B*, **321**, 206. Copyright © 2002 by Elsevier Science B. V.

precursor can be reacted with a divalent ion such as Mn^{2+} , which results in an amorphous magnet with a spontaneous magnetization below 6.5 K. Similar precursors can be assembled into crosslinked chains with still higher Curie temperatures, as shown in Figure 6.70. Note that even though these structures contain transition metals such as Mn and Cu, it is the entire *molecule*, including the metal ion, that exhibits the spin, and that can be used as a building block for larger structures.

One final example is a class of related materials that undergo reversible magnetic behavior through a mild dehydration-rehydration process. Because these materials show a reversible crossover under dehydration to a polymerized long-range, magnetically ordered state with spontaneous magnetization, and transformation back to isolated molecular units under rehydration, they are called *molecular magnetic sponges*. Coercivity values for these sponges are high (see Table 6.23), and some even undergo color changes that coincide with the change in magnetic properties. In addition to the “opba” anion described above, these molecular magnetic sponges are composed of “obbz” and “obze” ligands, where obbz = oxamido bis(benzoato) and obze = oxamido-*N*-benzoato-*N'*-ethanoato.

As this field continues to develop, look for improvements not only in the magnetic properties of these organic polymers, but also in the theoretical descriptions of intrinsic ferro- and ferrimagnetism in polymers.

6.2.4 Magnetic Properties of Composites

In this section, we describe the properties of two magnetic composites that represent extremes in terms of applications for magnetic materials. The first, flexible magnets illustrate how the incorporation of less-expensive components into a material can retain the functionality of the magnetic material while significantly reducing cost. The second, magnetic storage media illustrates how a simple concept such as a reversible magnetic moment can be utilized to create an entirely new industry and revolutionize the manner in which we conduct our daily lives.

6.2.4.1 Flexible Magnets. Flexible magnets are made by embedding ferrimagnetic ceramics in a polymer matrix, such as barium ferrite or strontium ferrite in nylon or

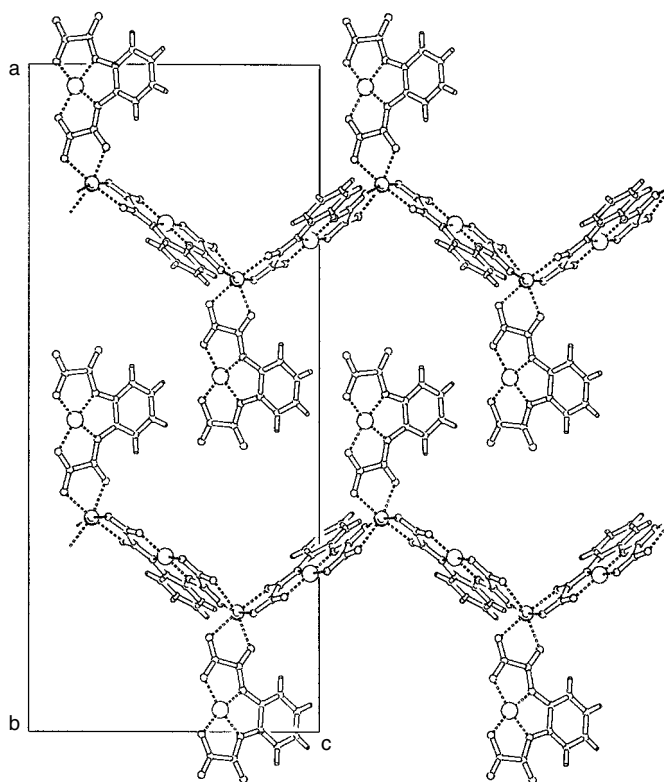


Figure 6.70 Structure of 1:2 Mn(II)Cu(II) compound consisting of a zigzag chain with terminal “opba” groups. Reprinted, by permission, from J. V. Yakhmi, *Physica B*, **321**, 207. Copyright © 2002 by Elsevier Science B. V.

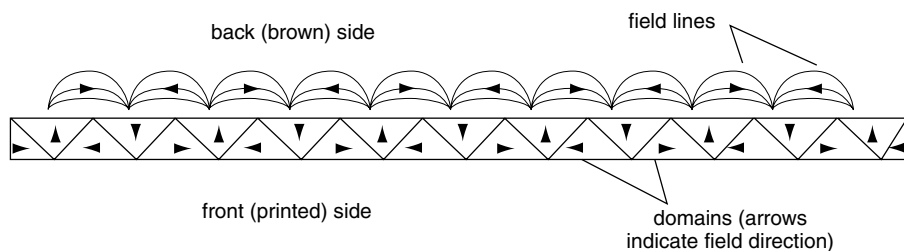
Table 6.23 Selected Magnetic Properties of Some CoCu-Based Molecular Magnetic Sponges

Compound	T_c (K)	H_c (kOe)
$\text{CoCu}(\text{pbaOH})(\text{H}_2\text{O})_3 \cdot 2\text{H}_2\text{O}$	38	5.66
$\text{CoCu}(\text{pba})(\text{H}_2\text{O})_3 \cdot 2\text{H}_2\text{O}$	33	3
$\text{CoCu}(\text{obbz})(\text{H}_2\text{O})_4 \cdot \text{H}_2\text{O}$	25	1.3
$\text{CoCu}(\text{obze})(\text{H}_2\text{O})_4 \cdot 2\text{H}_2\text{O}$	20	1

Source: J. V. Yakhmi, *Physica B*, Vol. 321, pp. 204–212. Copyright © 2002 by Elsevier Science B.V.

polyphenylene sulfide. In an anisotropic magnet (one-sided) the ferrite and polymer components are mixed and processed, usually by extrusion, into a thin sheet and are then coated or printed on one side. Typical tape thicknesses are 1–2 mm. To obtain maximum alignment, the ferrite particles are physically rotated in a magnetic field during the molding process. In this way, energy products equivalent to those of cobalt steel are obtained.

Side view



Side view

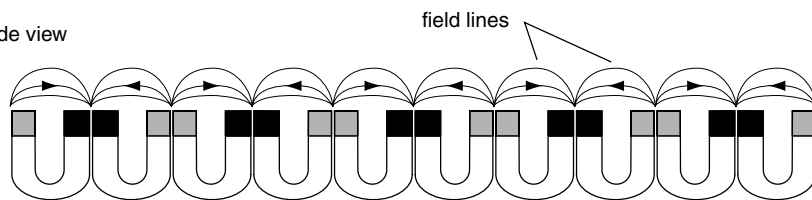


Figure 6.71 Side view of magnetic flux lines in an anisotropic flexible magnet. (mrsec.wisc.edu/edetc).

The magnetic field structure (see Figure 6.71) in an anisotropic magnet is made of a striped pattern of alternating pole alignments on the back side of the flexible magnetic sheet. This arrangement also channels the magnetic field to the back of the magnet so that maximum holding power is obtained, which is important for many applications. It is also possible to make isotropic, or two-sided, magnetic tapes and sheets, for which the field lines shown in Figure 6.71 are present on both sides of the sheet.

The magnetic properties of the flexible magnets depend upon the properties of the ferrite, of course, and the relative amounts of ferrite and binder, as well as processing conditions, but generally for strontium ferrite-based materials, residual inductions, B_r , range from 1.6 to 2.6 gauss, coercive forces, H_c , range from 1.3 to 2.3 kOe, and densities range from 3.5 to 3.8 g/cm³. The magnetic properties degrade linearly with increasing temperature, and there is generally an upper-use temperature of around 100°C at which point the polymeric component begins to melt or flow.

6.2.4.2 Magnetic Storage Media. Magnetic materials are ideal candidates for information storage media because magnets can be used like switches. They can be made to point in one direction or another in the presence of a magnetic field. Reverse the direction of the field, and the magnet will switch to point in the other direction. This represents a simple way to store binary information. The magnet represents a “1” when pointing in one direction and represents a “0” when pointing in the other. A magnetic memory can be constructed from an entire array of magnets, in which the binary data can be encoded by applying an external magnetic field to each magnet in turn, the direction of which determines whether a “1” or a “0” is written. As we have seen, individual atoms can act as magnets. In a ferromagnetic material such as iron, for example, the magnetic moments in each atom tend to line up so that they all point in the same direction. Furthermore, recall that the magnetic moments tend to align in domains, separated by domain walls, the net magnetic moments of which are randomly oriented to create a bulk material with no net magnetic moment.

The ability to influence the alignment of magnetic moment by the application of a magnetic field forms the basis of magnetic recording. By applying a strong, localized magnetic field to one region of a thin layer of a ferromagnetic material such as magnetite (above the Curie temperature), a domain can be created in which all the magnetic moments are aligned. The magnetized domains, in general, are larger than the magnetic particles. Application of the field in the opposite direction in another part of the magnetic medium creates a domain of opposite alignment. One alignment direction represents the “1” in the binary code, and the opposite direction represents the “0.” The alignment is generated by a *recording head*, which generates a magnetic field that changes the direction of alignment in the magnetic particles, as shown in Figure 6.72. The recording head contains an electromagnet in which the field is generated by flowing current across a small gap. When the recording head is magnetized, a magnetic field bridges the gap, and the flux lines spread out so that they pass through the magnetic medium lying below. The magnetic moments in the medium align themselves with the direction of the field across the recording head gap. Essentially the same process in reverse is used to retrieve information from the device.

Magnetic tape technology, while still important in limited applications, has been almost completely replaced by two-dimensional disk technology due to the limitations of the one-dimensionality of the tape. In order to retrieve information from one part of the tape, the entire preceding information must first be trawled through. Though the disk allows information to be retrieved from a specific site on the disk surface, the principles of magnetization and storage of binary information via alignment of magnetic particles is essentially the same. The primary principle leading to the development of new materials in this area is storage density. As illustrated in Figure 6.73, there must be a *transition region* between each oriented domain in the magnetic film. This buffer zone allows adjacent magnetic domains to retain their alignment without influencing each other. The resistance to alignment flipping due to an adjacent domain is related to the coercivity of the particles. The higher the coercivity, the more resistant the particle

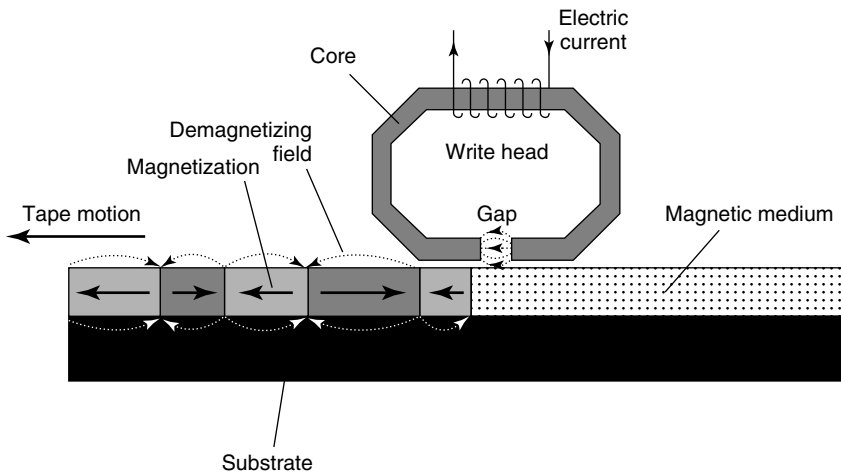


Figure 6.72 Schematic diagram of a magnetic recording device and magnetization in magnetic tape recording medium. Reprinted, by permission, from P. Ball, *Made to Measure*, p. 72. Copyright © 1997 by Princeton University Press.

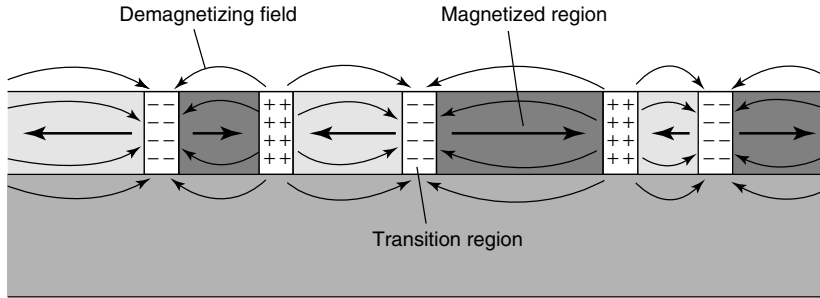


Figure 6.73 Schematic illustration of transition region between magnetic domains in a magnetic information storage medium. Reprinted, by permission, from P. Ball, *Made to Measure*, p. 75. Copyright © 1997 by Princeton University Press.

is to flipping, and the smaller the transition zone between domains can be. Smaller transition zone and magnetic domains translate directly into increased storage density.

Composite magnetic recording media consist of submicroscopic, single-domain particles of magnetic oxides or metals immersed in a polymeric binder that separates the particles and binds them to the substrate. The substrates used in tapes, magnetic cards, and floppy disks are generally made from poly(ethylene terephthalate), while rigid disks are fabricated from an Al–Mg alloy. Particles of $\gamma\text{-Fe}_2\text{O}_3$ have been used in tapes for a long time, but as the bit length of recorded signals becomes shorter, further improvements in coercivity are required. Coercive fields have been raised from 100 to 500 A/m by impregnating the surface of the iron oxide particles with cobalt.

In addition to magnetic particle/polymer composites, laminar magnetic composite thin films are used for information storage. The magnetic film is typically either a CoPtCr or CoCrTa alloy of thickness 10 to 50 nm on a substrate of pure chromium or chromium alloy (see Figure 6.74). The carbon layer overcoat is to improve mechanical stability, reduce corrosion of the magnetic layer, and provide a hard, low-friction surface for the head to glide over. The magnetic thin film is polycrystalline, with an average grain size of 10–30 nm. Each grain is a single magnetic domain, with the direction of easy magnetization for each grain aligned in the direction of disk motion. In these materials, it is desirable to have a relatively large and square hysteresis loop. Saturation flux densities range from 0.4 to 0.6 tesla, and coercivities range from

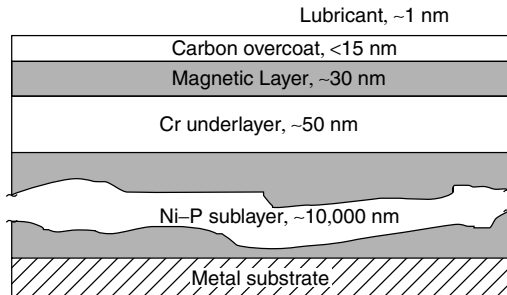


Figure 6.74 Schematic illustration of layers in a composite thin film for magnetic information storage.

1.5×10^5 to 2.5×10^5 A/m (2 to 3 kOe). These films are formed by a process called chemical vapor deposition, which will be described in more detail in the next chapter.

Laminar composite technology is also used in the readout heads. Instead of relying solely on the change in magnetic field strength from the magnetic storage medium to change an electrical signal in the head (essentially the reverse of the writing situation presented in Figure 6.72), these heads use a phenomenon known as *magnetoresistance*. The electrical resistance of magnetoresistive materials varies markedly with magnetization. The magnetic field from the information storage medium creates a change in resistivity in the readout head, which can be registered as a change in voltage across the material under conditions of constant current. The advantage of this device is that the head is far more sensitive to changes in the magnetic flux of the storage medium. As a result, magnetoresistive heads can be made very thin and can actually be placed within the gap of the induction loop used to write on the medium (see Figure 6.72). The magnetoresistive heads are made by alternating layers of two different metals, such as iron and chromium. Cobalt and chromium are also used. The layers are again formed by chemical vapor deposition and are only a few nanometers thick. Stacks of these thin layers are known as *superlattices*. In this way, iron–chromium superlattices can be made with resistances in the presence of magnetic fields of just half that in the absence of a field, as shown in Figure 6.75. The magnetic coupling between the layers is like that in an antiferromagnetic material, and it leads to changes in the mobility of the charge carriers in the superlattice.

Additional information storage phenomena such as compact disks (CDs) and digital video disks (DVD) involve laser technology and will be described in the next section. The area of information storage is an ever-evolving one and will potentially involve phenomena other than alignment of magnetic domains. At present, however, magnetic storage media are an excellent example of how composites are utilized in areas other than for structural applications.

6.2.5 Magnetic Properties of Biologics*

Much as was the case in general with polymeric materials, biologics do not possess significant magnetic activity. There is one topic related to the interaction of biological

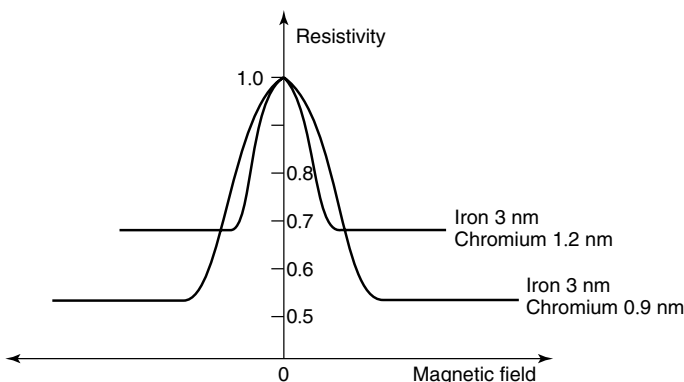


Figure 6.75 Variation in resistivity of two ironchromium superlattices of various layer thicknesses due to magnetoresistive effect. Reprinted, by permission, from P. Ball, *Made to Measure*, p. 77. Copyright © 1997 by Princeton University Press.

tissues with magnetic fields that is of such technological importance, and related enough to the chemical makeup of biologics, that it is worth describing here. *Nuclear Magnetic Resonance Imaging*, or MRI for short, has revolutionized diagnostic medicine. What is so intriguing about it from a scientific standpoint is that it is based upon the interaction of only one atom with a magnetic field—hydrogen.

6.2.5.1 Nuclear Magnetic Resonance Imaging. Virtually all of the topics in this textbook deal in some way with the chemical aspects of atoms and molecules—that is, how electrons and the electronic structure dictate interactions between atoms and molecules, and ultimately, the bulk properties of an assembly of atoms or molecules. This is why such a great deal of attention was devoted to potential energy functions, molecular orbital structure, and bonding in the first chapter. And, as we have seen in this section on magnetic properties, simple electronic orbital diagrams can provide very clear explanations for why certain materials behave as diamagnets while others behave as paramagnets. Indeed, all of the types of magnetism described in this section are related in some way to the pairing of electrons.

What we describe in this subsection is not a bulk magnetic property of a material and is not related to any of the types of magnetism described heretofore. *Nuclear magnetic resonance*, as the name implies, is related to the interaction of an atom's nucleus with a magnetic field. Let us take a moment to review a bit of nuclear chemistry, then describe the general topic of nuclear magnetic resonance, or NMR, before completing this section with a description of the application of NMR to imaging of hydrogen in biological tissues—MRI.

Recall from general chemistry that an atom consists not only of orbiting electrons, but of a central nucleus, composed of *nucleons* called protons and neutrons. The protons are positively charged, and the neutrons have no charge associated with them. In addition to electrons orbiting the nucleus, there are two other kinds of spins associated with an atom: (a) the spin of an electron on its own axis and (b) the spin of a nucleus on its own axis. We have concentrated a great deal upon the motion of electrons and have completely ignored the spin of the nucleus to this point. We must no longer ignore nuclear spin, since it is the basis upon which MRI functions.

Particles that spin have an associated angular momentum; and as dictated by quantum chemistry, the angular momentum has values that are integral or half-integral multiples of $h/2\pi$, where h is Planck's constant. The maximum spin component for a particular nucleus is its *spin quantum number*, I , and a nucleus has $(2I + 1)$ discrete states. The component of angular momentum for these states in any chosen direction will have values of $I, I - 1, I - 2, \dots, -I$, called the *magnetic quantum number*, m . In the absence of an external magnetic field, the various states have identical energies. The spin number for a proton is $1/2$; thus two spin states are possible: $I = +1/2$ and $I = -1/2$. Heavier nuclei have spin numbers that range from 0 to over $9/2$. As shown in Table 6.24, the spin number of a nucleus is related to the relative number of protons and neutrons it contains. Since the nucleus contains a charge, its spin gives rise to a magnetic field, much like the field produced when electricity flows through a coil of wire. The resulting magnetic dipole is oriented along the axis of spin and has a value that is characteristic for each type of nucleus. For a hydrogen atom, whose nucleus contains only one proton, the spin quantum number is $I = 1/2$, and the magnetic quantum number can have values of $+1/2$ and $-1/2$. These two quantum energies correspond to the two possible orientations of the spin axis: spin up and spin down. Those nuclei

Table 6.24 Spin Quantum Number for Various Nuclei

Number of Protons	Number of Neutrons	Spin Quantum Number I	Examples
Even	Even	0	^{12}C , ^{16}O , ^{32}S
Odd	Even	$\frac{1}{2}$	^1H , ^{19}F , ^{31}P
		$\frac{3}{2}$	^{11}B , ^{79}Br
Even	Odd	$\frac{1}{2}$	^{13}C
		$\frac{3}{2}$	^{127}I
Odd	Odd	1	^2H , ^{14}N

with a spin-up orientation are termed low energy, and those with spin-down orientation are termed high energy. In the absence of a magnetic field, the energies of these two states are identical, despite their names. Consequently, a large assemblage of hydrogen atoms will contain an identical number of nuclei with $m = +\frac{1}{2}$ and $m = -\frac{1}{2}$.

When brought into the influence of an applied magnetic field, the spins tend to become oriented parallel to the field, termed spin up, and the lower-energy spin state ($m = +\frac{1}{2}$) is more highly populated. Some spins do populate the high-energy state, however. In fact, at room temperature there is only a minute excess (< 10 ppm) of nuclei in the lower-energy state due to thermal energies that are several orders of magnitude greater than the magnetic energy differences. This small difference in spin orientations is sufficient, however, to result in a net magnetic moment, as characterized by the *net magnetization vector*, NMV. The orientation of nuclear spins in a magnetic field is shown in Figure 6.76.

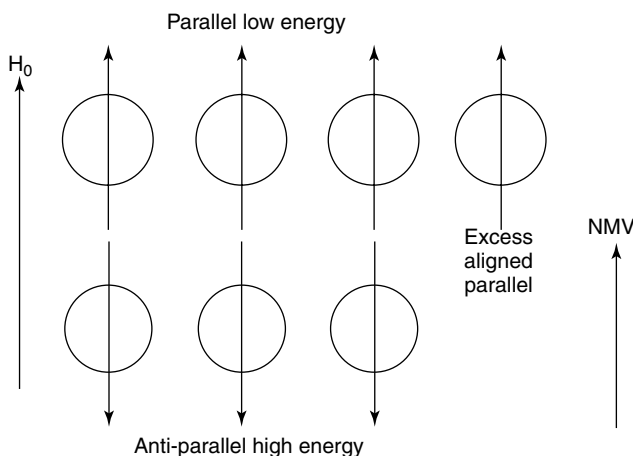


Figure 6.76 Orientation of nuclear spins in the presence of a magnetic field, and the resulting net magnetization vector (NMV) from excess low-energy spins aligned parallel to field. Adapted from C. Westbrook and C. Kaur, *MRI in Practice*, 2nd ed., p. 6. Copyright © 1998 by Blackwell Science Ltd.

The application of a magnetic field to the spinning nucleus creates an additional movement in the nucleus, called *precession*. Much like a compass needle that will swing back and forth indefinitely in the presence of an external magnet, a spinning particle will be forced to move in a circular path in the presence of a magnetic field. This is a gyroscopic effect similar to what occurs in a gyroscope when it is displaced from vertical by application of an external force. In this case, the external force is the applied magnetic field, which causes the spinning particle to move in a circular path, or precess, about the magnetic field, as illustrated in Figure 6.77. The *angular velocity of precession*, ω_0 , is directly proportional to the applied force and inversely proportional to the angular momentum of the spinning body. The force on a spinning nucleus in a magnetic field is the product of the field strength, H_0 , and the magnetic moment of the particle. When combined with the angular momentum, the magnetic moment creates a quantity called the *magnetogyric ratio*, γ , sometimes (inappropriately) called the gyromagnetic ratio. The result is the Larmor equation:

$$\omega_0 = \gamma H_0 \quad (6.67)$$

The magnetogyric ratio is then the ratio between the magnetic moment and the angular momentum of a rotating particle and has a characteristic value for each type of nucleus:

$$\gamma = \frac{\mu\beta}{I(h/2\pi)} \quad (6.68)$$

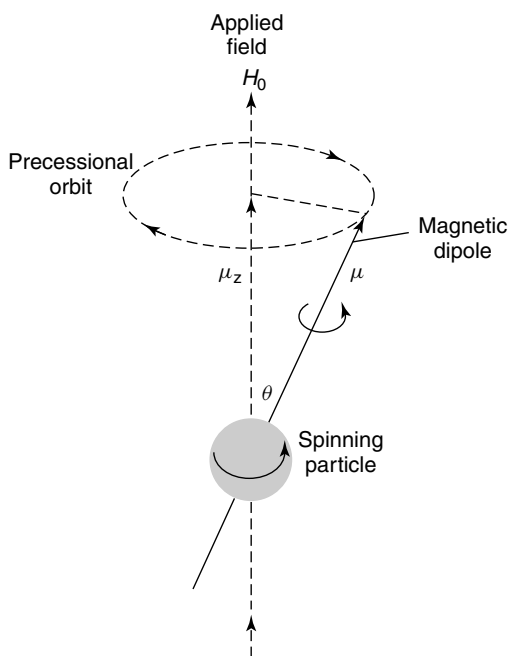


Figure 6.77 Precession of a spinning particle in a magnetic field. Reprinted, by permission, from D. A. Skoog and D. M. West, *Principles of Instrumental Analysis*, 2nd ed., p. 381. Copyright © 1980 by Saunders College.

where μ is the magnetic moment of the nucleus expressed in nuclear magnetons, β is a constant called the *nuclear magneton* (5.051×10^{-24} erg/G), I is the spin quantum number as described previously, and h is Planck's constant. For reference, the magnetic moment for the proton is 2.7927 nuclear magnetons. The angular velocity of precession given by the Larmor equation can be converted to a frequency of precession, ν_0 , by simply dividing by 2π . Thus, as the field strength is increased, the precessional frequency increases.

We turn our attention now to nuclear magnetic resonance, NMR, which forms the basis for MRI. *Resonance* is a phenomenon that occurs when an object is exposed to an oscillating perturbation that has a frequency close to its own natural frequency of oscillation. The nucleus gains energy and resonates if the energy is delivered at exactly its precessional frequency. If energy is delivered at a frequency different from that of the Larmor frequency of the nucleus, resonance does not occur. When this energy, typically in the form of radio-frequency electromagnetic radiation, is absorbed by the nucleus, *excitation* occurs, and the angle of precession, θ , shown in Figure 6.77, must change. If the frequency of the radio wave is the same as the precessional frequency, absorption and flipping can occur. The first result of resonance is that the NMV moves out of alignment away from the direction of the applied field. The angle to which the NMV moves out of alignment is called the *flip angle*. The magnitude of the flip angle depends upon the amplitude and duration of the electromagnetic pulse. Usually, the flip angle is 90° ; that is, the NMV is given enough energy by the pulse to move through 90° relative to H_0 (see Figure 6.78). With a flip angle of 90° the nuclei are given sufficient energy so that the longitudinal NMV is completely transferred into a transverse NMV. This transverse NMV rotates in the transverse plane at the Larmor frequency. We will see that the longitudinal and transverse components of the NMV are critical to NMR analysis.

The process is reversible, and the excited particle can thus return to the ground state by reemission of the radiation. This is known as the *relaxation process*. Relaxation following resonance is the basis for nuclear magnetic resonance spectroscopy. It turns

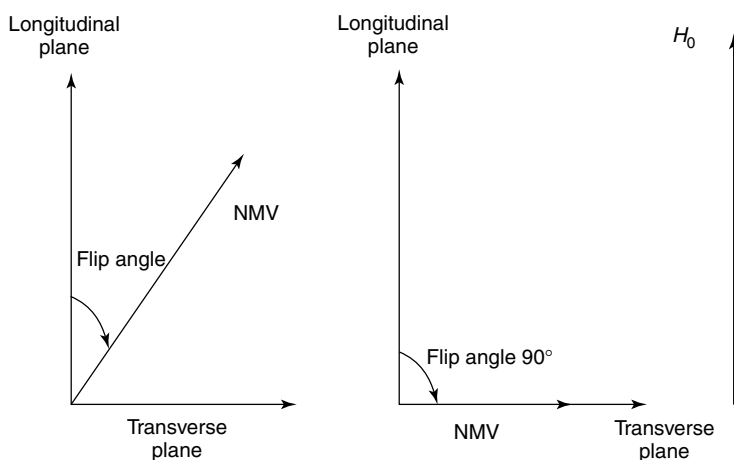


Figure 6.78 The flip angle with and without an applied field. Adapted from C. Westbrook and C. Kaur, *MRI in Practice*, 2nd ed., p. 9. Copyright © 1998 by Blackwell Science Ltd.

out that there is a low probability of emission of radiation of the exact frequency of resonance. Instead, relaxation processes usually involve radiationless mechanisms. In order to produce readily detectable signals, the relaxation processes should be as rapid as possible. Conversely, the lifetime of the excited state should be small. Due to line-broadening effects, which tend to counter the need for short lifetimes, the optimal half-life for an excited species is from about 0.1 to 1 s. There are two types of relaxation processes that are important in this regard: longitudinal, or *spin-lattice relaxation*, and transverse, or *spin-spin relaxation*. Each relaxation process is a first-order process that can be characterized by a time, T , which is the average lifetime of the nuclei in the higher energy state. Spin-lattice relaxation is characterized by a relaxation time T_1 , and spin-spin relaxation is characterized by time T_2 .

T_1 recovery is caused by the nuclei giving up their energy to the surrounding environment, or lattice. The rate of recovery is an exponential process, with a recovery time constant, T_1 , which is defined as the time it takes 63% of the longitudinal magnetization to recover. In addition to depending upon the magnetogyric ratio and the absorbing nuclei, T_1 is strongly affected by the mobility of the lattice. In crystalline solids and viscous liquids, where mobilities are low, T_1 is large. As the mobility increases, the vibrational and rotation frequencies increase, and T_1 becomes shorter. At very high mobilities, however, the probability for a spin-lattice transition begins to decrease. Thus, there is a minimum in the relationship between T_1 and lattice mobility.

T_2 is caused by nuclei exchanging energy with neighboring nuclei. The energy exchange is caused by the magnetic fields of each nucleus interacting with its neighbor. The rate of decay is also an exponential process, and it represents the time it takes 63% of the transverse magnetization to be lost. Values for T_2 are generally so small for crystalline solids and viscous liquids (as low as 10^{-4} s) that these samples are not typically used for high-resolution NMR spectra.

The NMR process, then, essentially involves placing a sample in a magnetic field, applying a radio-frequency (RF) pulse, and determining the decrease in power (attenuation) of the radiation caused by the absorbing sample. This process is shown schematically in Figure 6.79.

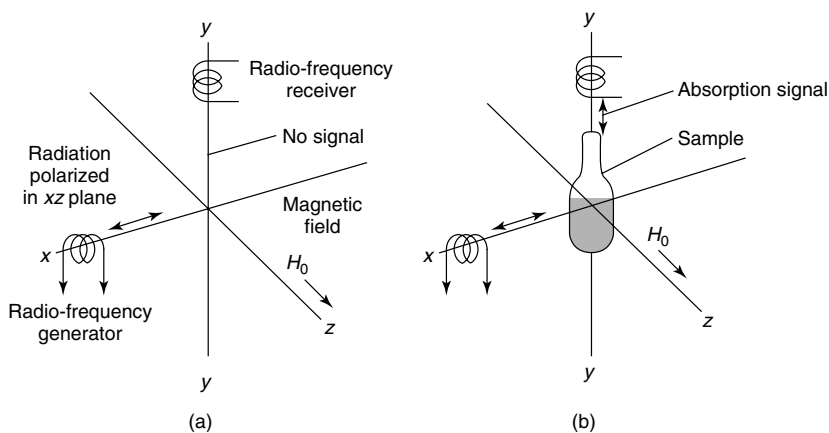


Figure 6.79 Schematic illustration of an NMR experiment (a) without sample and (b) with sample. Reprinted, by permission, from D. A. Skoog and D. M. West, *Principles of Instrumental Analysis*, 2nd ed., p. 285. Copyright © 1980 by Saunders College.

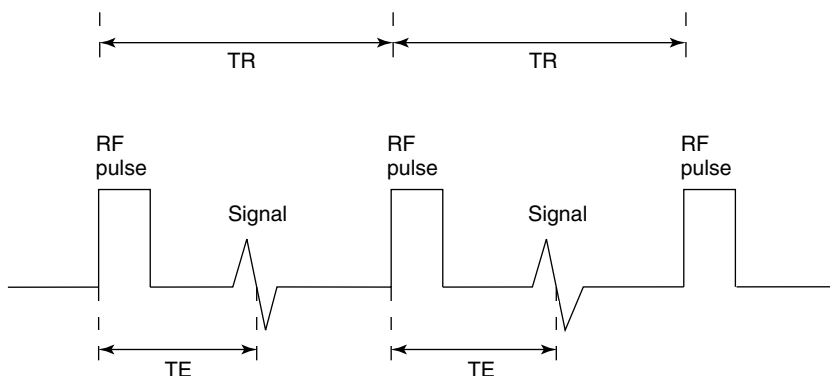


Figure 6.80 A basic NMR pulse sequence. Reprinted, by permission, from C. Westbrook and C. Kaur, *MRI in Practice*, 2nd ed., p. 15. Copyright © 1998 by Blackwell Science Ltd.

The manner in which the RF pulse is applied is critical to NMR analysis. A very simplified pulse sequence is a combination of RF pulses, signals, and intervening periods of recovery, as illustrated in Figure 6.80. The main components of the pulse sequence are the *repetition time*, TR, which is the time from the application of one RF pulse to the application of the next RF pulse (measured in milliseconds) and the *echo time*, TE. The repetition time determines the amount of relaxation that is allowed to occur between the end of one RF pulse and the application of the next. Therefore, the repetition time determines the amount of T_1 relaxation that has occurred. The echo time is the time from the application of the RF pulse to the peak of the signal induced in the coil (also measured in milliseconds). The TE determines how much decay of transverse magnetization is allowed to occur before the signal is read. Therefore, TE controls the amount of T_2 relaxation that has occurred.

Now that the basic principles of NMR have been described, we can describe how this phenomenon is adapted to the generation of images from biological tissues. Magnetic resonance imaging relies upon the nuclear magnet response of only one atom: hydrogen. Though there are certainly other magnetically susceptible atoms in the human body such as C^{13} , N^{15} , O^{17} , Na^{23} , and P^{31} , hydrogen is in such abundance and has such a relatively large magnetic moment owing to its single proton in the nucleus that its selection as the nucleus of choice for MRI is an easy one. As mentioned previously, the spin–spin relaxation time, T_2 , for an atom is influenced by its surroundings. As a result, hydrogen atoms in different environments within the body, in principle, can be differentiated according to their relaxation times. Practically, this means that the NMV can be separated into the longitudinal and transverse components for differing tissues such as fat, cerebrospinal fluid, and muscle.

A tissue has a large NMR signal if it has a large transverse component of magnetization. If there is a large component of transverse magnetization, the amplitude of the signal received by the coil is large, resulting in a bright area on the MRI image. A tissue returns a low signal if it has a small transverse component of magnetization, resulting in a dark area on the image. In general, the two extremes of image contrast in MRI are the result of hydrogens found in fat (lipids) and water (see Figure 6.81).

The hydrogens in lipids are linked to carbon, whereas the hydrogen in water is linked to electron-withdrawing oxygens. The removal of electrons from around the

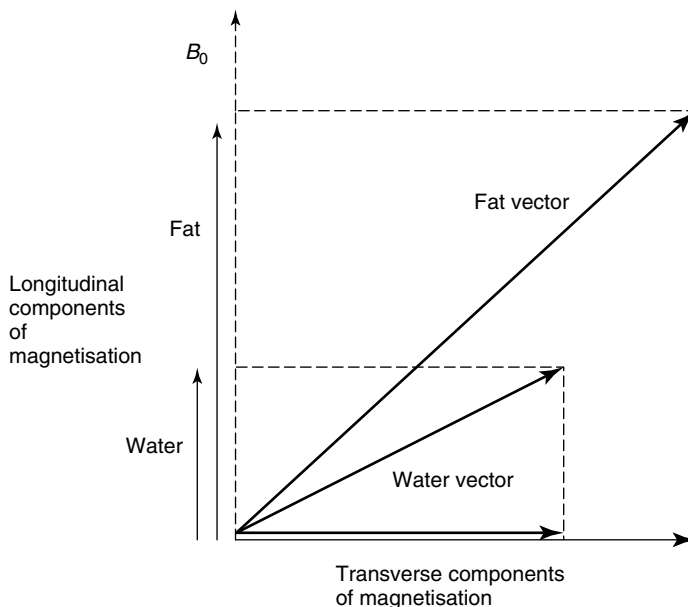


Figure 6.81 Magnitude of transverse and longitudinal magnetization for fat and water. Reprinted, by permission, from C. Westbrook and C. Kaur, *MRI in Practice*, 2nd ed., p. 18. Copyright © 1998 by Blackwell Science Ltd.

hydrogens in water causes its nucleus to be less shielded and to interact more strongly with the applied magnetic field. The carbon in lipids is less electron-withdrawing, so lipid hydrogens do not interact with the magnetic field as strongly. Therefore, the Larmor frequency of hydrogen in water is higher than that of hydrogen in lipids. Lipid hydrogens recover more rapidly along the longitudinal axis than water, and they lose transverse magnetization faster than water hydrogens. The result is different imaging characteristics in MRI.

Images obtain contrast mainly through T_1 and T_2 relaxation processes, as well as proton density. Let us briefly describe each of these effects in both fat and water. T_1 recovery occurs due to nuclei transferring their energy to the surroundings. The slow molecular tumbling in fat allows the recovery to proceed relatively rapidly. This means that the magnetic moments of hydrogens in fat are able to relax and regain their longitudinal magnetization quickly. The NMV of lipid hydrogens realigns rapidly with the applied field, and the T_1 for fat is short. In water, molecular mobility is high, resulting in less efficient T_1 recovery. The magnetic moments of water hydrogens take longer to relax and regain their longitudinal magnetization. The NMV of hydrogens in water take longer to realign with the applied field, so their T_1 is long. Because the T_1 time of hydrogens in fat is shorter than for those in water, its vector realigns with the applied field vector faster than that of water. The longitudinal component of magnetization of lipid hydrogens is therefore larger than water hydrogens. After a certain repetition time, TR, the next RF pulse is applied, flipping the longitudinal components of magnetization of both fat and water hydrogens into the transverse plane (assuming that a 90° pulse is applied). Since there is more longitudinal magnetization in the lipid hydrogens than before the RF pulse, there is more transverse magnetization

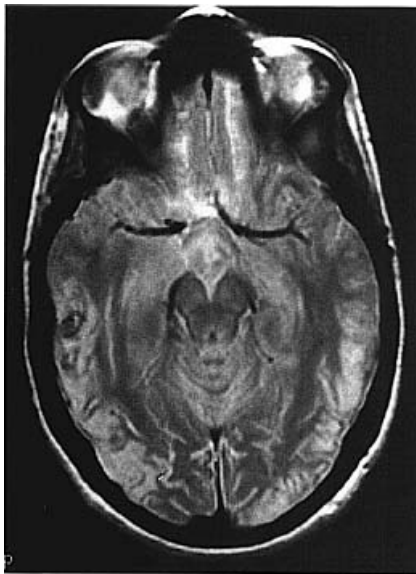
after the RF pulse. Lipid hydrogens therefore have a high signal and appear bright on a T_1 contrast image. The opposite is true for water hydrogens, which appear as dark on a T_1 contrast image. These images are called T_1 -weighted images.

Recall that T_2 occurs as a result of the nuclei exchanging energy with neighboring atoms. As energy exchange is more efficient for hydrogens in fat, the T_2 is short, approximately 80 ms. Energy exchange is less efficient in water than in fat, so the T_2 times for water hydrogens are longer, about 200 ms. As a result, the transverse component of magnetization decays faster for lipid hydrogens than water hydrogens. The magnitude of transverse magnetization in water is large, and it has a high signal, thus appearing bright on a T_2 contrast image. Similarly, fat appears dark on a T_2 contrast image.

The final effect on image contrast is proton density, or the relative number of protons per unit volume. To produce contrast due to proton density differences, the transverse

Table 6.25 Relative Repetition and Echo Times for Different MRI Image Contrasts

	T_1 Weighting	T_2 Weighting	Proton Density Weighting
TR	Short	Long	Long
TE	Short	Long	Short



(a)



(b)

Figure 6.82 (a) Proton density weighted axial MRI image of the brain, TE = 20 ms, TR = 2700 ms. (b) T_2 weighted coronal image of the brain, TE = 90 ms, TR = 2700 ms. Reprinted, by permission, from C. Westbrook and C. Kaur, *MRI in Practice*, 2nd ed., p. 35. Copyright © 1998 by Blackwell Science Ltd.

component of magnetization must reflect these differences. Tissues with high proton density, such as brain tissue, have a large transverse component of magnetization and therefore have a high signal. A bright *proton density contrast image* results. Tissues with low proton density, such as cortical bone, have small transverse components of magnetization and have low signal strengths, and they appear dark on proton density contrast images.

To demonstrate either T_1 , proton density or T_2 contrast, specific values of TR and TE are selected for a given pulse sequence (see Figure 6.80). The selection of appropriate TR and TE weights an image so that one contrast mechanism predominates over the other two (see Table 6.25). There are, of course, more topics and techniques associated with MRI imaging, such as spin echo and gradient pulse echo pulse sequences, but the basics of nuclear magnetic resonance and its application to MRI imaging have been presented. The result is astounding detailed images of biological tissue, like that of the human brain shown in Figure 6.82.

6.3 OPTICAL PROPERTIES OF MATERIALS

The final, general topic of this chapter deals, in a way, with a combination of the previous two properties: electricity and magnetism. The interaction of electromagnetic radiation with materials involves many of the same principles used to describe the electrical and magnetic properties of materials, such as magnetic moments, spins, and electronic configurations. However, we will see that both wave (frequency) and particle (photon) descriptions of light will be of benefit in this chapter. Thus, we will vacillate between the two with little fanfare or warning.

In this section, we are concerned with the interaction of electromagnetic radiation with a material. When electromagnetic radiation (which we will generally call “light” for ease of visualization, while recognizing that the visible spectrum is but a small portion of all electromagnetic radiation) strikes a surface, three types of processes may take place, either individually or in tandem. The light may be *absorbed*, *reflected*, or *transmitted*. Like many technical terms that find their way into common usage, these three terms are well known to us through their everyday occurrences. We know that black clothing absorbs energy, that a mirror reflects light, and that a pane of window glass transmits light. What is not always clear is that these three effects may occur simultaneously and that more than just the visible spectrum of light is involved. Since we are dealing primarily with “optical” properties of materials, this implies that we are primarily considering the visible portion of the electromagnetic spectrum. In some instances, radiation of other energies, such as infrared and ultraviolet radiation, will be examined. In these cases, more specificity will be exercised in the description of the type of “light.”

In all instances, the total intensity of the incident light striking a surface, I_0 , is the sum of the absorbed, reflected, and transmitted intensities, I_A , I_R , and I_T , respectively:

$$I_0 = I_A + I_R + I_T \quad (6.69)$$

The intensity is defined as the number of photons impinging on a surface per unit area per unit time. If we divide Eq. 6.69 through by the incident radiation, we end up with an equally useful relationship

$$1 = A + R + T \quad (6.70)$$

where A is the *absorptivity* (I_A/I_0), R is the *reflectivity* (I_R/I_0), and T is the *transmissivity* (I_T/I_0). The utility of Eq. (6.70) is that A , R , and T are material properties. Thus, it is not possible for a material to be simultaneously highly reflective, highly absorptive, and highly transmissive. We have some intuition as to which materials are absorptive, reflective, and transmissive, at least in terms of visible light. Let us utilize this knowledge to examine the fundamentals of how electromagnetic radiation interacts with materials from our four classes and how these interactions can be used in some important applications.

6.3.1 Optical Properties of Metals and Alloys

The “shininess” and inability to transmit visible light inherent in most metals indicates that absorptivity and reflectivity are high. In this section, we utilize our knowledge of electronic structure from previous sections to describe why this is so, and we investigate what happens to the energy that is absorbed in these materials.

Consider an incident beam of light interacting with a material as shown in Figure 6.83. Upon initial interaction, a certain fraction of the incident beam is reflected. According to Eq. (6.70), this fraction is R , or I_R/I_0 . The associated intensity is I_R , or

Cooperative Learning Exercise 6.8

The reflectivity of silicon at 633 nm is 35% and the absorption coefficient is $3.8 \times 10^5 \text{ m}^{-1}$. Calculate the following quantities for a 10 μm -thick sample of silicon at this wavelength.

Person 1: Calculate the fraction of incident light that is absorbed.

Person 2: Calculate the fraction of incident light that is transmitted through the sample.

Combine your information to check that Eq. (6.70) is satisfied.

Answers: If Eq. (6.72) is the fraction of light reaching the back face, then that portion subtracted from the light entering, $I_0(1 - R)$ is the fraction absorbed, so $I_A/I_0 = 0.35 - (1 - 0.35)\exp[-(3.8 \times 10^5)(1 \times 10^{-5})] = 0.6355$. Equation (6.73) gives $I_T/I_0 = (0.65)^2 \exp[-(3.8 \times 10^5)(1 \times 10^{-5})] = 0.00945$. $A + R + T = 0.6355 + 0.35 + 0.00945 \approx 1.0$.

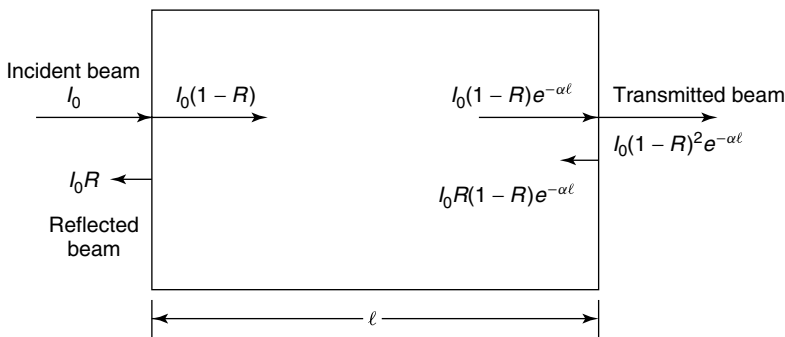


Figure 6.83 Reflection, absorption and transmission by a solid. From K. M. Ralls, T. H. Courtney, and J. Wulff, *Introduction to Materials Science and Engineering*. Copyright © 1976 by John Wiley & Sons, Inc. This material is used by permission John Wiley & Sons, Inc.

I_0R . Metals and alloys typically have high values of R , as high as 1.0 in some cases. The light that is not reflected enters the material, the intensity of which is thus $I_0 - I_R$, or $I_0(1 - R)$. Some or all of this remaining light will be absorbed through electronic interactions with the solid, and the result is a continuously decreasing intensity as the light passes through the length of the solid, indicated by l . The fractional change in light intensity, dI/I , over a distance x is directly proportional to a material property called the *linear absorption coefficient*, β :

$$\frac{dI}{I} = -\beta dx \quad (6.71)$$

where the minus sign indicates a decrease in intensity with distance, since β is taken as a positive quantity. Integration of Eq. (6.71) over the distance l in Figure 6.83 results in

$$I = I_0(1 - R) \exp\{-\beta \cdot l\} \quad (6.72)$$

This is the intensity of light reaching the back surface in Figure 6.83. At the back surface, a fraction of the light is once again reflected internally, which is R times the amount given in Eq. (6.72), and the remainder passes out of the material or is transmitted. Thus, the fractional amount of transmitted light, T , is one minus the amount reflected at the back face, or

$$T = (1 - R)^2 \exp\{-\beta \cdot l\} \quad (6.73)$$

provided that the same medium, e.g., air is on both the entering and exiting side of the solid. (We will return to this condition when we discuss refractive index in Section 6.3.2.1). These relationships indicate that the linear absorption coefficient, β , and reflectivity, R , are the two important parameters in determining how light interacts with a material. Let us investigate these two quantities more carefully, first for metals and alloys.

6.3.1.1 Reflectance and Color. Recall that in metals and alloys, there are many empty electronic states just above the occupied levels in the conduction bands. When incident radiation strikes a metallic surface, energy can be absorbed by promoting electrons from the occupied to the unoccupied electronic states. This generally occurs over a very short distance in the metal surface, and only very thin films of metals ($< 0.1 \mu\text{m}$) exhibit any transmittance at all. Once the electrons have been excited, they decay back to the lower energy levels, and reemission of light from the metal surface occurs. It is this immediate reemission process that gives rise to reflectivity. As we will see, there are other types of reemission processes, but they differ in time scale and frequency of the emitted light from reflectivity.

The efficiency of the reflection process depends on the frequency of the incident light, ν . For example, as shown in Figure 6.84, silver is highly reflective over the entire visible range. As a result, it has a white metallic *color* and a bright *luster**.

*The technical definition of *luster* is a bit elusive. In its common use, it is defined as “the quality, condition, or fact of shining by reflected light; gloss; sheen.” In fact, the term *metallic luster* is used in mineralogy as a distinguishing feature from *mineral luster*, which is less “shiny” than metallic luster. In this context, luster is defined as “the appearance of a mineral in reflected light.” However, this does not help us differentiate between the luster of two metals. So, while luster is commonly used to describe both metals and minerals, there is no absolute or relative scale for luster that makes it a useful quantity for describing metals.

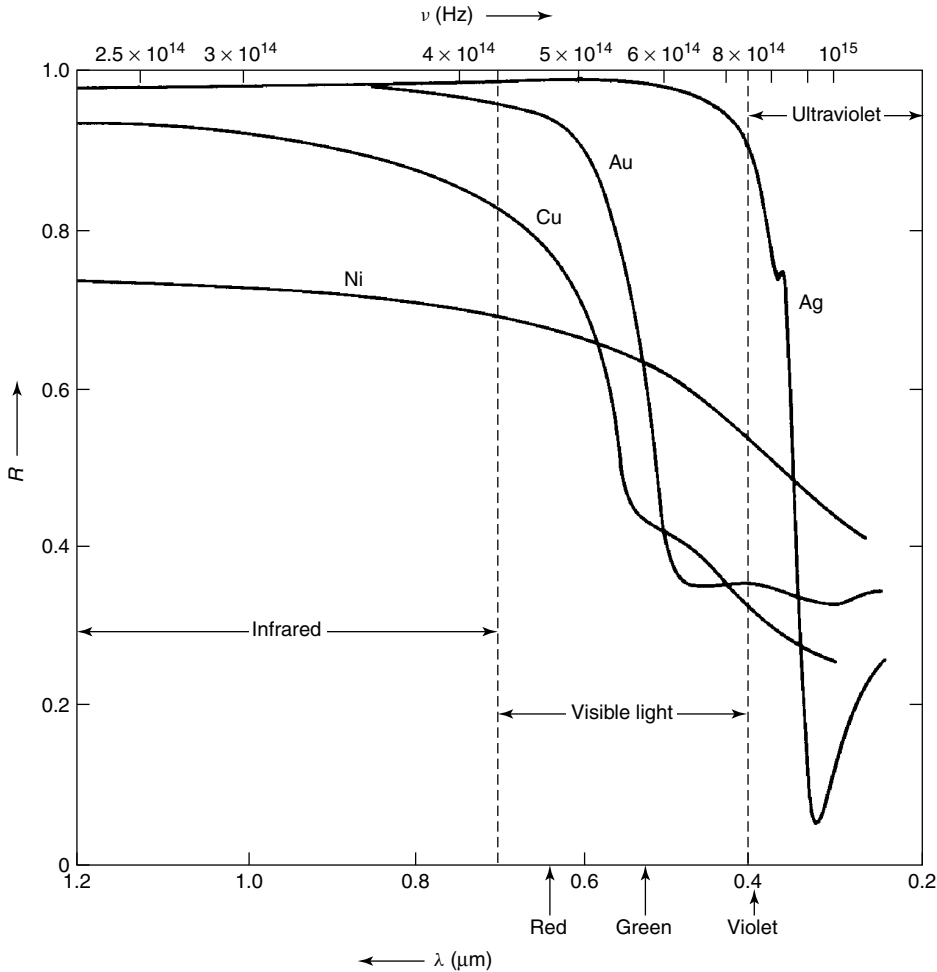


Figure 6.84 The frequency dependence of reflectivity for selected metals. From K. M. Ralls, T. H. Courtney, and J. Wulff, *Introduction to Materials Science and Engineering*. Copyright © 1976 by John Wiley & Sons, Inc. This material is used by permission John Wiley & Sons, Inc.

The white color of silver indicates that the reemitted photons cover much of the same frequencies and are comparable in number (intensity) to the incident photons. Metals like copper and gold exhibit characteristic red-orange and yellow colors, respectively, because incident photons above a certain frequency cause excitation of some electrons from a filled d electronic band to empty s electronic bands. Since this frequency falls in the visible region for Cu and Au (see Figure 6.84), strong absorption of light with higher frequencies occurs, and light with lower frequencies (red and yellow) is strongly reemitted. Many metals, like nickel, iron, and tungsten, have grayish colors because the density of electronic states both for occupied and unoccupied levels exhibit maxima and minima. This, in combination with the fact that the density of electronic states is very large in different parts of the d band, leads to relatively strong absorption and thus leads to a relatively low reflectivity in the visible region. We will return to a more

quantitative description of color in the section on ceramics and glasses, where there is more variability in color than is commonly found in metals and alloys. Outside of the visible region, most metals become highly reflective for photons having frequencies in the infrared region. This is because unlike free atoms where discrete frequencies are absorbed and emitted, photons having a virtually continuous band of frequencies are absorbed and emitted by a metal because of the almost continuous variation of energy levels in the conduction band. Of course, some intensity is lost because of phonon generation resulting from collisions suffered by the excited electrons in a metal and because of electronic polarization.

The color and luster of a metal can be affected by other factors, such as surface roughness. As illustrated in Figure 6.85, reflection from a smooth or mirror-like surface is termed *specular reflectance*, whereas reflection from surfaces that are not parallel to the average surface due to roughness is termed *diffuse reflectance*. On a completely rough surface, reflectance can occur at all angles, θ , relative to the incident light, as shown in Figure 6.86. The relative intensity of reflection, I_θ , varies as the cosine of

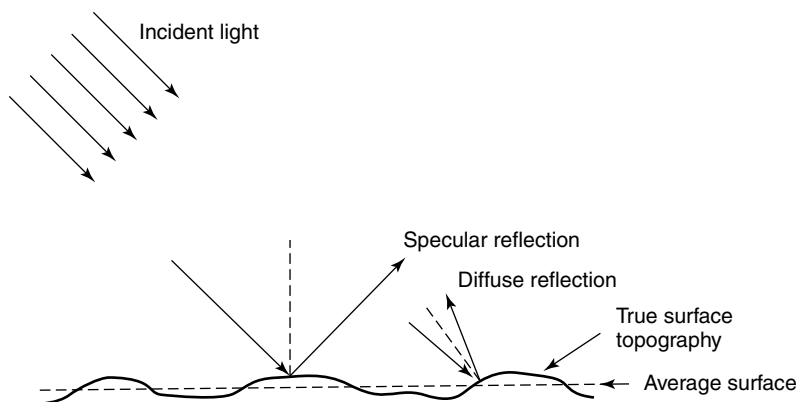


Figure 6.85 Schematic illustration of specular reflection from a flat surface and diffuse reflection from a rough surface, both relative to the average surface. Reprinted, by permission, from J. F. Shackelford, *Introduction to Materials Science for Engineers*, 5th ed., p. 597. Copyright © 2000 by Prentice-Hall, Inc.

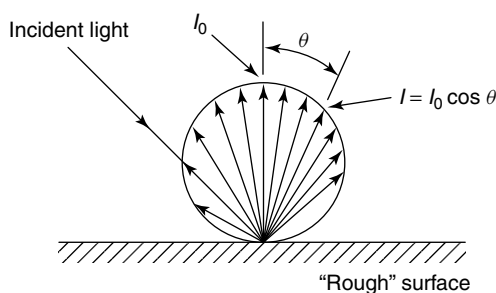


Figure 6.86 Polar diagram illustrating the directional intensity of reflection from a rough surface. Reprinted, by permission, from J. F. Shackelford, *Introduction to Materials Science for Engineers*, p. 598, 5th ed. Copyright © 2000 by Prentice-Hall, Inc.

the angle as

$$I_{\theta} = I_0 \cos \theta \quad (6.74)$$

where I_0 is the intensity of scattering at $\theta = 0^\circ$. Since any area segment, A_{θ} , will be reduced when viewed at an angle, the luster of the diffuse surface will be a constant independent of viewing angle:

$$\text{luster} = \frac{I_{\theta}}{A_{\theta}} = \frac{I_0 \cos \theta}{A_0 \cos \theta} = \text{constant} \quad (6.75)$$

This, at least in part, helps us understand the concept of luster.

6.3.1.2 The Photoelectric Effect. A phenomenon that is related to the bombardment of metallic surfaces with light (photons) is the *photoelectric effect*, which is the release of electrons due to the absorption of light energy. The photoelectric effect arises from the fact that the potential energy barrier for electrons is finite at the surface of the metal. This process is illustrated in Figure 6.87. The finite energy barrier at the surface is represented by W . In order for an electron to escape from the metal, it must possess a kinetic energy equal to or greater than W . Since the free electrons in the metal have kinetic energies ranging from nearly zero at the bottom of the potential energy well to E_f at the Fermi level, the electrons must absorb energy between W and $(W - E_f)$ to be ejected from the metal. The work that must be supplied to eject a free electron is called the *work function* and is denoted by the Greek lowercase phi, ϕ , where:

$$\phi = W - E_f \quad (6.76)$$

The critical energy required for a photon to remove an electron is then $h\nu_c = \phi$, where ν_c is the critical frequency of the photon and h is Planck's constant. When the frequency of the incident radiation is less than the critical frequency, electrons will not be ejected. Similarly, when the wavelength of the incident radiation is greater than the *critical wavelength*, λ_c , electrons will also not be emitted (recall that $\nu = c/\lambda$, where c is the speed of light in vacuum). This relationship between photon energy (in terms of wavelength) and electron emission for several alkali metals is shown in Figure 6.88. The decrease in number of emitted electrons at short wavelengths (high energy) is due to a decrease in the efficiency of the electronic excitation. In this way, the work function for each element, in principle, can be determined and can be used to identify a metallic sample.

We will see that a number of important optical phenomena are functions of the wavelength of light. This is probably a good time to review the various categories

HISTORICAL HIGHLIGHT

It is somewhat surprising that despite all of his contributions to science and engineering, including his work on Brownian motion and the theory of relativity, Albert Einstein (1879–1955) won his only Nobel Prize in 1921 “for his services to Theoretical Physics, and especially for his discovery of the law of the photoelectric effect.”

Source: www.nobel.se/physics/laureates/1921

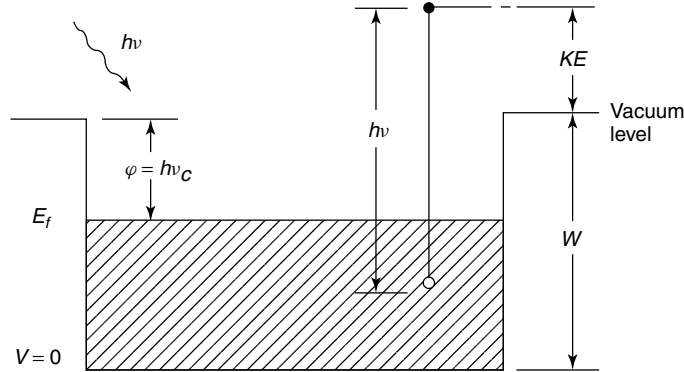


Figure 6.87 Illustration of potential energy well for the surface of a metal, and the energy required by an incident photon to remove an electron from it.

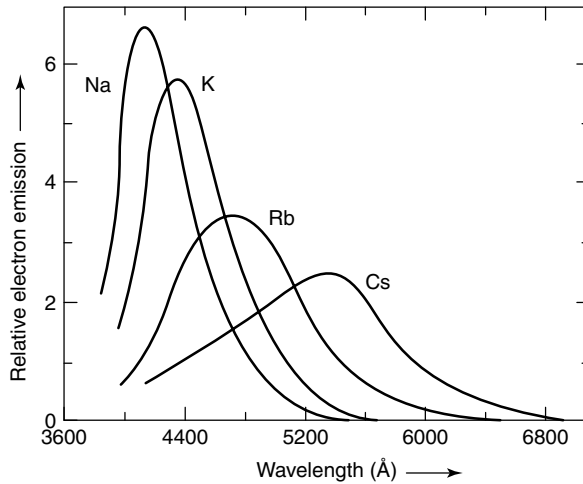


Figure 6.88 Dependence of photoelectric emission on wavelength of incident light for various alkali metals. Reprinted, by permission, from C. R. Barrett, W. D. Nix, and A. S. Tetelman, *The Principles of Engineering Materials*, p. 378. Copyright © 1973 by Prentice-Hall, Inc.

and associated wavelengths (and frequencies) of electromagnetic radiation through the summary in Figure 6.89.

6.3.2 Optical Properties of Ceramics and Glasses

6.3.2.1 Refractive Index and Dispersion. The velocity of light varies depending upon the density of the medium in which it is propagating. In a vacuum, the speed of light is a constant, c , which has a value of 3.08×10^8 m/s. In any other medium, such as a gas, liquid, or solid, the velocity is given by the variable, v . The ratio between these two velocities determines the *index of refraction*, n , sometimes called the *refractive index*:

$$n = \frac{c}{v} \quad (6.77)$$

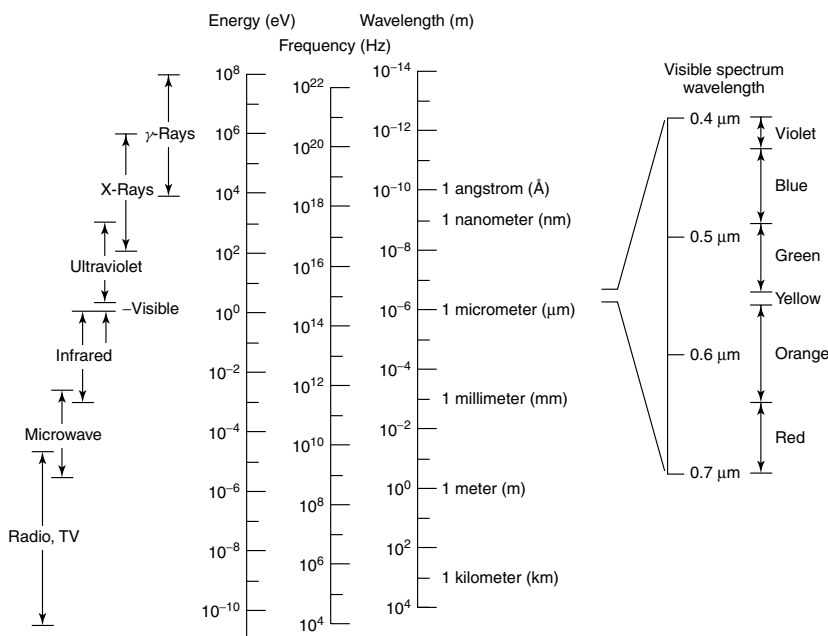


Figure 6.89 Energies, wavelengths, and frequencies of various categories of electromagnetic radiation. Reprinted, by permission, from W. Callister, *Materials Science and Engineering: An Introduction*, 5th ed., p. 709. Copyright © 2000 by John Wiley & Sons, Inc.

Hence, the refractive index is a dimensionless quantity. The velocity of light in a vacuum can be related to the electric permittivity in a vacuum, ϵ_0 [cf. Eq. (6.32)], and the magnetic permeability in a vacuum, μ_0 [cf. Equation (6.60)]:

$$c = \frac{1}{\sqrt{\epsilon_0 \mu_0}} \quad (6.78)$$

Similarly, the velocity of light in a medium is related to the electric permittivity and magnetic permeabilities in the medium, ϵ and μ , respectively:

$$v = \frac{1}{\sqrt{\epsilon \cdot \mu}} \quad (6.79)$$

Thus, we see the initial connection between optical properties and the electrical and magnetic properties from the two previous sections. Substitution of Eqs. (6.78) and (6.79) into (6.77) shows that the refractive index can be expressed in terms of the relative electric permittivity (dielectric constant), ϵ_r (cf. Table 6.5), and relative magnetic permeability of the medium, $(1 + \chi)$ [cf. Eq. (6.63)], where χ is the magnetic susceptibility:

$$n = \sqrt{\frac{\epsilon_r}{(1 + \chi)}} \quad (6.80)$$

Since most ceramic substances (and most nonmetallic substances, for that matter) possess small magnetic susceptibilities, the quantity $(1 + \chi)$ is approximately unity, and the refractive index can be approximated as the square root of the dielectric constant:

$$n \approx \sqrt{\epsilon_r} \quad (6.81)$$

Refractive index values vary from 1.0003 for air to over 2.7 for some solid oxide ceramics. Silicate glasses have a much narrower range of values, from about 1.5 to 1.9. The refractive indices (or indexes) of other materials can be found in Appendix 9.

The relationship between refractive index and the dielectric constant is a logical one, and brings into play many of the considerations of electronic structure utilized in Section 6.1.2.2 to describe the dielectric constant. A dielectric material interacts with electromagnetic radiation because it contains charge carriers that can be displaced. Light waves are retarded in a dielectric; that is, the velocity is decreased because of the interactions of the electromagnetic radiation with the electrons. Recall from Section 6.1.2.2 that the polarizability, α , is a measure of the average dipole moment per unit field strength [cf. Eq. (6.39)]. The polarizability can be related to the index of refraction for a simple, monatomic gas through the Lorentz–Lorenz equation

$$\alpha = \frac{3\varepsilon_0 M(n^2 - 1)}{N_A \rho(n^2 + 2)} \quad (6.82)$$

where ε_0 is again the electric permittivity in vacuum, M is the atomic weight of the gas, ρ is its density, N_A is Avogadro's number, and n is the refractive index.

In ionic solids, we expect the ionic polarizability to dominate. Ionic polarization should increase with the size of the ion and with the degree of negative charge on isoelectric ions. Since the index of refraction increases with polarizability in accordance with Eq. (6.82), large refractive indices arise with large ions (e.g., $n_{\text{PbS}} = 3.912$) and low refractive indices occur with small ions (e.g., $n_{\text{SiCl}_4} = 1.412$). However, as we know, the electronic environment of the ions also affects the polarizability and, in turn, the refractive index. Only in glasses and in cubic crystals is the refractive index independent of direction. In other crystal systems, the refractive index is larger in directions that are close-packed. This also follows directly from Eq. (6.82). Similarly, the more open structures of high-temperature polymorphic forms have lower refractive indices than do crystals of the same composition; for example, for SiO_2 , $n_{\text{glass}} = 1.46$, $n_{\text{tridymite}} = 1.47$, $n_{\text{cristobalite}} = 1.49$, and $n_{\text{quartz}} = 1.55$. The refractive index of a typical soda-lime glass is about 1.5. The addition of large ions such as lead and barium have the effect of increasing the index of refraction. For example, glasses containing 90 wt % PbO have an index of refraction of around 2.1, which is about the upper limit of the obtainable values for practical optical glasses.

In the same way that close-packed directions in a crystal have larger refractive indices, so too can the application of a tensile stress to an isotropic glass increase the index of refraction normal to the direction of the applied stress. Uniaxial compression has the reverse effect. The resulting variation in refractive index with direction is called *birefringence*, which can be used as a method of measuring stress.

The refractive index is a function of the frequency of the light, and it normally decreases with increasing wavelength, as illustrated in Figure 6.90 for some typical glasses. The variation in refractive index with wavelength, λ , is called *dispersion*, and it is given in one definition by

$$\text{Dispersion} = \frac{dn}{d\lambda} \quad (6.83)$$

As can be seen in Figure 6.90, the slope of the refractive index versus wavelength—the dispersion—varies with wavelength. However, most practical measurements are made

Cooperative Learning Exercise 6.9

It can be shown that for some ionic crystals, such as LiF, both ionic and electronic polarization can contribute to the overall dielectric constant, ϵ_r . In such cases, Eq. (6.81) is not entirely correct, and the electronic contribution to the polarizability, α_e , is given by Eq. (6.82), since the refractive index affects only the frequencies in the electronic range, and the number of ions per unit cell, in this case two, must be included in the denominator. The total polarizability, $\alpha = \alpha_e + \alpha_i$, is then given by

$$\alpha = \frac{3\epsilon_0 M}{N_A \rho} \left(\frac{\epsilon_r - 1}{\epsilon_r + 2} \right),$$
 where ϵ_r is the dielectric constant as given in Table 6.3 and the remaining quantities are all the same as in Eq. (6.82). The index of refraction for LiF is 1.395, its density is $2.635 \times 10^3 \text{ kg/m}^3$, and its molecular weight is $26 \times 10^{-3} \text{ kg/mol}$. Recall that $\epsilon_0 = 8.854 \times 10^{-12} \text{ C/V-m}$.

Person 1: Calculate the total polarizability for LiF.

Person 2: Calculate the electronic contribution to the total polarizability.

Combine your information to calculate the ionic polarizability, α_i .

$$\alpha_i = \frac{3\epsilon_0 M}{N_A \rho} \left(\frac{\epsilon_r - 1}{\epsilon_r + 2} \right) - \alpha_e$$

$$= \frac{3(8.854 \times 10^{-12} \text{ C/V-m})(26 \times 10^{-3} \text{ kg/mol})}{(6.02 \times 10^{23} \text{ mol}^{-1})(2.635 \times 10^3 \text{ kg/m}^3)} \left(\frac{1.395^2 - 1}{1.395^2 + 2} \right) - 3.166 \times 10^{-40} \text{ C}^2\text{m}^2/\text{V}$$

$$= 1.2 \times 10^{-40} \text{ C}^2\text{m}^2/\text{V}$$

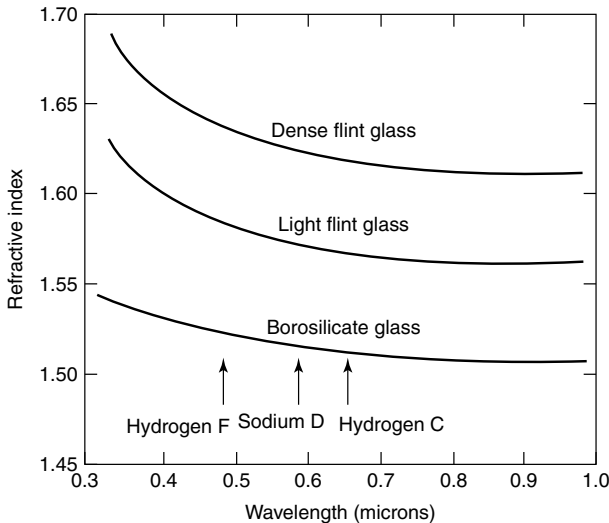


Figure 6.90 Effect of light wavelength on refractive index for some common glasses. From W. D. Kingery, H. K. Bowen, and D. R. Uhlmann, *Introduction to Ceramics*. Copyright © 1976 by John Wiley & Sons, Inc. This material is used by permission of John Wiley & Sons, Inc.

by determining the dispersion at specific wavelengths, such as the hydrogen F line ($\lambda = 486.1 \text{ nm}$), sodium D line ($\lambda = 589.3 \text{ nm}$), and hydrogen C line ($\lambda = 656.3 \text{ nm}$), as indicated in Figure 6.90. The complete dispersion curves for some common inorganic materials are shown in Figure 6.91.

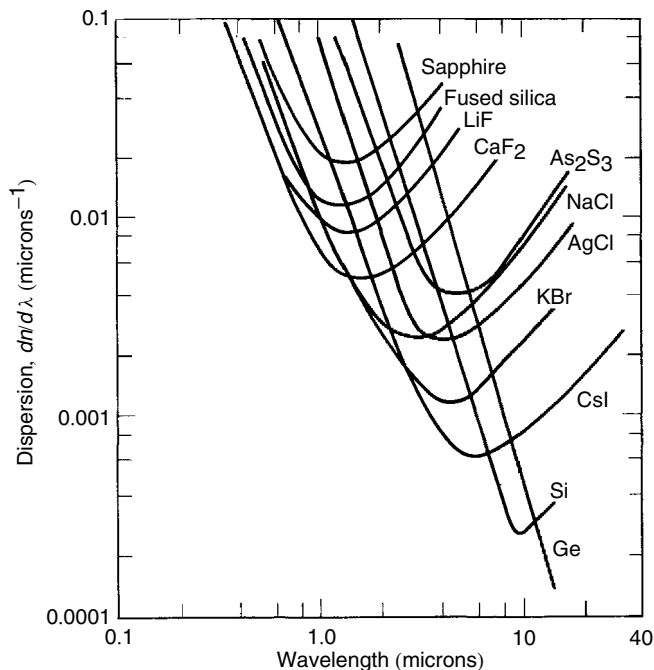


Figure 6.91 Effect of light wavelength on dispersion for some common inorganic materials. From W. D. Kingery, H. K. Bowen, and D. R. Uhlmann, *Introduction to Ceramics*. Copyright © 1976 by John Wiley & Sons, Inc. This material is used by permission of John Wiley & Sons, Inc.

The data shown in Figures 6.90 and 6.91 are a subset of the more general behavior, which is composed of two types of dispersion: *normal dispersion* and *anomalous dispersion*. Normal dispersion arises in the visible range of light, and the index of refraction increases with decreasing wavelength (increasing energy), as in Figure 6.90. In this region, the refractive index can be correlated with wavelength according to the following empirical expression, known as the Cauchy formula:

$$n = A + \frac{B}{\lambda^2} + \frac{C}{\lambda^4} \quad (6.84)$$

where A , B , and C are constants. In the region where refractive index decreases with decreasing wavelength (typically in the ultraviolet), anomalous dispersion occurs. Anomalous dispersion is the result of interactions between the light and the electronic oscillators in the material. At the so-called *resonant frequencies* of the electronic oscillators, absorption of the electromagnetic radiation can occur, resulting in reinforcement of the natural electronic oscillations. This resonance tends to decrease the refractive index.

6.3.2.2 Reflection and Refraction. With the principle of refractive index now in mind, we can return momentarily to the concept of reflection, which was first introduced in Section 6.3.1. Recall that the velocity of light changes as it passes from

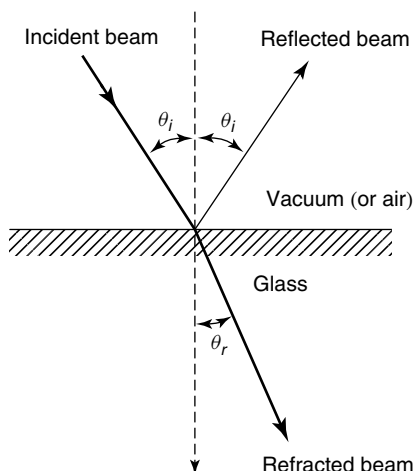


Figure 6.92 Reflection and refraction at a solid surface. Reprinted, by permission, from J. F. Shackelford, *Introduction to Materials Science for Engineers*, 5th ed., p. 597. Copyright © 2000 by Prentice-Hall, Inc.

vacuum to a medium, such as air. The velocity also changes at any interface between two phases with different indices of refraction, such as at an air–solid interface as illustrated in Figure 6.92. The change in velocity causes the light to bend upon passing through the interface. The bending of transmitted light at an interface is more properly termed *refraction*—hence the term refractive index. We also know that some of the light is reflected. The ratio of reflected to refracted (transmitted) light at the interface is a function of (a) the refractive index difference between the two phases and (b) the angle of the incident light.

If the *angle of incidence* from a normal to the surface is θ_i (see Figure 6.92) and the *angle of refraction* is θ_r , the refractive index of the solid medium, n (provided that the incident light is coming from a phase of low refractive index such as vacuum or air), is given by

$$n = \frac{\sin \theta_i}{\sin \theta_r} \quad (6.85)$$

Recall from Figure 6.85 that the light that is reflected at the same angle of incidence, θ_i , is due to specular reflectance. We can now use the refractive index to show that the reflectivity, R [cf. Eq. (6.70)], at the interface in Figure 6.92 is given by

$$R = \frac{(n - 1)^2}{(n + 1)^2} \quad (6.86)$$

Equation (6.86) holds for a solid–gas interface where the refractive index of the gas (or vacuum) is approximately unity. It is a simplification of a more general expression for light propagating through a medium of refractive index n_1 , striking perpendicular to a surface ($i = 0$) of refractive index n_2 , which is presented here without derivation:

$$R = \frac{(n_2 - n_1)^2}{(n_2 + n_1)^2} \quad (6.87)$$

Thus, the higher the refractive index of the solid, the greater the reflectivity. For example, the reflectivity of a typical silicate glass, with $n = 1.5$, is about 0.04. Just as the refractive index varies with wavelength, so too does the reflectivity.

6.3.2.3 Absorbance and Color. Once the light that is not reflected enters the medium, it can either continue to be transmitted or be absorbed by the medium (cf. Figure 6.83). The absorption process, too, is a function of the energy (wavelength) of the light.

Recall from Eq. (6.71) that the fractional change in light intensity, dI/I , over a distance x within the absorbing medium is directly proportional to the linear absorption coefficient, β :

$$\frac{dI}{I} = -\beta dx \quad (6.71)$$

The absorption coefficient is a material property and is a function of the wavelength of light, λ :

$$\beta = \frac{4\pi k}{\lambda} \quad (6.88)$$

where k is called the *index of absorption*.

Light is absorbed by two basic mechanisms: electronic polarization and electronic excitation. Electronic polarization and its effect on refractive index were described in the previous section and will not be elaborated upon here. The process of electronic excitation is an important one, however, and has implications to a number of optical phenomena such as lasing and luminescence.

Absorption of a photon of light may occur by the promotion or excitation of an electron from the valence band to the conduction band. In doing so, the promoted electron leaves behind a hole in the valence band and is free to move in the conduction band. Absorption and excitation occur only if the photon has energy greater than that of the band gap, E_g :

$$h\nu \geq E_g \quad (6.89)$$

Cooperative Learning Exercise 6.10

Use the data in Figure 6.89 to perform the following calculations.

Person 1: Calculate the maximum band gap energy for which absorption of visible light is possible.

Person 2: Calculate the minimum band gap energy for which absorption of visible light is possible.

Compare your answers. What type of electrical properties will materials within these band gap energy limits possess?

$$\text{Answers: } E_g(\text{max}) = hc/\lambda_{\text{min}} = (6.626 \times 10^{-34} \text{ J}\cdot\text{s})(3.0 \times 10^8 \text{ m/s})/(4.1 \times 10^{-7} \text{ m}) = 4.8 \text{ eV}$$

The magnitude of the band gap energy, then, will determine whether the material absorbs no light, and is transparent, or absorbs certain wavelengths of light, thus becoming *opaque*.

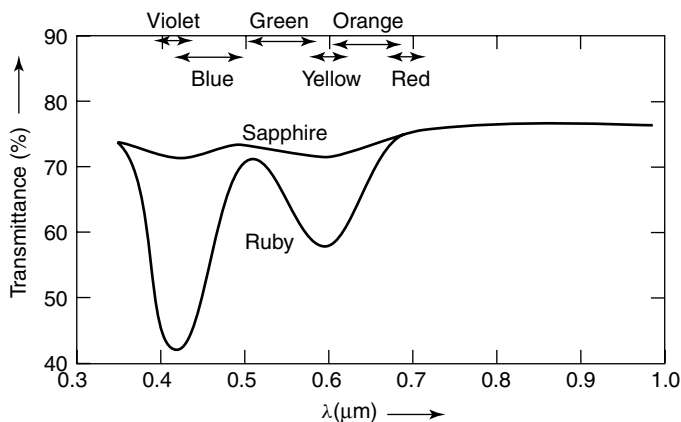


Figure 6.93 Transmission spectrum for sapphire and ruby. From K. M. Ralls, T. H. Courtney, and J. Wulff, *Introduction to Materials Science and Engineering*. Copyright © 1976 by John Wiley & Sons, Inc. This material is used by permission John Wiley & Sons, Inc.

The absorption of certain wavelengths of light in the visible spectrum results in *color*. As illustrated in Figure 6.93 for a ruby, the absorption of light centered at 0.42 and 0.6 μm (represented here as decreases in transmittance rather than increases in absorbance) correspond to absorption of blue-violet and yellow-green light, respectively. The result is that red is the most strongly transmitted visible light, giving ruby its characteristic red color. The transmission spectrum for sapphire, which has a slight bluish color, is also shown in Figure 6.93. The interesting fact is that both ruby and sapphire are primarily Al_2O_3 , with only trace amounts of Ti^{3+} or Cr^{3+} substituted for Al^{3+} in sapphire and ruby, respectively. In the case of ruby, the Cr^{3+} ions are point defects with associated energy states that lie between the valence and conduction bands of Al_2O_3 . The separation of levels is such that blue-violet light can be absorbed and red light emitted. A characteristic of such an absorption–emission process is that the emitted light cannot be of a higher energy than the absorbed light. We will further describe these radiative transitions when we get to the topics of luminescence and phosphorescence.

In general, the most commonly used ions for creating color in ceramics are transition elements with their incomplete *d* shells, such as V, Cr, Mn, Fe, Co, Ni, and Cu, and, to a lesser extent, the rare-earth elements with their incomplete *f* shells. In addition to the individual ion and its oxidation state, absorption phenomena are affected by their ionic environment. The introduction of impurity atoms to affect color is also utilized in glasses. In this case, a single ion such as Co^{2+} can give different colorings in different glasses, since it can have different coordination numbers associated with it (cf. Section 1.2.4.3). Some common metal ions and their effect on the color of silicate glasses are listed in Table 6.26.

6.3.2.4 Transmittance, Transparency, and Translucency. The descriptions of absorption processes and their relationship to transmittance and color in the preceding section serve to underscore the relationship first presented by Eq. (6.70)—namely, that the fractions of light reflected, absorbed, and transmitted must sum to unity. In this

Table 6.26 Selected Metal Ions and their Effect on Color in Silicate Glasses

Ion	In Glass Network		In Modifier Position	
	Coordination Number	Color	Coordination Number	Color
Cr ²⁺				Blue
Cr ³⁺			6	Green
Cr ⁶⁺	4	Yellow		
Cu ²⁺	4		6	Blue-green
Cu ⁺			8	Colorless
Co ²⁺	4	Blue-purple	6–8	Pink
Ni ²⁺		Purple	6–8	Yellow-green
Mn ²⁺		Colorless	8	Weak orange
Mn ³⁺		Purple	6	
Fe ²⁺			6–8	Blue-green
Fe ³⁺		Deep brown	6	Weak yellow
U ⁶⁺		Orange	6–10	Weak yellow
V ³⁺			6	Green
V ⁴⁺			6	Blue
V ⁵⁺	4	Colorless		

Source: Shackelford, J.F., *Introduction to Materials Science for Engineers*, 5th ed. Copyright © 2000 by Prentice-Hall, Inc.

section, we complete our description of these three processes with some issues related to transmittance—namely, transparency and translucency.

A material is transparent if it transmits a clear image through it. Dielectrics tend to be transparent to visible radiation because they possess such large energy gaps that light cannot cause electronic excitation. Thus, materials such as diamond, sodium chloride, and silicate glasses readily transmit light. When the energy of the incident radiation is sufficiently high, as in ultraviolet radiation, electrons can be excited across the energy gap, and strong absorption occurs, as described in the previous section.

Many inherently transparent materials appear “milky” because of diffusive transmission, also known as *translucency*. Translucence results from multiple internal reflections. In noncubic polycrystalline materials that possess an anisotropic refractive index, light is reflected or scattered at grain boundaries where the index of refraction undergoes a discontinuous change. This effect is similar to that which results in reflection at a free surface. Translucency is slightly different from opacity, which was first described in the previous section, insofar as a diffuse image is transmitted through a translucent medium, whereas a total loss of image occurs in an opaque medium. In both cases, however, a certain fraction of some light of certain wavelengths is transmitted.

In addition to surface roughness and absorbing chemical species that affect transmittance and have already been described, such factors as porosity and particulate inclusions can affect translucence and opacity, mostly through a process called *scattering*. Figure 6.94 illustrates how scattering can occur at a single pore by refraction. The light is refracted as it exits a medium of higher refractive index and enters one of lower refractive index, such as air, inside the pore. This is essentially a miniaturized, reversed situation of the refraction process illustrated in Figure 6.92. A similar

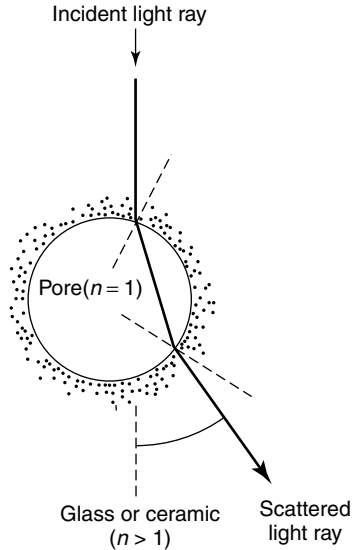


Figure 6.94 Schematic illustration of light scattering in a solid due to a pore. Reprinted, by permission, from J. F. Shackelford, *Introduction to Materials Science for Engineers*, 5th ed., p. 599. Copyright © 2000 by Prentice-Hall, Inc.

scattering result can be created with second-phase particles such as SnO_2 with a higher index of refraction ($n = 2.0$) than that of the medium, such as glass ($n = 1.5$). Such materials are called *opacifiers*. The degree of scattering and opacification created by the pores or particles depends on their average size and concentration, as well as the mismatch between the refractive indices. If individual pores or particles are significantly smaller than the wavelength of light, they are ineffective scattering centers. Conversely, particles or pores in the 400- to 700-nm size range maximize the scattering effect. This effect is what leads to transparent ceramics, such as glass ceramics (cf. Section 1.2.5) where the crystallite sizes are carefully controlled through nucleation and growth to be less than the wavelength of visible light (cf. Figure 1.52).

6.3.2.5 Decay Processes: Luminescence and Lasers*. The absorption and reemission of electromagnetic radiation leads to some interesting phenomena that can be utilized for important applications. Both lasers and luminescence are built upon the principle of emission processes and will be described here in brief.

As we have already seen, the absorption of photons by a material can lead to the reemission of other photons of equal or lesser energy. When photon absorption is accompanied by emission of photons in the visible spectrum, the process is called *photoluminescence*, or simply *luminescence*. In fact, luminescence can be used to describe the emission of visible light as a result of absorption of any number of forms of energy, including thermal, mechanical, or chemical energy. The photon emission is the result of excited electrons returning to their ground state. The duration of this relaxation process is used to distinguish between the two main types of luminescence: *fluorescence* and *phosphorescence*. If the relaxation process occurs in less than about 10 ns (10^{-8} s), it is termed fluorescence. The fluorescent process also involves additional internal or

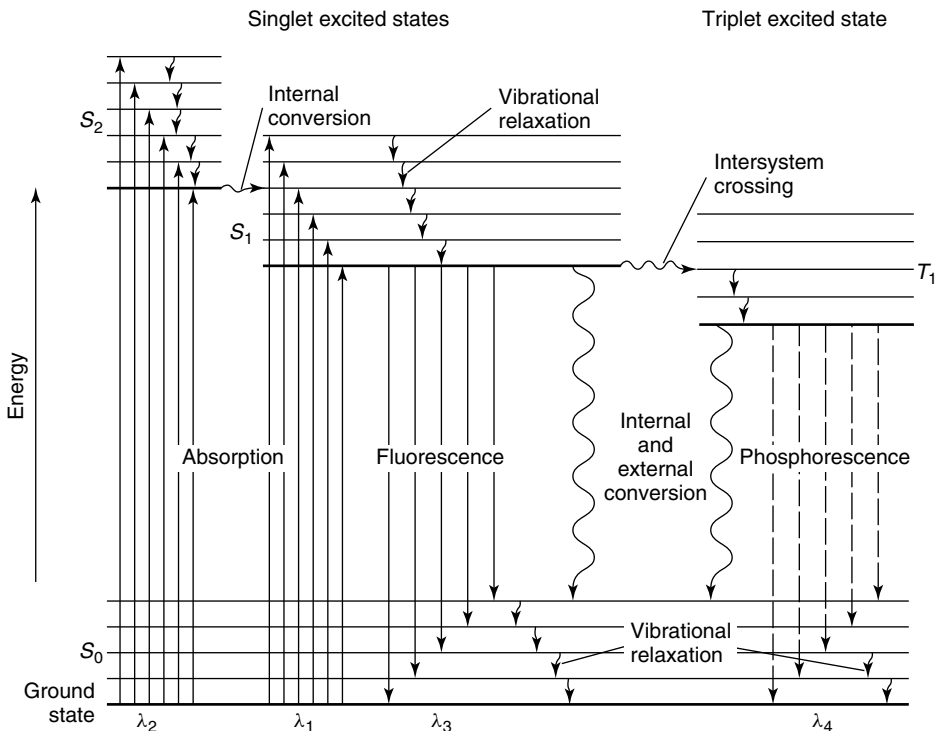


Figure 6.95 Schematic diagram of transitions between electronic energy levels involved in fluorescence and phosphorescence. Reprinted, by permission, from D. A. Skoog and D. M. West, *Principles of Instrumental Analysis*, 2nd ed., p. 282. Copyright © 1980 by Saunders College.

external energy conversion, as illustrated with the energy diagrams in Figure 6.95. In this way, the energy of the reemitted photons is less than the energy of the absorbed photons. If the reemission process takes longer than about 10 nanoseconds, it is termed phosphorescence.

Luminescence is generally produced through the addition of impurities to compounds. For example, zinc sulfide containing small amounts of excess zinc, or impurities such as gold or manganese, emits light in the visible spectrum after excitation with ultraviolet radiation (see Figure 6.96). Zinc sulfide and a similar compound, Mn-activated zinc orthosilicate, Zn_2SiO_4 , are also examples of compounds used as *phosphors*. Phosphors are useful for detecting X-ray or γ -ray radiation because they emit visible light upon exposure. They are used for other, more mundane purposes as well, such as the luminous hands on watches and clocks.

Light amplification by stimulated emission of radiation, or *LASER*, is another application of radiative relaxation processes. Unlike most radiative processes, such as luminescence, which produce *incoherent* light (light waves are out of phase with each other), the light produced by laser emission is *coherent* (light waves are all in phase with each other). The principal benefit of coherent light is that the photons do not disperse as they do in an incoherent beam of light. Consequently, the laser beam does not spread out in the same way that an incoherent beam can. Additionally, lasers produce a beam of light that is monochromatic—that is, entirely of one wavelength. This is

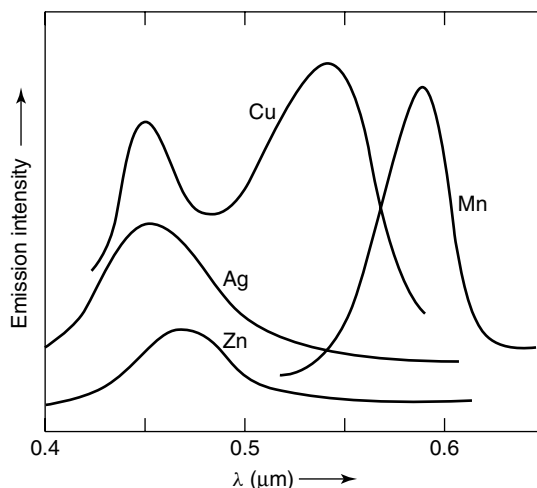


Figure 6.96 Luminescence spectra for Zn doped with Cu, Ag, Mn, and excess Zn. From W. D. Kingery, H. K. Bowen, and D. R. Uhlmann, *Introduction to Ceramics*. Copyright © 1976 by John Wiley & Sons, Inc. This material is used by permission of John Wiley & Sons, Inc.

in contrast to most light sources, even phosphors, that produce a range of wavelengths, or polychromatic light. Polychromatic light is not entirely a bad thing—we much prefer white light (all or most of the wavelengths in the visible spectrum) to monochromatic light for our daily and nightly operations. But the monochromatic, coherent, and collimated (photons directed along the same straight line) beam of a laser opens up a realm of possible applications. Let us see how this type of beam can be produced.

The radiative transitions of the previous descriptions have all been spontaneous: Relaxation from the excited state to the ground state and emission of photons occur without external aid. In contrast, a stimulated emission occurs when the half-life of the excited state is relatively long, and relaxation can occur only through the aid of a stimulating photon. In stimulated emission, the emitted photon has the same direction as, and is in phase with, the stimulating photon. The example of Cr^{3+} -doped Al_2O_3 that we utilized earlier for our description of the color of ruby works equally well for a description of stimulated emission. Recall that the presence of chromium in alumina alters the electronic structure, creating a metastable state between the valence and conduction bands. Absorption of a blue-violet photon results in the excitation of an electron from

HISTORICAL HIGHLIGHT

The physical principles that give rise to the emission of coherent light were elucidated in the first half of [the 20th] century, by Albert Einstein among others. But not until 1954 were these principles put into practice in a working device that emitted coherent radiation. This device, developed by Charles Townes of the University of California at Berkeley, was not really a laser at all but a *maser*, which generated coherent microwave radiation rather than light. Townes and others strove in the ensuing years to create devices that would emit coherent light at visible wavelengths, and the first genuine laser was demonstrated in 1960 by H. Maiman, who obtained red laser light from a ruby laser.

Source: Ball, *Made to Measure*, p. 29.

the ground state to the excited state, as illustrated in Figure 6.97. The excited electron relaxes to a metastable electronic state through a non-radiative process involving the transfer of energy to a phonon. *Spontaneous decay* results in the emission of a photon with wavelength in the red part of the visible spectrum ($\lambda = 694.3 \text{ nm}$). However, most of the electrons reside in this metastable state for up to 3 ms before decaying to the ground state. This time span is sufficiently long that several electrons can occupy this metastable state simultaneously. This fact is utilized to create artificially large numbers of electrons in the metastable state through a process known as *optical pumping*, in which a xenon flash lamp excites a large number of electrons into the excited state, which decay rapidly (in the nonradiative process) to the metastable state. When spontaneous emission finally occurs due to a few electrons, these electrons stimulate the emission of the remaining electrons in the metastable state, and an avalanche of emission occurs. The photons are of the same energy and are in phase (coherent).

The beam is collimated through the use of a tube with silvered mirrors at each end, as illustrated in Figure 6.98. As stimulated emission occurs, only those photons traveling nearly parallel to the long axis of the ruby crystal are reflected from the fully silvered surface at the end of the tube. As these reflected photons travel back through the tube, they stimulate the emission of more photons. A fraction of these photons are re-reflected at the partially silvered face at the other end of the tube. Thus, photons travel up and down the length of the crystal, producing ever-increasing numbers of stimulated photons. When the beam is finally emitted through the partially silvered face, it is a high-energy, highly collimated, monochromatic beam of coherent light. Typical power densities for a ruby laser are on the order of a few watts.

In addition to ruby, lasers can be constructed from gases such as CO_2 or He–Ne and from semiconductors such as GaAs (cf. Section 6.1.2.5) and InGaAsP. Gas lasers generally produce lower intensities and powers, but are more suitable for continuous operation since solid-state lasers generate appreciable amounts of heat. The power in a solid-state laser can range from microwatts to 25 kW, and more than a megawatt in lasers for defense applications. Some common lasers and their associated powers are listed in Table 6.27. Lasers that can selectively produce coherent light of more than one wavelength are called *tunable lasers*.

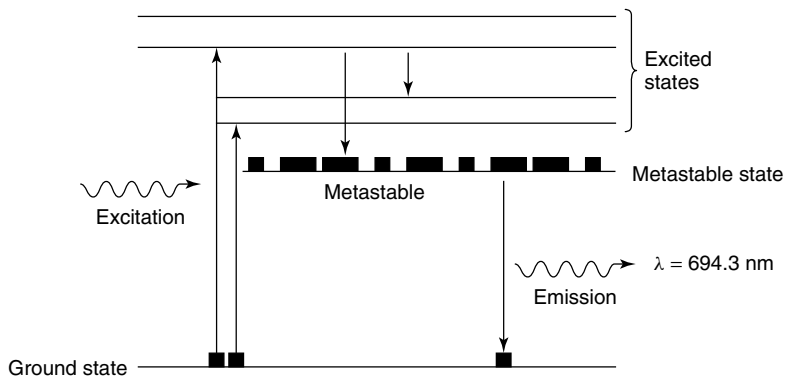


Figure 6.97 Schematic illustration of energy levels in ruby that are used to create a populated metastable electronic state, which can then be stimulated to emit monochromatic, coherent radiation for a laser. Reprinted, by permission, from J. F. Shackelford, *Introduction to Materials Science for Engineers*, 5th ed., p. 607. Copyright © 2000 by Prentice-Hall, Inc.

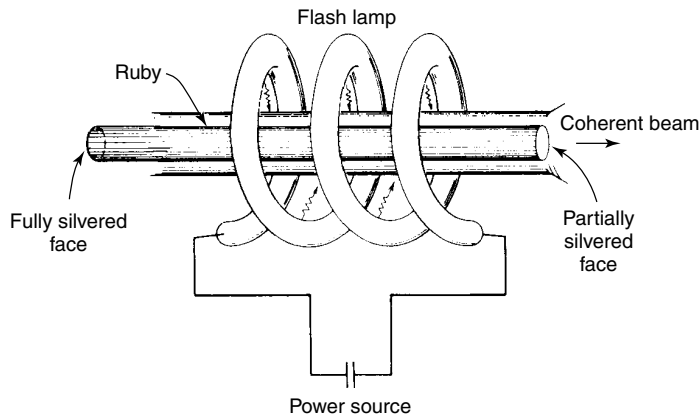


Figure 6.98 Schematic illustration of a ruby laser. From K. M. Ralls, T. H. Courtney, and J. Wulff, *Introduction to Materials Science and Engineering*. Copyright © 1976 by John Wiley & Sons, Inc. This material is used by permission of John Wiley & Sons, Inc.

Table 6.27 Characteristics and Applications of Some Common Lasers

Laser	Type	Common Wavelengths (μm)	Maximum Output Power (W) ^a	Applications
He-Ne	Gas	0.6328, 1.15, 3.39	0.0005–0.05 (CW)	Line-of sight communications, recording/playback of holograms
CO ₂	Gas	9.6, 10.6	500–15,000 (CW)	Heat treating, welding, cutting, scribing, marking
Argon	Gas ion	0.488, 0.5145	0.005–20 (CW)	Surgery, distance measurements, holography
HeCd	Metal vapor	0.441, 0.325	0.05–0.1	Light shows, spectroscopy
Dye	Liquid	0.38–1.0	0.01 (CW) 1×10^6 (P)	Spectroscopy, pollution detection
Ruby	Solid state	0.694	(P)	Pulsed holography, hole piercing
Nd-YAG	Solid state	1.06	1000 (CW) 2×10^8 (P)	Welding, hole piercing, cutting
Nd-glass	Solid state	1.06	5×10^{14} (P)	Pulse welding, hole piercing
Diode	Semiconductor	0.33–40	0.6 (CW) 100 (P)	Bar-code reading, CDs and video disks, optical communications

^a“CW” denotes continuous; “P” denotes pulsed.
 Source: W. Callister, *Materials Science and Engineering: An Introduction*, 5th ed. Copyright © 2000 by John Wiley & Sons, Inc.

Semiconducting lasers have become increasingly important in information storage, such as in the use of compact discs (CDs) and digital video discs (DVDs). In these materials, a voltage is applied across a layered semiconductor (see Figure 6.99), which excites electrons into the conduction band, just as in the ruby laser. However, the holes created in the valence band play an important role in the emission process. It is the recombination of the electron–hole pairs that results in the emission of photons with a specific wavelength. As in the ruby laser, the ends of the semiconducting “sandwich” are fully and partially silvered, and a voltage is continuously applied to ensure that there is a steady source of holes and electrons. These devices are extremely temperature-sensitive, since the current required to cause lasing, the wavelength of emitted radiation, and the lifetime of the diode all depend on temperature.

The conventional III–V compound semiconductors such as GaAs are limited to infrared or red emitting diode lasers and are not capable of generating shorter wavelength light, which is a requirement for size reduction in information storage devices. Short-wavelength LEDs and laser diodes require a different class of semiconductor materials; principally, the group III nitrides. The growth of high-quality (AlGaIn)N single-crystalline layer sequences has been a challenge, and only recent developments in fabrication processes have produced blue lasers that can be used in commercially available devices such as DVD players. The wavelengths of some common compound semiconductors are listed in Table 6.28.

6.3.2.6 Photoconductivity*. In Section 6.3.1.2 we saw how electricity can be generated from the surface of a metal when it is bombarded with photons. A similar process occurs when certain semiconductors absorb photons and create electron–hole pairs that can be used to generate current. This process is called *photoconductivity* and is slightly different from the photoelectric effect, since it is an electron–hole pair that is being generated instead of a free electron and since the energy of the electron–hole pair is related to the band gap energy, and not the energy of the Fermi level.

When a semiconductor is bombarded with photons equal to or greater in energy than the band gap, an electron–hole pair is formed. The current that results is a direct function of the incident light intensity. Photoconductive devices consist of a *p–n* junction called a *photodiode*, or a *p–i–n* junction commonly used in a photodetector, an

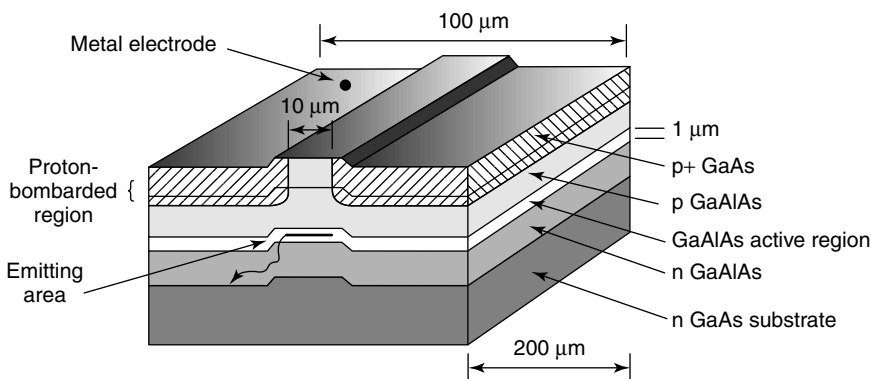


Figure 6.99 Schematic diagram of a layered compound semiconductor laser. (www.mtmi.vu.lt/pfk/funkc_dariniai/diod/led.htm).

Table 6.28 Some Common Compound Semiconductor Lasers and Their Characteristic Wavelengths

Compound	Wavelength (μm)	Compound	Wavelength (μm)
ZnS	0.33	GaAs	0.84–0
ZnO	0.37	InP	0.91
GaN	0.40	GaSb	1.55
ZnSe	0.46	InAs	3.1
CdS	0.49	Te	3.72
ZnTe	0.53	PbS	4.3
GaSe	0.59	InSb	5.2
CdSe	0.675	PbTe	6.5
CdTe	0.785	PbSe	8.5

Source: www.mtmi.vu.lt/pfk/funkc_dariniai/diod/led.htm

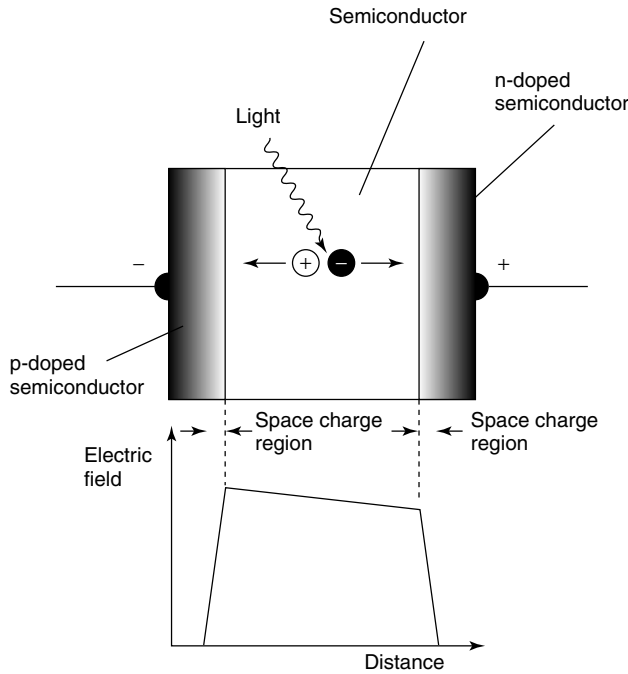


Figure 6.100 Schematic illustration of *p-i-n* junction used in a photodiode. Reprinted, by permission, from P. Ball, *Made to Measure*, p. 46. Copyright © 1997 by Princeton University Press.

example of which is schematically illustrated in Figure 6.100. When light is absorbed in the undoped region (*i* region), the electron–hole pair is created, and the two charge carriers are pulled in opposite directions by the applied electric field to the two poles, thus creating current. Silicon can be used to detect infrared wavelength light, and InGaAs is used for longer wavelengths, including visible light. However, optical detectors tend to be relatively slow and have low sensitivity. CdS is widely used for the detection

of visible light, as in photographic light meters. Photoconductivity is also the underlying principle of the *photovoltaic cell*, commonly called the *solar cell*, used for the conversion of solar energy into electricity.

6.3.2.7 Optical Fiber*. One of the benefits that lasers have provided is a method for transmitting information in binary code (cf. Section 6.1.1.6). This is easily performed by assigning a “one” to a high-intensity pulse (on) and assigning a “zero” to a low intensity pulse (off). The key to utilizing this technology for telecommunications, however, is the ability to transmit this digital information over long distances. One method for transmitting optical information has been through the optical analog to copper wire, the optical fiber. The conversion from the transmission of information via analog signals (such as telephone conversations) on copper wires to the transmission of information via digital signals on fiber-optic cable has been a rapid one and is due primarily to the advantages of optical fiber over copper wire, some of which are listed in Table 6.29. In Table 6.29, the number of two-way transmissions is a measure of information capacity, and the repeater distance is the distance between amplifiers, indicative of the attenuation loss associated with each medium. It is ironic that even with the proliferation of wireless communications (e.g., cellular telephones), the use of land-based transmission media, such as optical fiber, has grown in a concurrent manner, since for every cellular transmission tower, there needs to be the associated land-based components that connect the tower to the communications “backbone.” Hence, it is worthwhile to describe how this important materials technology works.

Optical fiber operates on the principle of *total internal reflectance*. Recall from Eq. (6.85) that when light encounters a change in refractive index, it is bent at an angle. Consider now the case where light goes through three media, each of differing refractive index, as illustrated in Figure 6.101. The angles of refraction are related to the refractive index change at each of the interfaces, through the more general form of Eq. (6.85) known as *Snell’s Law*:

$$\frac{n_2}{n_1} = \frac{\sin \theta_1}{\sin \theta_2} \tag{6.90}$$

and

$$\frac{n_3}{n_2} = \frac{\sin \theta_2}{\sin \theta_3} \tag{6.91}$$

Note that Eq. (6.90) reduces to Eq. (6.85) for the case where medium 1 is air ($n_1 = 1$).

Table 6.29 Comparison of Transmission Characteristics for Copper Wire and Optical Fiber

Characteristic	Copper Wire	Optical Fiber
Diameter, mm	1.5	0.025
Density, g/cm ³	8.96	2–4
Repeater distance, km	2	30
No. of two-way transmissions	24	1344
Corrosion resistance	Low	High
Susceptibility to EM interference	High	Low

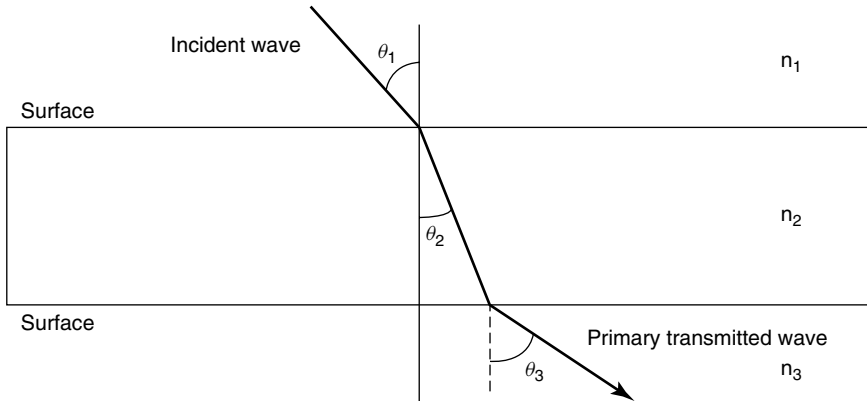


Figure 6.101 Schematic illustration of light propagating through three media of differing refractive indices.

At some angle of θ_2 , the transmitted wave will travel parallel to the second interface (*i.e.*, $\theta_3 = 90^\circ$), and all of the light is reflected back into medium 2. This value of θ_2 is called the *critical angle for total internal reflectance*, θ_c . For example, if medium 3 were air ($n_3 = 1$) and medium 2 were a glass of $n_2 = 1.5$, the condition for which $\theta_3 = 90^\circ$ could be found from Eq. (6.91) to be $\theta_c = 42^\circ$. You should be able to visualize, with the aid of Figure 6.101, that total internal reflectance can also be accomplished by selecting an index of refraction for medium 3 such that $\theta_3 = 90^\circ$. This is called the *core and cladding* structure, where medium 1 is air at the entrance to the optical fiber, medium 2 is the core, and medium 3 is the cladding. The core–cladding structure is the principle behind fiber optics, and simply consists of a center core, through which the optical signal is transmitted, surrounded by a cladding of different refractive index. The indices of refraction are selected such that $n_{\text{cladding}} < n_{\text{core}}$. Once the light enters the core from the source, it is reflected internally and propagates along the length of the fiber. Typically, both the core and cladding are made of special types of glass with carefully controlled indices of refraction. A polymeric coating is usually applied to the outside of the fiber for protection only.

The sharp change of refractive index between the core and cladding results in what is called a *step-index optical fiber*, as illustrated in Figure 6.102a. It is also possible, through chemical manipulation of the glass components, to vary the index of refraction in a continuous, parabolic manner, resulting in a *graded-index optical fiber*, as shown in Figure 6.102b. This results in a helical path for the light rays, as opposed to a zigzag path in a step-index fiber. The digital pulse is less distorted in a graded-index fiber, which allows for a higher density of information transmission. Both step- and graded-index fibers are termed *multimode fibers*. A third type of optical fiber is called a *single-mode fiber*, as shown in Figure 6.102c, in which light travels largely parallel to the fiber axis with little distortion of the digital light pulse. These fibers are used for long transmission lines, in which all of the incoming signals are combined, or *multiplexed*, into a single signal.

Core and cladding materials are selected not only on the basis of their refractive index, but also for their processability, attenuation loss, mechanical properties, and dispersion properties. However, density, ρ , and refractive index, n , are critical and have been correlated for over 200 optical glasses, for which the following formula

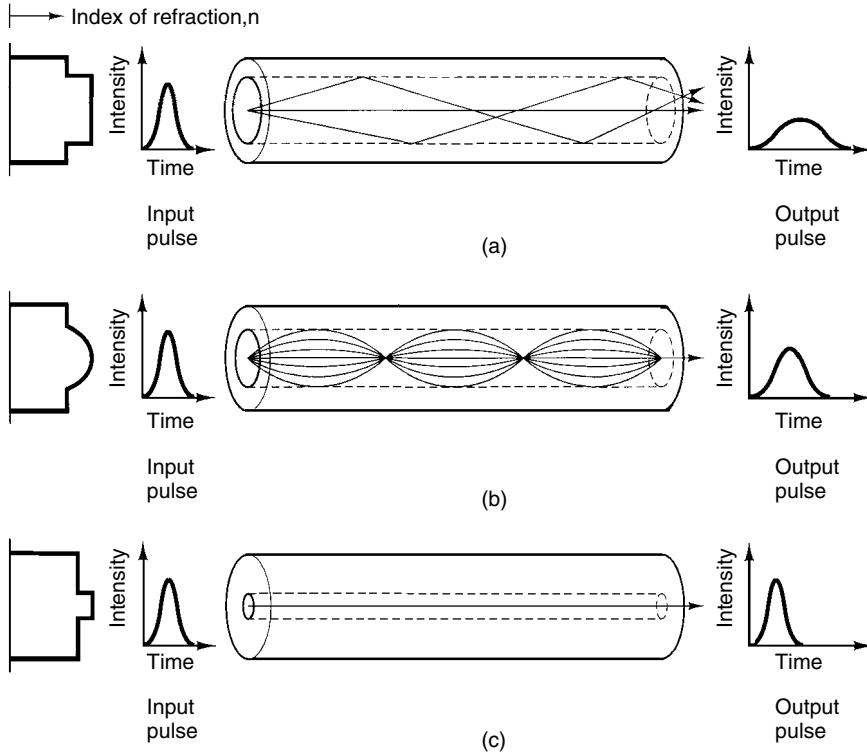


Figure 6.102 Schematic illustration of (a) step-index, (b) graded-index, and (c) single-mode optical fibers. Reprinted, by permission, from J. F. Shackelford, *Introduction to Materials Science for Engineers*, 5th ed., p. 611. Copyright © 2000 by Prentice-Hall, Inc.

applies with an accuracy of 2% or better:

$$n = \frac{\rho + 10.4}{8.6} \quad (6.92)$$

Refractive index can also be found from the weighted average of the refractive index of its components, to a first approximation.

High-purity silica-based glasses are used as the fiber material, with fiber diameters ranging between about 5 and 100 μm . The fibers are carefully fabricated to be virtually free of flaws and, as a result, are extremely strong and flexible. We will examine this unique fabrication process in more detail in the next chapter.

6.3.3 Optical Properties of Polymers

As with virtually every other material property, if a polymer possesses optical properties comparable to those of a glass or metal, it will be utilized simply on the basis of weight savings, all other factors being equal. As a result, much of the development in the optical properties of polymers is related to creating glass-like transmissivities or metal-like reflectivities. There are also a few unique optical characteristics of polymers that

make them useful for applications for which there is no true glass or metal analogue. We investigate some of these optical characteristics of polymers in this section.

6.3.3.1 Polymer Structure, Transmittance and Birefringence. There is a great deal of variability in the light transmission properties of polymers. Some of this variability is due to structural differences, and some is due to the presence of fillers and colorants that are purposely added to make otherwise translucent polymers appear opaque. We will focus for the moment on structural differences in polymers that lead to differences in the transmission of light.

The primary structural characteristic affecting the transmission of light in polymers is crystallinity. As in ceramic materials, the presence of grain boundaries, pores and particles that are of the order in size of the wavelength of light will create scattering. Crystallites in polymers act as these scattering centers. An example is found in polyethylene. Low-density polyethylene is semicrystalline, with only a few crystallites to act as scattering centers, so that it is mostly transparent. However, high-density polyethylene, which is highly crystalline, is translucent. In fact, most polymer crystals are of the right size to cause scattering, so a rule of thumb is that crystalline polymers are translucent (or opaque), whereas noncrystalline polymers are transparent. Some examples of noncrystalline, transparent polymers are polycarbonate, acrylics such as poly(methyl methacrylate), and polystyrene. There are some transparent, crystalline polymers, such as polyethylene terephthalate (PET), in which the crystallites are smaller than the wavelength of light.

An interesting artifact of polymer crystallinity is the anisotropic nature of the refractive index, which leads to birefringence, as first introduced in Section 6.3.2.1. When the topic of polymer crystallinity was first introduced back in Chapter 1, we presented a photomicrograph of polyethylene spherulites that was produced under cross-polarized light (cf. Figure 1.62). This image is obtained by placing a sample of the polymer between two quarter-wave plate optical filters, or *polarizers*, which allow the light passing through to vibrate only along one plane. In this way, if the second filter, called the *analyzer*, is rotated 90° from the polarizer, no light will pass through the filter combination, since the plane of vibration allowed through the polarizer is extinguished in the analyzer. However, when a crystalline sample such as polyethylene is placed between the polarizer and analyzer, an interesting pattern is transmitted through the analyzer, which includes some dark regions (no transmission) and light regions (complete transmission). An idealized form of the resulting *Maltese cross* is shown in Figure 6.103, and an actual image of which was shown in Figure 1.62. This image is the result of birefringence, or refractive index differences in the oriented polymer chains. The index of refraction for most polymers is greater parallel to the chain than normal to the molecular axis. As a result, the refractive index in the tangential direction of the spherulite is greater (see Figure 1.61) than that along the spherulite radius. This birefringence, coupled with the spherical geometry of the spherulite, produces light extinction along the axis of each of the filters, hence the 90° angles in the Maltese cross.

Birefringence can also be used to analyze polymer samples after melt processing. As we will see in the next chapter, the shear produced in certain molding techniques, such as injection molding, can orient polymer chains in certain parts of the mold, especially near the mold walls, whereas the chains in low-shear regions, such as in the middle of the mold, are not as oriented. Figure 6.104 shows the variation in birefringence, as

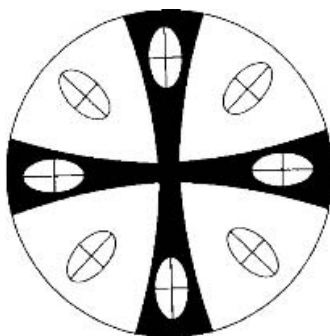


Figure 6.103 Schematic of Maltese cross produced by spherulites in crosspolarized filters. Reprinted, by permission, from Strobl, G., *The Physics of Polymers*, 2nd ed., p. 146. Copyright © 1997 Springer-Verlag.

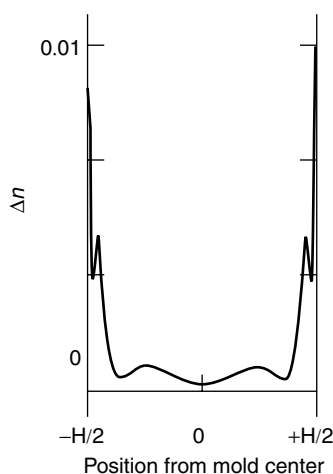


Figure 6.104 Variation in birefringence of injection molded polymer of width H . Adapted from P. C. Powell and A. J. Ingen Housz, *Engineering with Polymers*, p. 314. Copyright © 1998 by P. C. Powell and A. J. Ingen Housz.

measured by the refractive index difference along two directions, with position in the mold for an injection-molded polymer. The birefringence is largest at the periphery of the mold, where shear rates are highest and the polymer is most highly oriented.

6.3.3.2 Electroluminescence*. In Section 6.3.2.5, we saw that some materials—in particular, semiconductors—can reemit radiation after the absorption of light in a process called photoluminescence. A related type of emission process, which is common in polymer-based semiconductors, called *electroluminescence*, results when the electronic excitation necessary for emission is brought about by the application of an electric field rather than by incident photons. The electric field injects electrons into the conduction band, and holes into the valence band, which upon recombination emit light.

As we saw in Section 6.1.3.2, most electrically conducting polymers contain poly-conjugated structures, such as extended double bonds along the polymer backbone. It is not surprising, then, that electrically conducting polymers such as polyacetylene can also be electroluminescent. The first visible-light-emitting polymer was made from poly(phenylene vinylene), or PPV, the structure for which is shown in Figure 6.105a. PPV exhibits luminescence in the yellow part of the spectrum, and it can be fabricated into a *light-emitting diode* (LED) by sandwiching a micron-thick layer of PPV between contacts made of indium-tin oxide (a transparent electrode material) on the bottom and cadmium metal on the top. These contact materials are selected to match their electronic bands to that of the polymer. When 12 volts are applied across the contacts, electrons and holes enter the polymer and recombined to generate photons of yellow light. Other polymers with different band gaps can be used to emit light of various wavelengths, such as polythiophene-based compounds (see Figure 6.105b) for the emission of blue light. The applications for polymer LEDs (PLEDs) continue to grow, including paper-thin computer and television displays, which will ultimately require a single polymer that is capable of emitting blue, red, or yellow light, depending upon the applied voltage. The requirements that must be met before PLEDs can become viable candidates for use in flat panel displays include sufficiently high brightness, good photoluminescence profiles, high efficiency (i.e., low operating voltage and current), good color saturation, and long lifetime. A good display device must have at least a brightness of 100 cd m^{-2} at an operating voltage of between 5 and 15 V and a lifetime of 10,000 h. Moreover, charge conduction in the PLEDs requires electric fields in the range of $2\text{--}5 \text{ MV cm}^{-1}$.

6.3.3.3 Liquid Crystal Displays (LCDs)*. Liquid crystalline polymers, first introduced in Section 1.3.6.3, are utilized for a different type of computer and television display, the *liquid crystal display* (LCD). Most of today's laptop computers and handheld devices utilize color flat panel displays where the light transmission from the

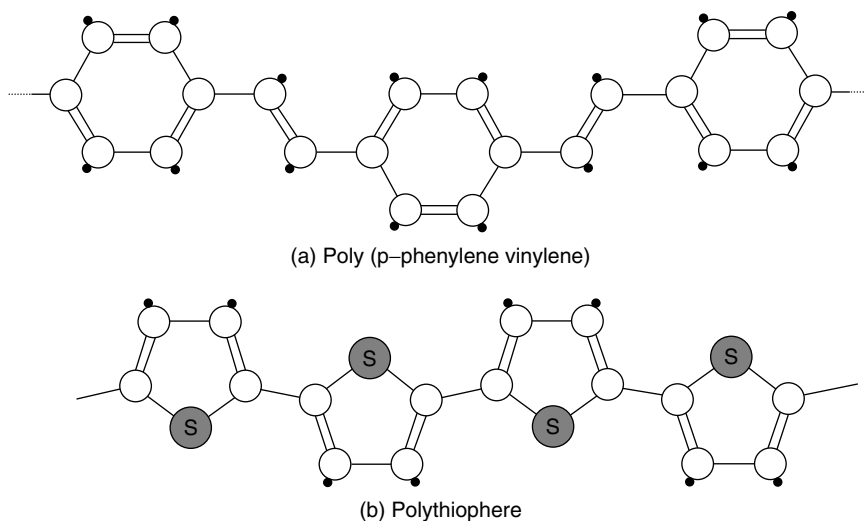


Figure 6.105 Molecular structure of two electroluminescent polymers. Reprinted, by permission, from P. Ball, *Made to Measure*, p. 381. Copyright © 1997 by Princeton University Press.

back to the front of the display is modulated by orientational changes in liquid crystal molecules. As illustrated in Figure 6.106, liquid crystalline polymers are sandwiched between two transparent polarizers. The types of liquid crystalline polymers can vary, but generally they are of the cholesteric or twisted nematic type. The LC polymers are initially oriented in the display manufacturing process using a “rubbing process.” The mechanism of alignment is not well understood, however, and is an expensive step in the fabrication process. The transparent substrates between which the liquid crystals are deposited are usually polyimides.

Under an applied electric field, the liquid crystal molecules tend to align parallel to each other, resulting in optical anisotropy. The liquid crystal cell is thus a tiny shutter that is controlled by the applied electric field. When the area encompassed on the top, bottom, and sides by electrodes, called a *pixel*, is turned on, the liquid crystal molecules align, allowing only one plane of the electromagnetic wave (polarized light) to penetrate to the front panel, where it is absorbed in the second polarizer, effectively blocking the light (left image in Figure 6.106). When the field is turned off, the shutter filters the light by rotating its optical plane, as shown on the right in Figure 6.106. Changing bright pixels into colored ones requires yet another filter. As a result, LCDs

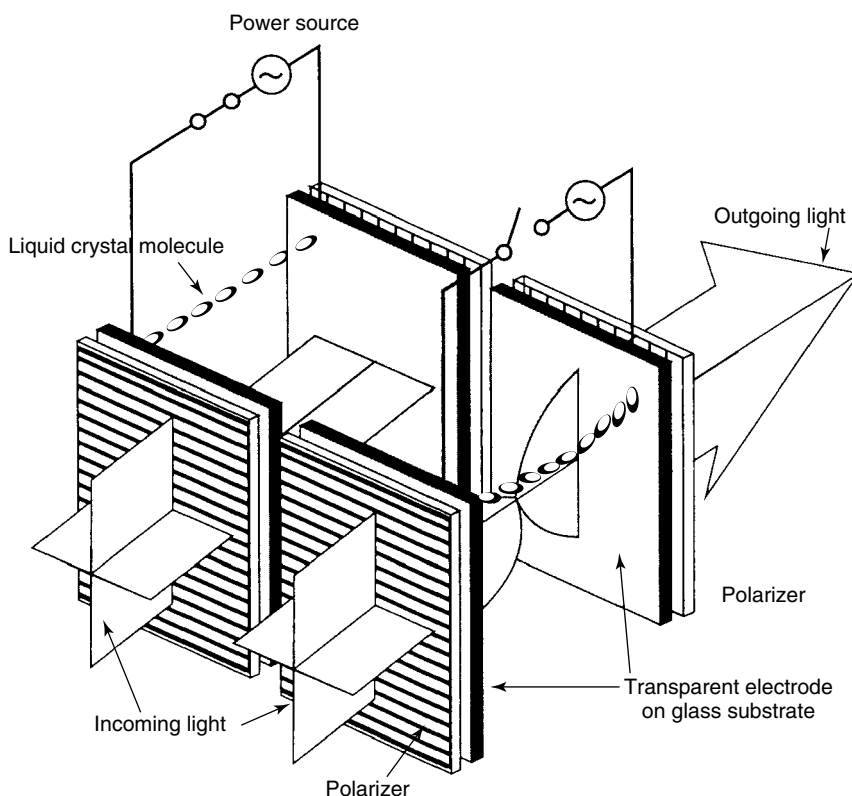


Figure 6.106 Schematic illustration of liquid crystalline polymers sandwiched between polarizers and effect on light in a liquid crystal display. From Jun-ichi Hanna and Isamu Shimizu, Materials in active-matrix liquid-crystal displays, *MRS Bulletin*, 21(3), 35 (1996). Reproduced by permission of MRS Bulletin.

are very dim, and must be back-illuminated with a lamp, which is an energy-intensive process. LCDs also suffer from a limited viewing angle. These are the primary reasons behind the interest in the electroluminescent materials of the previous section for flat panel displays.

6.3.3.4 Nonlinear Optical Materials*. We have seen several examples in the previous sections of how photons can be used to generate and transmit data. Though it is beyond the scope of this text, there are also devices for storing data in an optical fashion. This emerging area of using photons to replace what was previously performed by electrons is called *photonics*. The integration of photonic and electronic devices is called *optoelectronics*. In this section, we describe how the optical properties of materials can be used in yet another manner to create devices that can act as switches, multiplexers, and mirrors and even change the wavelength of light. The materials that exhibit these effects and that are used in these photonic and optoelectronic devices are generally referred to as *nonlinear optical materials* (NLO), because their outputs are not a linear response to some input. We are most familiar with linear responses of materials; for example, the intensity of photons emitted from a tungsten filament in a light bulb increases (more or less) linearly with the power we put into it. But even in this example, nonlinear behavior can occur in the form of *saturation*, where further increases in power do not result in more output, or in the form of *breakdown*, when the filament burns out. The diodes described in the preceding sections are nonlinear electronic components—their output currents remain negligibly low until the driving voltages reach a threshold value whereupon the output current increases sharply.

The best way to describe a nonlinear optical response is first through some examples, then through some mathematics. Shortly after the invention of lasers, it was observed that a ruby laser beam passing through a quartz crystal produced a faint beam at the laser's second harmonic—that is, at twice the fundamental frequency of the ruby laser (cf. Section 6.3.2.5). A much simpler-to-perform example of nonlinear optical behavior is found when the polarization of light passing through a crystal is modified upon application of an electric field to the crystal. The origin of both of these NLO effects is related to the change in refractive indices that result by an applied electric field and the modulation of light beams by these field-dependent indices. We have already seen the relationship between refractive index and polarizability, and this is where our mathematical description of NLO effects begins.

We can examine how induced polarization behaves as a function of an applied electric field, \mathcal{E} , by considering the induced electric dipole moment (cf. Section 6.1.2.2), p_e , as a Taylor series expansion in \mathcal{E} :

$$p_e = p_{e,0} + \mathcal{E}(\partial p_e / \partial \mathcal{E})_{\mathcal{E} \rightarrow 0} + 1/2 \mathcal{E}^2 (\partial^2 p_e / \partial \mathcal{E}^2)_{\mathcal{E} \rightarrow 0} + 1/6 \mathcal{E}^3 (\partial^3 p_e / \partial \mathcal{E}^3)_{\mathcal{E} \rightarrow 0} + \cdots \quad (6.93)$$

or, more simply,

$$p_e = p_{e,0} + \alpha \mathcal{E} + (\beta/2) \mathcal{E}^2 + (\gamma/6) \mathcal{E}^3 + \cdots \quad (6.94)$$

where $p_{e,0}$ is the static dipole of the molecule, α is the linear polarizability [previously called just “polarizability”; cf. Eq. (6.35)], and the higher-order terms β and γ are called the *first* and *second hyperpolarizabilities*, respectively. Note that once again, we consider only the magnitude of the electric field, which is actually a vector quantity.

The terms beyond $\alpha\mathcal{E}$ in Eq. (6.94) are not linear in \mathcal{E} , so they are referred to as the *nonlinear polarization* and give rise to NLO effects. You should now see why nonlinear polarization becomes more important at higher electric field strengths, since it scales with higher powers of the field. For most materials, $\alpha\mathcal{E} > (\beta/2)\mathcal{E}^2 > (\gamma/6)\mathcal{E}^3$, so the first few observations of NLO effects were made prior to the invention of lasers and their associated large electric fields. The bulk polarization, P , which you will recall is the dipole moment per unit volume, can then be expressed as

$$P = P_0 + \chi^{(1)}\mathcal{E} + \chi^{(2)}\mathcal{E}^2 + \chi^{(3)}\mathcal{E}^3 + \dots \quad (6.95)$$

where the $\chi^{(n)}$ *susceptibility coefficients* (not to be confused with the magnetic susceptibility of the same symbol) are tensors of order $n + 1$, and P_0 is the intrinsic static dipole moment density of the material.

We now consider the polarization induced by an oscillating electric field, such as that found in electromagnetic radiation (light), which can be expressed as

$$\mathcal{E} = \mathcal{E}_0 \cos(\omega t) \quad (6.96)$$

where ω is the frequency of the electric field and t is time. Substitution of Eq. (6.96) into Eq. (6.95) yields

$$P = P_0 + \chi^{(1)}\mathcal{E}_0 \cos(\omega t) + \chi^{(2)}\mathcal{E}_0^2 \cos^2(\omega t) + \chi^{(3)}\mathcal{E}_0^3 \cos^3(\omega t) + \dots \quad (6.97)$$

Because $\cos^2(\omega t) = 1/2 + 1/2 \cos(2\omega t)$, the first three terms of Eq. (6.97) become

$$P = (P_0 + 1/2\chi^{(2)}\mathcal{E}_0^2) + \chi^{(1)}\mathcal{E}_0 \cos(\omega t) + 1/2\chi^{(2)}\mathcal{E}_0^2 \cos(2\omega t) + \dots \quad (6.98)$$

Equation (6.98) indicates that the polarization consists of a second-order, direct-current (not dependent upon ω) field contribution to the static polarization (the first term), a frequency component, ω , corresponding to the incident light frequency (the second term), and a new, frequency-doubled component, 2ω (the third term). Thus, if an intense light beam passes through a second-order NLO material, light at twice the input frequency will be produced, as well as a static electric field. The process of frequency-doubling, which explains the first example of NLO behavior from the beginning of this section, is called *second harmonic generation* (SHG). The oscillating dipole reemits at all of its polarization frequencies, so light is observed at both ω and 2ω . The process of static field production is called *optical rectification*.

The general condition of second-order NLO effects involves the interaction of two distinct waves of frequencies ω_1 and ω_2 in an NLO material. In this case, polarization occurs at sum ($\omega_1 + \omega_2$) and difference ($\omega_1 - \omega_2$) frequencies. This electronic polarization will therefore reemit radiation at these frequencies, with contributions that depend on $\chi^{(2)}$, which is itself frequency-dependent. The combination of frequencies is called *sum* (or *difference*) *frequency generation* (SFG). SHG is a special case of SFG, in which the two frequencies are equal.

An applied electric field can also change a material's linear susceptibility, and thus its refractive index. This effect is known as the *linear electro-optic* (LEO) or *Pockel's effect*, and it can be used to modulate light by changing the voltage applied to a second-order NLO material. The applied voltage anisotropically distorts the electron

density within the material, and the optical beam “sees” a different polarizability and anisotropy of the polarizability. As a result, a beam of light can have its polarization state changed by an amount related to the strength of the orientation of the applied voltage and can travel at a different speed, and possibly in a different direction. The change in refractive index as a function of the applied field is approximated by the general expression

$$1/N_{ij}^2 = 1/n_{ij}^2 + r_{ijk}\mathcal{E}_k + s_{ijkl}\mathcal{E}_k\mathcal{E}_l + \dots \quad (6.99)$$

where N_{ij} are the induced refractive indices, n_{ij} are the refractive indices in the absence of the electric field, r_{ijk} are the linear or Pockels coefficients, s_{ijkl} are the quadratic or Kerr coefficients, and \mathcal{E} is the applied field. Subscripts indicate the orientation of the field with respect to a material coordinate system. Equation (6.99) indicates that light traveling through an electro-optic material can be phase- or polarization-modulated by refractive index changes induced by an applied electric field. Devices exploiting this effect include optical switches, modulators, and wavelength filters.

An example of an electro-optic switch based on NLO materials is shown in Figure 6.107. The switch is comprised of two parallel waveguides made of NLO materials. The waveguide channels have a different refractive index from the surrounding material. The light can be switched back and forth between the channels by applying and removing a voltage across the bottleneck. In the absence of an electric field, the light traveling through the lower waveguide interacts with the upper waveguide in a nonlinear manner at the bottleneck, causing the light to switch channels. Switching *does not* occur when an electric field is applied. The electric field polarizes the NLO material and alters the refractive indices of the two channels, such that the nonlinear interaction at the bottleneck is modified and the light stays in the lower waveguide.

Many current NLO devices are based upon crystalline materials (such as lithium niobate for the electro-optic switch) and nonlinear optical glasses, but there is intense

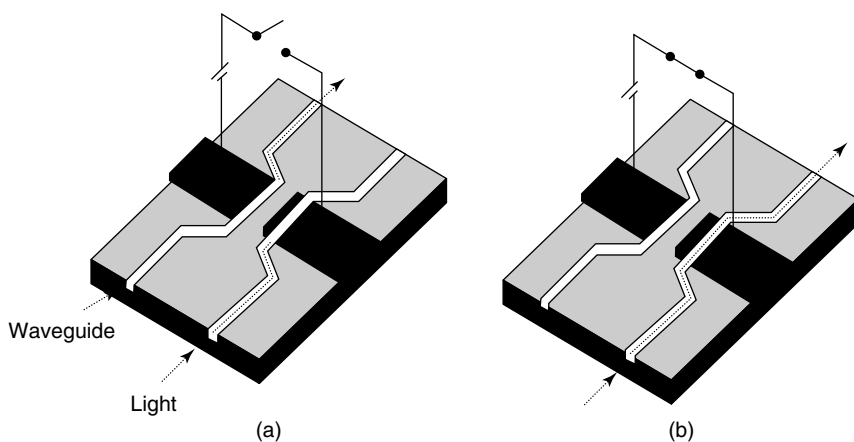


Figure 6.107 Schematic illustration of an electro-optic switch. (a) An open circuit causes light to switch channels, and (b) a closed switch keeps light in the same channel. Reprinted, by permission, from P. Ball, *Made to Measure*, p. 53. Copyright © 1997 by Princeton University Press.

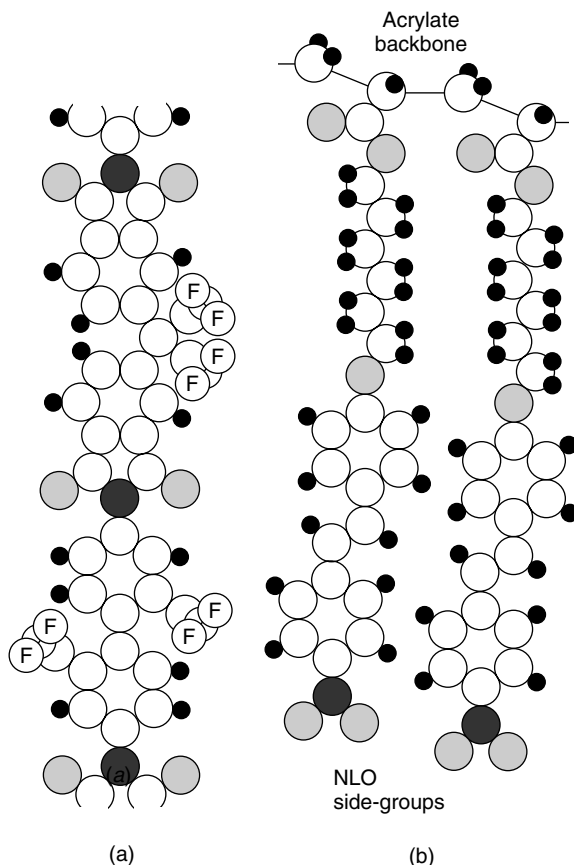


Figure 6.108 Examples of nonlinear optical polymers (a) fluorinated polyimide and (b) polyacrylate with NLO side groups. Reprinted, by permission, from P. Ball, *Made to Measure*, p. 55. Copyright © 1997 by Princeton University Press.

interest in utilizing polymers for these applications, due to their inherently low densities and potential ease of processing. Some of the polymers that have been used for photonic devices are based upon architectures that have highly polarizable electronic structures. Several polyimides fall into this category (Figure 6.108a), as do polyacrylates and polyurethanes with optically responsive side groups (Figure 6.108b).

6.3.4 Optical Properties of Composites and Biologics*

Of the three physical properties covered in this chapter, optical properties have the least importance in composite and biological applications. This is not to say that there are no applications of optical properties in composites or biological materials. There are indeed, such as the use of birefringence in the analysis of stress distribution and fiber breakage in fiber–matrix composites [14] and in the development of materials for ophthalmic implants such as intraocular devices [15]. These topics are beyond the scope of this text, however, even as optional information, and introduce no new concepts from a material property standpoint. There are many interesting articles and

books on these topics, however, and the interested reader is encouraged to consult them as these, and many more, new uses for the optical properties of materials are applied to composite and biological materials systems.

REFERENCES

Cited References

1. Solymar, L., and D. Walsh, *Lectures on the Electrical Properties of Materials*, 5th ed., Oxford University Press, Oxford, 1993, p. 425.
2. Sheahan, T., *Introduction to High-Temperature Superconductivity*, Plenum, New York, 1994, p. 3.
3. Cava, R. J., Oxide superconductors, *J. Am. Ceram. Soc.*, **83**(1), 5–28 (2000).
4. Sheahan, T., *Introduction to High-Temperature Superconductivity*, Plenum Press, New York, 1994, p. 223.
5. Zawodzinski, T. A., C. Derouin, S. Radzinski, R. J. Sherman, V. T. Smith, T. E. Springer, and S. Gottesfeld, *J. Electrochem. Soc.*, **140**, 1041 (1993).
6. Schmidt, C. E., V. R. Shastri, J. P. Vacanti, and R. Langer, Stimulation of neurite growth using an electrically-conducting polymer, *Proc. Natl. Acad. Sci. USA*, **94**, 8948–8953 (1997).
7. Sun, A., H. Xu, Z. Chen, L. Cui, and X. Hai, Research on electrical properties of amphiphilic lipid membranes by means of interdigital electrodes, *Mater. Sci. Eng. C*, **2**(3), 159–163 (1995).
8. Hontsu, S., T. Matsumoto, J. Ishii, M. Nakamori, H. Tabata, and T. Kawai, Electrical properties of hydroxyapatite thin films grown by pulsed laser deposition, *Thin Sol. Films*, **295**, 214–217 (1997).
9. Gatteschi, D., P. Carretta, and A. Lascialfari, Molecular magnets and magnetic nanoparticles: new opportunities for μ SR investigations, *Physica B*, **289–290**, 94–105 (2000).
10. Yakhmi, J. V., Magnetism as a functionality at the molecular level, *Physica B*, **321**, 204–212 (2002).
11. Chavan, S. A., J. V. Yakhmi, and I. K. Gopalakrishnan, Molecular ferromagnets—a review, *Mater. Sci. Eng. C*, **3**, 175–179 (1995).
12. Miller, J. S. and A. J. Epstein, Molecular magnets: An emerging area of materials chemistry, in *Materials Chemistry: An Emerging Discipline*, L. V. Interrante, L. A. Casper, and A. B. Ellis, eds., American Chemical Society, Washington, D.C., 1995, p. 161.
13. Hanna, J., and I. Shimizu, Materials in Active-Matrix Liquid Crystal Displays, *MRS Bulletin*, March, 35 (1996).
14. Schuster, D. M., and E. Scala, *Trans. AIME*, **230**, 1639 (1964).
15. Obstbaum, S. A., Ophthalmic Implantation, in *Biomaterials Science*, B. D. Ratner, A. S. Hoffman, F. J. Schoen, and J. E. Lemons, eds., Academic Press, San Diego, 1996, p. 435.

Electrical Properties of Materials

Electrical Properties of Bone and Cartilage, C. T. Brighton, J. Black, and S. Pollack, eds., Grune & Stratton, New York, 1979.

Solymar, L., and D. Walsh, *Lectures on the Electrical Properties of Materials*, 5th ed., Oxford University Press, New York, 1993.

Magnetic Properties of Materials

Moorjani, K., and J. M. D. Coey, *Magnetic Glasses*, Elsevier, Amsterdam, 1984.

Westbrook, C., and C. Kaut, *MRI in Practice*, Blackwell Science, Oxford, 1998.

Optical Properties of Materials

Campbell, S. A., *The Science and Engineering of Microelectronic Fabrication*, Oxford University Press, New York, 1996.

Wolf, S., and R. N. Tauber, *Silicon Processing for the VLSI Era*, Vol. 1, Lattice Press, Sunset Beach, CA, 1986.

Fox, M., *Optical Properties of Solids*, Oxford University Press, New York, 2001.

PROBLEMS

Level I

- 6.I.1** What will be the resistance of a copper wire 0.08 in. in diameter and 100 ft long if its resistivity is $1.7 \mu\Omega \cdot \text{cm}$?
- 6.I.2** A maximum resistance of 1Ω is permitted in a copper wire 25 ft long. What is the smallest wire diameter that can be used?
- 6.I.3** What is the electrical conductivity of iron (a) at room temperature? (b) at 212°F ?
- 6.I.4** Silicon has a density of 2.40 g/cm^3 . (a) What is the concentration of the silicon atoms per cubic centimeter? (b) Phosphorus is added to the silicon to make it an *n*-type semiconductor with a conductivity of 1 mho/cm and an electron mobility of $1700 \text{ cm}^2/\text{V}\cdot\text{s}$. What is the concentration of the conduction electrons per cubic centimeter?
- 6.I.5** (a) How many silicon atoms are there for each conduction electron in problem 6.I.4? (b) The lattice constant for silicon is 5.42 \AA , and there are eight atoms per unit cell. What is the volume associated with each conduction electron?
- 6.I.6** Germanium used for transistors has a resistivity of $2 \Omega \cdot \text{cm}$ and an electron “hole” concentration of $1.9 \times 10^{15} \text{ holes/cm}^3$. (a) What is the mobility of the electron holes in the germanium? (b) What impurity element could be added to germanium to create electron holes?
- 6.I.7** Calculate the mobility of electrons in Cu. The resistivity of Cu is $1.72 \times 10^{-8} \Omega \cdot \text{m}$ at 25°C and its density is 8.9 g/cm^3 . Assume each copper atom donates one valence electron to the conduction band.
- 6.I.8** A coil of wire 0.1 m long and having 15 turns carries a current of 1.0 A. (a) Compute the magnetic induction if the coil is within a vacuum. (b) A bar of molybdenum is now placed in the coil, and the current adjusted to maintain the same magnetic induction as in part (a). Calculate the magnetization.
- 6.I.9** Why is there a maximum power loss when the dielectric is changing most rapidly as a function of temperature and frequency?

- 6.I.10** Crown glass has a refractive index of 1.51 in the visible spectral region. Calculate the reflectivity of the air–glass interface, and determine the transmission of a typical glass window.
- 6.I.11** Look up the refractive indices for fused silica and dense flint glass, and calculate the ratio of their reflectivities. Cite the source of your information.

Level II

- 6.II.1** At room temperature, the temperature dependence of electron and hole mobilities for intrinsic germanium is found to be proportional to $T^{-3/2}$ for temperature in degrees Kelvin. Thus, a more appropriate form of Eq. (6.31) is

$$\sigma = C'' T^{-3/2} \exp\left(\frac{-E_g}{2k_B T}\right)$$

where C'' is a temperature-independent constant. (a) Calculate the intrinsic electrical conductivity using both Eq. (6.31) and the equation above for intrinsic germanium at 150°C, if the room temperature electrical conductivity is $2.2 (\Omega \cdot \text{m})^{-1}$. (b) Compute the number of free electrons and holes for intrinsic germanium at 150°C assuming this $T^{-3/2}$ dependence of electron and hole mobilities.

- 6.II.2** Assume there exists some hypothetical metal that exhibits ferromagnetic behavior and that has a simple cubic structure, an atomic radius of 0.153 nm, and a saturation flux density of 0.76 tesla. Determine the number of Bohr magnetons per atom for this material.
- 6.II.3** The formula for yttrium iron garnet ($\text{Y}_3\text{Fe}_5\text{O}_{12}$) may be written in the form $\text{Y}_3^c\text{Fe}_2^a\text{Fe}_3^d\text{O}_{12}$, where the superscripts a , c , and d represent different sites on which the Y^{3+} and Fe^{3+} ions are located. The spin magnetic moments for the Y^{3+} and Fe^{3+} ions positioned in the a and c sites are oriented parallel to one another and antiparallel to the Fe^{3+} ions in d sites. Compute the number of Bohr magnetons associated with each Y^{3+} ion, given the following information: (1) Each unit cell consists of eight formula ($\text{Y}_3\text{Fe}_5\text{O}_{12}$) units; (2) the unit cell is cubic with an edge length of 1.2376 nm; (3) the saturation magnetization for this material is 1.0×10^4 A/m, and (4) assume that there are 5 Bohr magnetons associated with each Fe^{3+} ion.
- 6.II.4** The detectors used in optical fiber networks operating at 850 nm are usually made of silicon, which has an absorption coefficient of $1.3 \times 10^5 \text{ m}^{-1}$ at this wavelength. The detectors have coating on the front face that make the reflectivity at the design wavelength negligibly small. Calculate the thickness of the active region of a photodiode designed to absorb 90% of the light.

Level III

- 6.III.1** The *magnetocaloric effect* (*Scientific American*, May 1998, p. 44) relies on the ability of a ferromagnetic material to heat up in the presence of a magnetic field and then cool down once the field is removed. When a ferromagnet is

placed in a magnetic field, the magnetic moments of its atoms become aligned, making the material more ordered. But the amount of entropy must be conserved, so the atoms vibrate more rapidly, raising the material's temperature. When the material is taken out of the field, the material cools. Water, or some other heat transfer fluid, can be cooled down by running it through the ferromagnetic material as it cools. (a) The magnitude of the magnetocaloric effect reaches a maximum at the Curie temperature of the ferromagnet. Based upon the above description of the application and the Curie temperature, which of the following three materials will make the best ferromagnetic material for a typical household refrigeration unit? *Justify your selection.*

Material	Saturation Magnetization ^a at Room Temperature	Curie Temperature (K)	Melting Point (K)
Iron	1707	1043	1811
Gadolinium	1090	289	1585
Nickel	485	631	1728

^aMaximum possible magnetization that results when all magnetic dipoles are aligned with the external field.

(b) The amount of refrigeration is also determined by the strength of the applied magnetic field. Superconducting magnets are used to generate massive magnetic fields that cause large magnetizations in the ferromagnetic inductor. Below are three candidate materials for the superconducting magnet. Based on what you know about superconductors, which of these three materials will make the best superconducting magnet for this application? *Justify your selection.*

Material	T _c , K	H _c , tesla
Bi ₂ Sr ₂ Ca ₂ Cu ₃ O ₁₀	110	100
Gadolinium	5.9	0.0001
NbTi	9.5	10

6.III.2 A team of chemical engineers [*Proc. Natl. Acad. Sci. USA*, **94**, 8984 (1997)] has shown that oxidized polypyrrole supports the growth of structural support cells needed for nerve regeneration in rats. In particular, the team showed that rat nerve cells responded to electrical stimulus from the polymer by producing extensions called neurites that are twice as long as neurites produced in the absence of the stimulus. (a) Calculate the current generated in a 10-mm-long, 10.0×10^{-6} -m-diameter polypyrrole filament that is subjected to a electric field gradient of 12 V. Assume that the conductivity of oxidized polypyrrole is $1.5 \times 10^7 \, \Omega^{-1}\text{m}^{-1}$. (b) One drawback for this application is that polypyrrole is very fragile and not biodegradable. Suggest a method for evaluating the long-term biocompatibility of polypyrrole fibers *in vivo*.